2011

The Aspects of Fouling on the Performance of Diesel Exhaust Gas Recirculation Coolers

Ahmed J. Sobh
University of Windsor

The Aspects of Fouling on the Performance of Diesel Exhaust Gas Recirculation Coolers

by

Ahmed Sobh

A Thesis
Submitted to the Faculty of Graduate Studies
through Mechanical, Automotive and Materials Engineering
in Partial Fulfillment of the Requirements for
the Degree of Master of Applied Science at the
University of Windsor

Windsor, Ontario, Canada

2011

The Aspects of Fouling on the Performance of Diesel Exhaust Gas Recirculation Coolers

by

Ahmed Sobh

APPROVED BY:

_____
Dr. Xiang Chen, Outside Reader
Department of Electrical and Computer Engineering

_____
Dr. Graham Reader, Program Reader
Faculty of Engineering

_____
Dr. Jimi S. Tjong, Co-advisor
Department of Mechanical, Automotive and Materials Engineering

_____
Dr. Ming Zheng, Co-advisor
Department of Mechanical, Automotive and Materials Engineering

_____
Dr. Andrzej Sobiesiak, Chair of Defence
Department of Mechanical, Automotive and Materials Engineering

May 17, 2011

AUTHOR'S DECLARATION OF ORIGINALITY

I herby certify that I am the sole author of this thesis and that no part of this thesis has been published or submitted for publication.

I certify that, to the best of my knowledge, my thesis does not infringe upon anyone's copyright nor violate my proprietary rights and that any ideas, techniques, quotations, or any other material from the work of other people included in my thesis, published or otherwise, are fully acknowledged in accordance with the standard referencing practices. Furthermore, to the extent that I have included copyrighted material that surpasses the bounds of fair dealings within the meaning of the Canada Copyright Act. I certify that I have obtained a written permission from the copyright owner(s) to include such material(s) in my thesis and have included copies of such copyright clearances to my appendix.

I declare that this is a true copy of my thesis, including my final revisions, as approved by my thesis committee and the Graduate Studies office, and that this thesis has not been submitted for a higher degree to any other University or Institution.

ABSTRACT

A study was conducted to develop a standardized method to evaluate and compare the performance of various EGR cooler designs on a common fouling test. Several leading competitive EGR coolers were tested for fouling performance utilizing a common test method and from the results of the investigation the best design was recommended for optimal fouling resistance. The Ford research group at the Powertrain Engineering Research and Development Centre selected the competitive cooler designs for the investigation based on similar cost and compactness. The evaluation of the EGR coolers was based on the performance measures of heat exchangers such as effectiveness and pressure drop. Additional analysis was also required in order to normalize the performance measures to develop trends of fouling. Heat exchanger effectiveness was normalized with respect to heat transfer surface area using the definition of fouling factor where as the pressure drop data was non-dimensionalized with the friction factor.

The aspects of coolant flow configuration, fin density, and particulate filtration were also investigated under standardized experiments and general conclusions were formed from the results. More importantly, the studies provided insight on some of the critical factors which contribute to cooler fouling and EGR cooler degradation. Further research studies can be designed to help better understand these critical factors of concern and the design of EGR coolers can be optimized.

DEDICATION

This work is dedicated to my parents,
JAWDAT and AMIRA SOBH:

ACKNOWLEDGEMENTS

The author would like to thank Dr. Jimi Tjong, and Dr. Ming Zheng as well as the committee for all of their support and guidance in the completion of this work. A special thanks to the group at the Powertrain Engineering Research and Development Centre (PERDC). Special regards to Dr. Usman Asad, Dr. Doug Chang, and Dr. Clarence Mwila Mulenga for their guidance and support with the development of the project.

TABLE OF CONTENTS

LIST OF FIGURES

LIST OF TABLES

NOMENCLATURE

A	Overall heat transfer surface area	[m^2]
A_o	Minimum free flow area	[m^2]
API	American Petroleum Institute	
ASTM	American Society for Testing and Materials	
BMEP	Brake Mean Effective Pressure	[bar]
BSFC	Brake Specific Fuel Consumption	[g/kW-hr]
CAC	Charge Air Cooler	
CO	Carbon Monoxide	
CO_2	Carbon Dioxide	
c_p	Specific heat capacity @ constant pressure	[J/kg-K]
CF	Counter flow configuration	
DPF	Diesel Particulate Filter	
D_h	Hydraulic Diameter	[m]
EGR	Exhaust Gas Recirculation	
f	Fanning friction factor	
FSN	Filter Smoke Number	
FPI	Fins per inch	
HC	Hydrocarbon	
H-FID	Heated Flame Ionization Detector	
HPL	High Pressure Loop	
HT	High Temperature	
IAT	Intake Air Temperature	[°C]
L	Cooler characteristic length	[m]
LPL	Low Pressure Loop	
LT	Low Temperature	
$\dot{m}_{EGR}$	Mass flow rate of EGR	[kg/hr]
MAF	Mass air flow of fresh intake charge	[kg/hr]
MAF_{TOTAL}	Mass air flow (fresh intake + EGR)	[kg/hr]
NDIR	Non-Dispersive Infra-Red	
NO_x	Oxides of Nitrogen	

OBD	On-Board Diagnostic	
PC	Personal Computer	
PCM	Powertrain Control Module	
PM	Particulate Matter	
r_{EGR}	Rate of EGR	[%]
R_f	Fouling factor (thermal resistance of fouling deposits)	[m^2-K/W]
SCR	Selective Catalytic Reduction	
T_i	Temperature of i	[°C]
THC	Total Hydrocarbons	
U	Overall heat transfer coefficient	[W/m^2-K]
U_f	Overall heat transfer coefficient for a fouled cooler	[W/m^2-K]
U_c	Overall heat transfer coefficient for a clean cooler	[W/m^2-K]
V	Average velocity of fluid stream	[m/s]

Greek Alphabet

ε	Effectiveness of heat exchanger	[%]
$\Delta\varepsilon_{abs}$	Absolute degradation in effectiveness	[%]
Δh	Change in enthalpy	
Δp	Pressure drop	[kPa]
ΔT_m	Log mean temperature difference	
∇T	Temperature gradient	
ρ_i	Density of fluid i	[kg/m^3]

CHAPTER I

1 INTRODUCTION

1.1 Background / Motivations

A diesel engine is a power producing device that possesses many desirable characteristics when compared to other power generating systems thus resulting in its diverse application worldwide. In addition to powering buses, boats, ships, cars, trains, and many other vehicles on the ground, in the air and in the water, diesel engines are also applied in the underground mining industry for their low emissions of carbon monoxide. In the North American automotive sector diesel engines can be found in all types of vehicles including heavy duty truck applications. Two major advantages of the diesel engine are the relatively high power output and thermal efficiency which result from the high compression ratio and fuel lean operation [1]. Unfortunately the diesel operation exhibits several drawbacks which limit the usefulness and wider application of the technology.

In today's society, people have become more concerned with the environment and have taken action to protect the earth and its atmosphere. In the past decade, automotive manufacturers have been put under a great deal of pressure to reduce the harmful exhaust emission levels of their vehicles in order to meet the stringent standards set forth by the governing bodies such as the Environmental Protection Agency (EPA). The conventional high temperature diesel combustion process produces high levels of particulate matter (PM) and oxides of nitrogen (NOx) which are a main focus of this investigation. The demanding emission regulations required automakers to invest time and money into the research and development of various technologies that could effectively reduce the emissions of PM and NOx. In the case of particulate matter, several types of aftertreatment devices have already been designed, tested, and implemented in industry. Many of today's diesel engines are equipped with diesel particulate filters (DPF) to reduce PM emissions to near zero levels. The case for NOx, however, is more challenging. The most popular aftertreatment technology for NOx reduction is selective

catalytic reduction (SCR). Although this technology is efficient in reducing the total NOx, it requires a continuous supply of urea (ammonia) solution which limits its application. As the study of aftertreatment technologies progresses, it is extremely important to investigate some of the in-cylinder strategies that can be used to reduce the NOx emissions from diesel engines. The most effective in-cylinder technique in diesel engine operation is the use of exhaust gas recirculation (EGR).

The effects of EGR on the combustion process have been investigated in great detail by many researchers and studies have proven that cooled EGR is essential for reduction of diesel NOx emissions. Modern diesel EGR systems are equipped with heat exchangers, also referred to as EGR coolers, whose function is to cool down the exhaust gases before introducing them into the intake stream to achieve further reduction of NOx emissions. With the application of EGR, particulates and hydrocarbons adhere to the cooled cooler wall surfaces and the accumulation of deposits effectively deteriorates the cooling performance of the heat exchanger. EGR cooler designs are generally oversized to compensate for fouling effects and to assure that the cooler performance will be sufficient throughout its useful life. The concepts of EGR cooler fouling are extremely complex and not fully understood causing some difficulty for designers. The following section highlights the main goals of this investigation which contribute to this research area.

1.2 Research Objectives

The following items identify the aim of this study:

- To develop a common EGR cooler fouling experiment with standardized experimental procedures which can be used to evaluate and compare the performance characteristics of competitive EGR cooler designs.
- To establish the effects of EGR cooler fouling on the regulated NOx emissions of diesel engines.
- To investigate the aspects of coolant flow configuration, fin density, and particulate filtration on the EGR cooler fouling process.
- And finally, to gain insight on the critical factors contributing to EGR cooler fouling.

CHAPTER II

2 REVIEW OF LITERATURE AND THEORY

2.1 Exhaust Gas Recirculation (EGR)

The EGR concept has been used for more than a decade in small passenger vehicles as a NOx reduction mechanism. However, it was the application of EGR techniques in heavy duty diesel engines that initiated the significant technological advancements as EGR systems became highly sophisticated [2,3]. EGR technology is known to be the most effective in-cylinder NOx reduction strategy and is used in parallel with exhaust aftertreatment devices such as selective catalytic reduction to bring the tailpipe NOx emissions to acceptable levels [3]. The following sections describe the concepts of EGR and operation principles in addition to implementation methods, effects on pollutant formation, and EGR treatment techniques.

2.1.1 EGR Operation Principles

EGR involves the introduction of exhaust gas species from combustion into the intake stream of an engine for the sole purpose of reducing in-cylinder NOx formation. The recycling of exhaust gases into the engine intake has several effects on the combustion process; the single most important factor that results from the use of EGR is the reduction of the peak flame temperature [4,5]. It is best to break down the different effects of EGR and discuss each individually in order to properly understand the various contributing factors influencing peak combustion temperatures. The four effects are the *dilution effect, thermal effect, chemical effect,* and *added mass effect*.

Exhaust gases are recycled into the engine intake stream essentially 'displacing' the intake oxygen mass fraction available for combustion resulting in what is called the *dilution effect*. Diesel engines are overall lean burn systems; however, the diffusion controlled combustion tends to localize at near stoichiometric conditions [1]. Without EGR, fuel evaporates and mixes with air to form locally stoichiometric conditions around the rich region of the fuel spray. As oxygen is displaced by the induction of non-reacting

exhaust gases, the evaporated fuel must diffuse further away from the rich region of the fuel spray in order to maintain stoichiometric conditions for combustion; thus, broadening the flame region. The lack of oxygen availability significantly decreases the peak combustion temperature and the strong relationship has been established in several studies [4,7-11,14].

The *thermal effect* explains how the application of EGR increases the average specific heat capacity of the mixture in the combustion zone. Carbon dioxide (CO_2) and water vapour (H_2O) inherently have higher specific heat capacities than air. Moreover, these species are the major constituents of exhaust gases; consequently, with EGR, the average specific heat capacity of the diluted fresh charge increases [7-11]. The thermal effect is more clearly established through consideration of the change in heat absorption of the non-reacting species in the combustion chamber [11]. From Equation 2.1, the heat absorption of the non-reacting species (ΔQ_{nr}) is dependent on the change in mass of species in the cylinder (Δm_0), the average specific heat at constant pressure (C_p), and the temperature difference between combustion and EGR [3].

$$\Delta Q_{nr} = \Delta m_0 C_p (T_{combustion} - T_{EGR}) \qquad \text{Equation 2.1}$$

Where:

ΔQ_{nr}	heat absorption of the non-reacting species in the combustion chamber
Δm_0	mass of species in the combustion chamber
C_p	average specific heat at constant pressure of the non reacting species
$T_{combustion}$	in-cylinder combustion temperature
T_{EGR}	temperature of the recirculated exhaust gases

The thermal effect strictly deals with the change in the C_p value of Equation 2.1 as a result of applying EGR and it is clear that heat absorption increases with average specific heat of the non-reacting species. This implies that heat is being stolen from the combustion process, ultimately reducing peak combustion temperatures.

In a similar fashion, the *added mass effect* can be clarified by means of Equation 2.1, such that any additional mass resulting from the application of EGR is accounted for with the Δm_0 term of the expression [3,7-11]. Evidently, an increase in the mass of non-reacting species (i.e. $\Delta m_0 > 0$) yields an increase in the heat absorbed by the non-reacting species (ΔQ_{nr}) and ultimately a lower peak combustion temperature is produced.

Finally, the *chemical effect* is defined in consideration of the diluent gases which may dissociate or actively participate in the combustion process [3]. Important reactions include the dissociation of H_2O and CO_2. The dissociation of these exhaust species are endothermic reactions which implies that heat energy is required for the dissociation to take place. Thus, heat from the combustion process is used to initiate the dissociation causing a reduction in peak combustion temperatures [9].

Although it is difficult to completely isolate these effects from one another, significant research by several authors has been conducted and the consensus is that the effect of EGR dilution on peak combustion temperatures is paramount [1,7-11].

2.1.2 Effects of EGR on Combustion and Pollutants

In the preceding sections of the report it was established that NOx formation has a strong dependency on combustion flame temperature which in turn is correlated to oxygen mass fraction. Accordingly, the application of EGR results in the displacement of intake oxygen, reduction in combustion temperature and decrease of in-cylinder NOx generation. In a study performed by Wagner et al. [12], a 1.9L DI diesel engine was operated at 30% of full load and a constant speed of 1200rpm. The percentage of EGR applied was varied as the emissions of NOx, PM, and HCs were measured and the results indicated that tradeoffs exist between NOx and PM emissions in addition to NOx and HC emissions [12]. Similar conclusions were also reported in the work conducted by Ladommatos et al. [7-10], where increased EGR levels produced lower NOx emissions, but higher PM, HC, and CO emissions. These relationships were also witnessed in several other research studies [1,13-15]. The trends observed were explained by considering the dilution effect of EGR on intake oxygen. With increased levels of EGR, oxygen availability becomes limited for forming adequate air-fuel mixtures for complete

combustion; moreover, the lack of oxygen decays the soot oxidation rate [12,16]. Incomplete combustion yields higher levels of unburned hydrocarbons and slower soot oxidation leads to higher particulate matter emissions [3]. This trend is often referred to as the classical NOx/PM tradeoff.

2.1.3 EGR Implementation

Many contending systems are available for the implementation of EGR in diesel engines; the first distinction of EGR systems is between *internal* and *external* configurations.

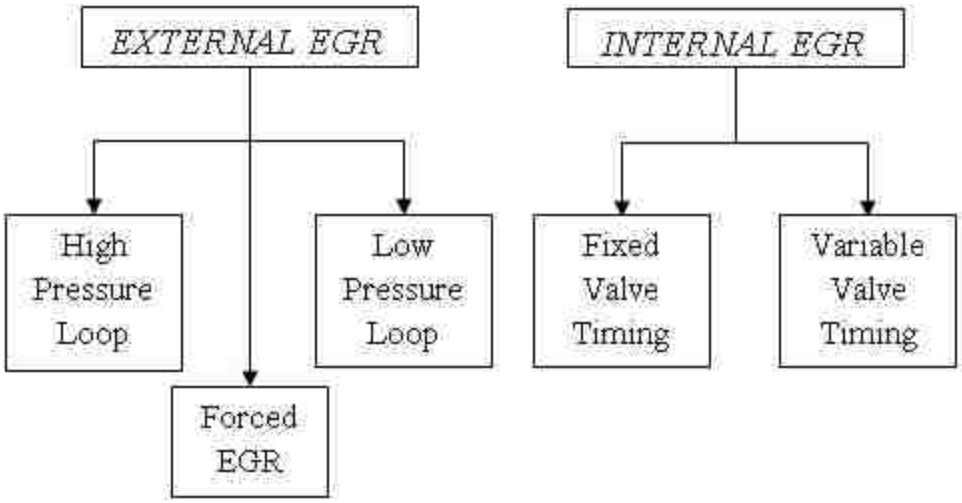

Figure 2.1: EGR configuration classifications [adapted from Tomazic et al. [14]]

Internal EGR systems involve the use of valve overlap to retain combustion products in the cylinder until the next combustion cycle takes place. *External EGR systems*, on the other hand, require the combustion products to leave the cylinder and return via the intake manifold [3,14,17]. Further classifications of these systems are illustrated in Figure 2.1 [14].

Current diesel engines (medium and heavy duty) are ordinarily equipped with turbochargers which generate exhaust gas pressures that are typically lower than intake charge pressures. The lack of pressure difference is insufficient to promote the flow of

exhaust gases into the intake stream complicating the implementation of EGR systems in turbocharged diesel engines [1,3,14,17]. External EGR is differentiated into Low Pressure Loop (LPL) and High Pressure Loop (HPL) systems [16]. Figure 2.2 is a schematic illustrating the HPL EGR system that is most popular in medium and heavy duty diesel applications. Considering constraints such as packaging, cost, durability, and reliability the HPL EGR system is deemed as the most promising configuration with highest potential for success [1,3,14].

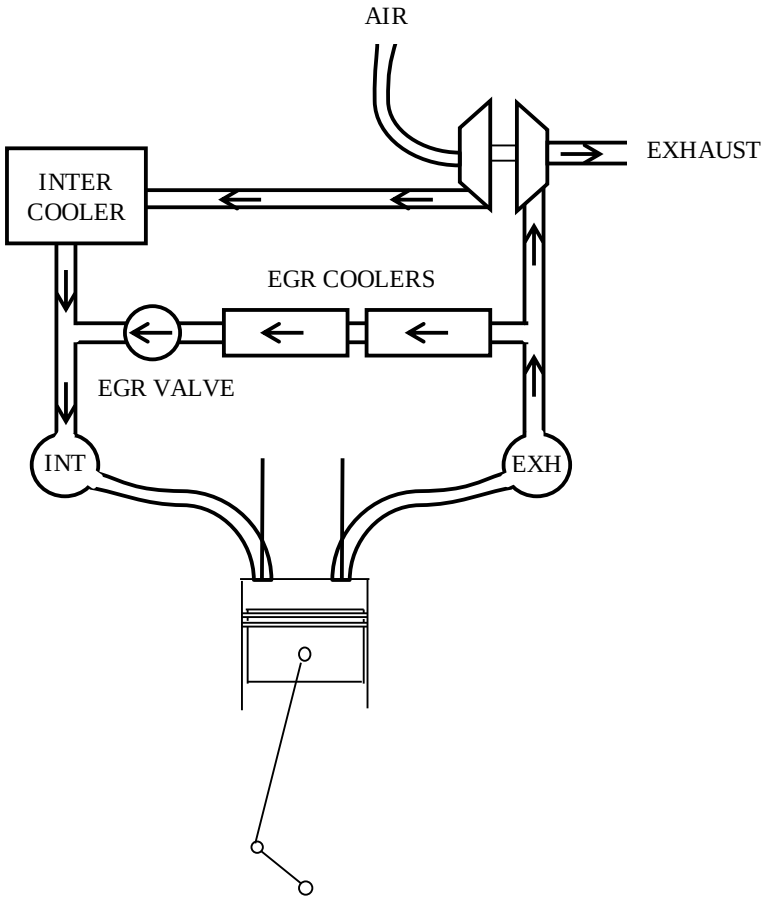

Figure 2.2: HPL EGR system configuration [adapted from Zheng et al. [1]]

The main components of an EGR system, as illustrated in Figure 2.2, are the EGR cooler and the EGR control valve. EGR coolers and their importance to engine operation are discussed in forthcoming sections. As for control valves, former systems utilized pneumatic actuators; however, hysteresis effects of such systems caused a push towards electronically actuated valves containing stepper motors which are hysteresis-free [3]. A

control signal sent from the Engine Control Module (ECM) to the EGR valve demands the opening or closing of the valve, essentially controlling the quantity of EGR flowing through the loop. Nonetheless, the quantity of EGR is also dependent on other key parameters such as [1,3,15]:

- EGR loop differential pressure,
- EGR cooling efficiency,
- in cylinder combustion efficiency,
- exhaust and intake temperatures.

2.1.4 EGR Cooling

The application of hot EGR simultaneously increases inlet charge temperature and decreases inlet charge mass of an engine. The resulting reduction of inlet charge mass and oxygen is commonly referred to as thermal throttling [11,14]. Effects of thermal throttling intensify with high levels of EGR causing a degradation of engine performance and operability. Such drawbacks can be moderated by treating the EGR stream thermally and/or chemically [1]. EGR cooling provides an increase in density, which yields an increase of intake charge [1,11]. Thus, the operational instabilities caused due to thermal throttling are effectively reduced. Other available EGR treatment methods, such as EGR oxidation and fuel reforming can be found in the literature [18,19].

In a study conducted by Tomazic et al. [14], the impacts of cooled and uncooled EGR on engine performance were highlighted. The results of the investigation showed that use of cooled EGR has a lesser negative impact on brake specific fuel consumption (bsfc) and smoke emissions [14]. Similar results were observed in studies by Ladommatos et al. [7-11]. The effects of hot and cooled EGR on NOx production were also compared in a study by Zheng et al. [1] where the application of enhanced cooled EGR was achieved, resulting in reduced exhaust NOx.

2.2 Heat Exchanger Design Fundamentals

The following sections introduce the fundamental governing equations used for heat exchanger design and analysis. General design criterion and methodologies used for

compact heat exchangers are also discussed. Moreover, specific performance characteristics used to evaluate and compare different EGR cooler designs are defined.

2.2.1 Thermal Design

Thermal design of heat exchangers, in its entirety, is governed by the following important relationships [20-22]:

- Enthalpy rate equations

$$q = q_h = q_c = \dot{m}\Delta h \qquad \text{Equation 2.2}$$

One for each of the two fluids (i.e., hot and cold) where:

q	heat transfer rate for the hot (h) and cold (c) fluids
ṁ	fluid mass flowrate
Δh	change in enthalpy

- Heat transfer rate equation

$$q = UA\Delta T_m \qquad \text{Equation 2.3}$$

Where:

U	overall heat transfer coefficient
A	heat transfer surface area
ΔT_m	log mean temperature difference

Equation 2.2 is derived from the first law of thermodynamics relating the heat transfer rate, q, to the rate of change in enthalpy, Δh, for an open non-adiabatic system with a single bulk flow stream under isobaric conditions [22]. Performing an energy balance by applying Equation 2.2 to a counter-flow EGR cooler as illustrated in Figure 2.3 yields:

$$\dot{m}_c \, \Delta h_c = \dot{m}_h \, \Delta h_h \qquad \text{Equation 2.4}$$

For single-phase fluids in a heat exchanger, the enthalpy rate of change is $\Delta h = c_p \Delta T$, where c_p is the specific heat of the fluid at constant pressure. With this, Equation 2.4 becomes:

$$\dot{m}_c \, c_{p,c} (T_{c,out} - T_{c,in}) = \dot{m}_h \, c_{p,h} (T_{h,in} - T_{h,out}) \qquad \text{Equation 2.5}$$

The effectiveness of a heat exchanger is defined as the fraction of actual heat transferred to the maximum possible heat transferrable [20-22, 23]:

$$\varepsilon = \frac{q_{actual}}{q_{\max}} \qquad \text{Equation 2.6}$$

For EGR coolers, the maximum heat transfer possible is determined as:

$$q_{\max} = \dot{m}_h \, c_{p,h} (T_{h,in} - T_{c,in}) \qquad \text{Equation 2.7}$$

Using the right hand side of Equation 2.5 as the actual heat transfer and Equation 2.7 as the maximum possible heat transfer, the heat exchanger effectiveness of Equation 2.6 simplifies to:

$$\varepsilon = \frac{(T_{h,in} - T_{h,out})}{(T_{h,in} - T_{c,in})} \qquad \text{Equation 2.8}$$

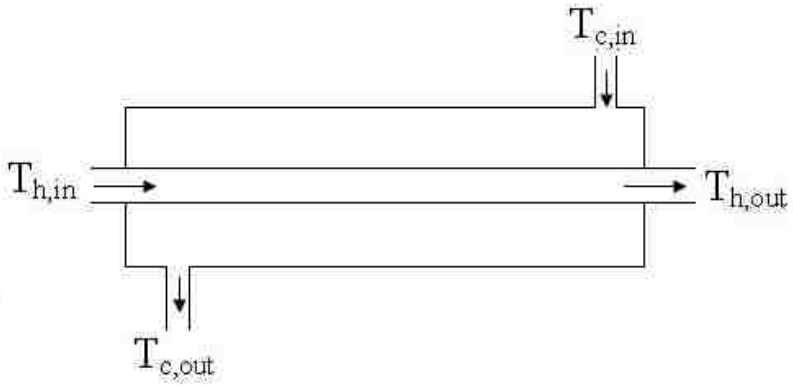

Figure 2.3: Schematic of a counter flow shell and tube heat exchanger

Equation 2.3 describes the conduction-convection heat transfer phenomenon in a two-fluid heat exchanger [22]. Where the heat transfer rate is a function of the heat transfer area, A, and mean temperature difference between the fluids, ΔT_m. The proportionality constant, U, is better known as the overall heat transfer coefficient and can be expressed as follows with reference to Figure 2.4 [20-22].

$$\frac{1}{UA} = \frac{1}{U_c A_c} = \frac{1}{U_h A_h} = \frac{1}{(\eta_0 hA)_c} + \frac{R_{f,c}}{(\eta_0 A)_c} + R_w + \frac{R_{f,h}}{(\eta_0 A)_h} + \frac{1}{(\eta_0 hA)_h} \qquad \text{Equation 2.9}$$

Where:

U_c overall heat transfer coefficient based on cold side heat transfer area (A_c)

U_h overall heat transfer coefficient based on hot side heat transfer area (A_h)

h convective heat transfer coefficient

$R_{f,c}$ fouling factor (resistance to heat transfer) on cold side surfaces

$R_{f,h}$ fouling factor (resistance to heat transfer) on hot side surfaces

R_w thermal resistance of the wall thickness

η_0 overall fin surface efficiency

η_f single fin efficiency

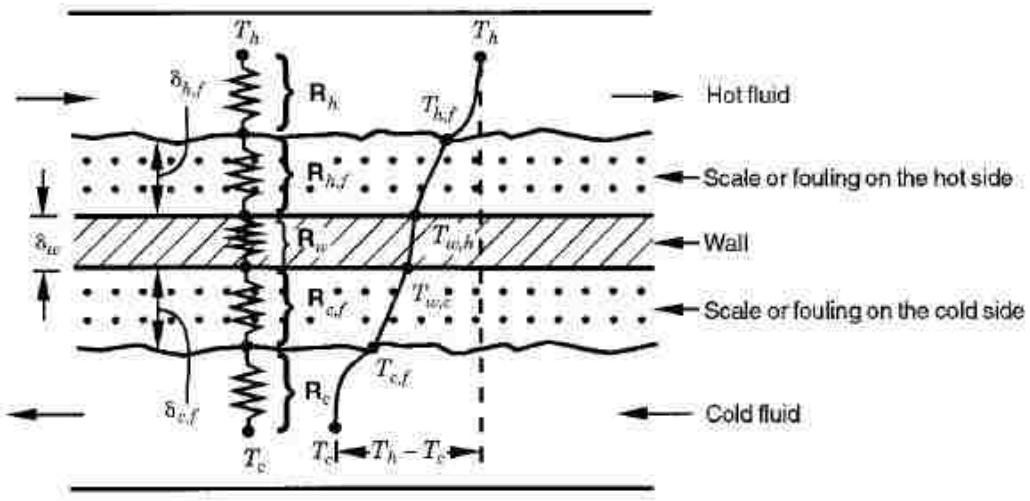

Figure 2.4: Thermal resistance schematic [22]

2.2.2 Pressure Drop Analysis

The pumping power required to pump a fluid through a heat exchanger is proportional to the fluid pressure drop [22]. From Figure 2.5, the core pressure drop can be expressed as:

$$\Delta p_{core} = f \frac{4L}{D_h} \frac{\rho V^2}{2} + G^2 \left(\frac{1}{\rho_{out}} - \frac{1}{\rho_{in}}\right) \qquad \text{Equation 2.10}$$

Where:

f friction factor

L characteristic length of the heat exchanger core

D_h hydraulic diameter of the heat exchanger inlet

G mass velocity of the stream ($G = \rho V$)

ρ density of fluid stream through the cooler core

V average velocity of fluid stream through cooler core

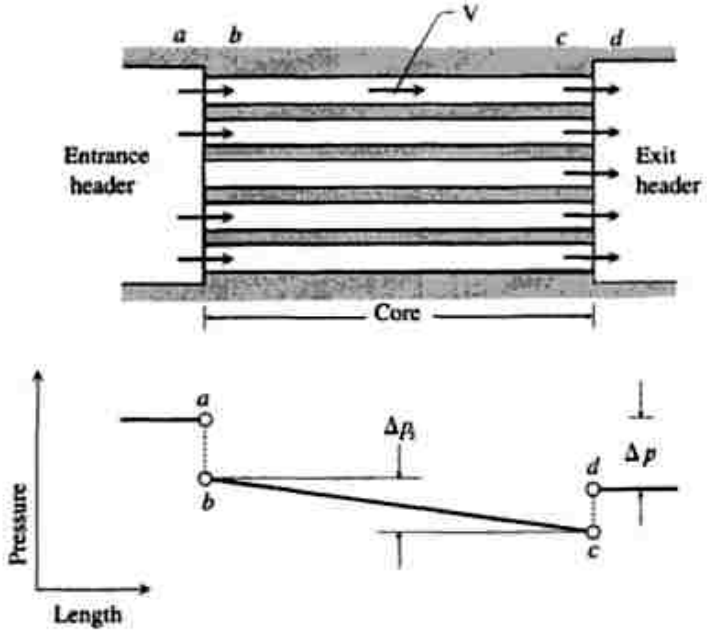

Figure 2.5: Core pressure drop of a compact heat exchanger [20]

It should be noted that the total pressure drop across a heat exchanger, Δp, consists of the core pressure drop plus the contributions made by entrance contractions, and exit enlargements. Pressure drop contributions of this kind are determined as the product of the dynamic pressure, $\frac{1}{2}\rho V^2$, and the corresponding loss coefficient, K, as found in literature [20]. For the coolers in this investigation, the contraction ratio equals the enlargement ratio and the fluid density does not vary appreciably along the short length EGR cooler passages resulting in the following simplified total pressure drop equation:

$$\Delta p = \frac{1}{2}\rho V^2 [K_c + f\frac{4L}{D_h} + K_e] \qquad \text{Equation 2.11}$$

Where, K_c and K_e are the contraction and enlargement loss coefficients respectively.

2.2.3 EGR Cooler Design and Performance

EGR coolers are multifaceted systems whose design involves not only the calculation of the heat transfer rate and pumping power needed to circulate the fluids but also the flow arrangement, the construction of the actual hardware, and the ability to disassemble the apparatus for periodic cleaning [20]. More specifically, designers are challenged with

meeting industry requirements such as compactness, low weight, and low cost while optimizing the main performance requirements listed below [22]:

- Durability – To meet customer expectations, the coolers must meet pressure and thermal cycling, vibrations, shock, operating temperatures, corrosion, fouling, etc.
- Low Pressure Drop – Minimizing pressure drops across heat exchangers results in reduced pumping power loses.

Generally, there are two measures of performance used to evaluate the functionality of a heat exchanger over its useful life [13]:

- Effectiveness, and
- Pressure drop.

In this study, competitive EGR cooler designs employed in industry will be investigated and compared based on their performance characteristics. In addition to this, effects of fouling on other measures such as recovery characteristics, EGR flow rate, and engine emissions will also be developed. The details of the cooler designs can be found in Appendix A.4.

2.3 Fouling Concepts

Concepts of EGR cooler fouling are introduced in the following sections of the report with emphasis on deposit constituents, deposit formation, removal mechanisms, and stabilization.

2.3.1 Deposit Constituents

The main constituents of deposits in diesel EGR coolers are particulate matter, hydrocarbons, and acids. The primary composition of PM in non-premixed internal combustion engines is soot [13,25,26,28]. Soot represents the elemental carbon portion of the total particulate matter and consists of small roughly spherical particles (20-30 nm), which tend to agglomerate on cooler wall surfaces. The hydrocarbon based particulates, also referred to as soluble organic compounds make up the remaining portion of total PM. According to literature, the soluble organic fraction is a measure of HC and sulfate in the exhaust stream which condenses onto the surface of the soot

particles after the gases have been mixed, diluted and cooled with air [28]. Since the temperatures of EGR gases are relatively high, the SOF of total PM is small in comparison to elemental carbonaceous soot [26,28].

Hydrocarbons will condense on the EGR cooler surface when the temperature is below the dew point for the partial pressure of the compound, and so the heavier, highly concentrated species will condense most [26,27]. This concept was illustrated in a study conducted by Hoard et al. [27] where the extractable fraction of the HC deposits was measured and the results indicated that the heavier chain hydrocarbons and aromatics constitute the majority of hydrocarbon condensate species.

Organic acids such as formic and acetic acid are present in diesel exhaust, but are not of great concern with respect to cooler fouling. More important is the condensation of sulfuric and nitric acids onto the EGR cooler walls. The dew point for nitric acid is approximately 40°C which is slightly below normal operating temperatures of diesel EGR coolers [26]. Sulfuric acid, on the other hand has a dew point of roughly 100°C which is near the EGR cooler temperature range. In a study conducted by Girard et al. [29], liquid condensate was removed from an EGR cooler system at a rate of 20-24 ml/hr with a cooler outlet temperature of 103°C. Up to 1.3% of the condensate collected was sulfuric acid.

2.3.2 Deposition Mechanisms

The main mechanisms by which deposits form are a complex combination of the following [26,27,30,31]:

- Thermophoretic Particle Deposition
- Diffusion
- Condensation
- Turbulent Impaction

Thermophoretic Particle Deposition: Soot particles that are dispersed in the gas stream are constantly subjected to various external forces such as thermophoretic forces,

gravitational settling forces, electrostatic forces, and Brownian motion forces caused by random actions of neighboring particles. Most significant are the thermophoretic forces which are caused due to the large temperature gradient within EGR coolers. Figure 2.6 (adapted from [31]) illustrates the unbalanced molecular forces on a soot particle in a gas stream with a temperature gradient, ∇T. The higher energy (i.e. higher temperature) molecules on the upper half of the soot particle will force the particle to drift away from the gas stream towards the cooler wall surface. This drift motion creates the potential for the particle to adhere to the wall surface via Van der Waals forces [26,27,31].

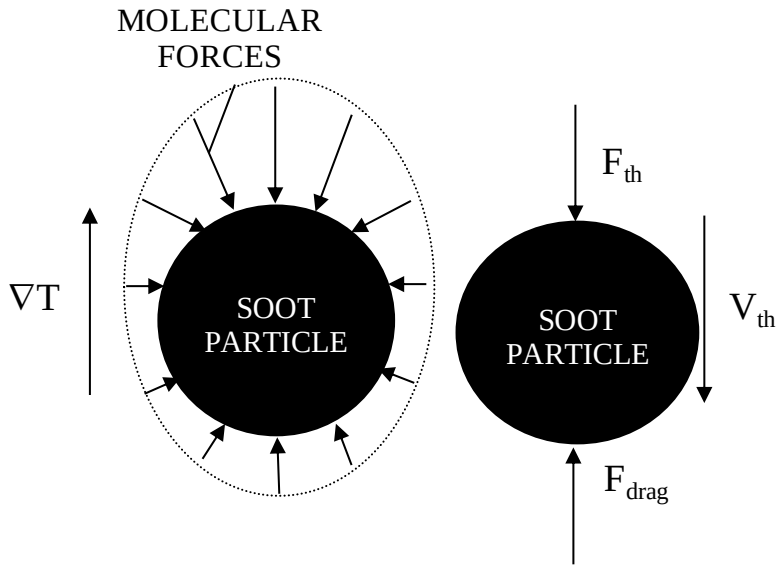

Figure 2.6: Thermophoretic force on a soot particle [adapted from Teng et al. [31]]

Diffusion and Condensation: In accordance to Graham's Law, the diffusion velocity of a molecule or particle in a gas flow is inversely proportional to the square root of molecular weight (i.e. heavier molecules/particles will diffuse slower). This implies that particulates diffuse slowly as compared to heavy hydrocarbons and hydrogen [26]. As species diffuse through the gas stream they will condense on the cooler surface if the wall temperature is below the dew point of that particular species at the local partial pressure [27]. Condensation formation creates a local concentration gradient which in turn drives the diffusion of species from high concentration areas (within the gas stream) to relatively low concentration areas (at the wall and condensate film) [26].

Turbulent Impaction: Turbulence within a gas flow causes the larger, heavier particulates to stray from the main gas stream, thus creating the potential for deposition due to turbulent impaction on the cooler wall surfaces. Since diesel particulates are small, they are less likely to randomly follow rapid turbulent changes in the gas flow direction. Essentially, turbulent impactions are less significant in EGR applications as compared to thermophoretic mechanisms [26,32].

2.3.3 Deposit Removal Mechanisms

The following summary of suggested removal mechanisms was presented by Hoard et al. [26]:

- *Blow Out*: Accumulated deposits might 'blow off' the surface at high flow conditions due to the shear force induced by the high gas flow.
- *Flaking*: Water, liquid HC, and/or acids reduce the strength of deposit adhesion causing the deposits to flake off of the surface.
- *Cracking*: Deposits may harden over time and eventually crack due to thermal or other stresses, causing portions to break away from the surface.
- *Evaporation/Oxidation*: The portion of deposits which are semi-volatile may evaporate off of the surface if the temperatures are high enough. Similarly oxidation of soot particulates may occur with sufficient temperatures. However, oxidation of soot is unlikely in EGR coolers as the required oxidation temperature is above 500°C.
- *Wash Out*: Condensation of water, HC, and/or acids may form a liquid film that would carry deposits out of the cooler.

Although the aforementioned removal mechanisms have been reported in several studies [26,27,32-34], there is a lack of experimental data that clarifies these mechanisms or conditions under which they occur.

2.3.4 Stabilization and Recovery

The results of many studies by various researchers have shown that cooler effectiveness follows an exponential characteristic involving an initial rapid decline in performance before approaching a steady state value. This trend is illustrated in Figure 2.7 taken from

a previous study conducted by the author. Two theories, found within the literature, are used to explain the stabilization behaviour [26]:

- Over time, the buildup of deposits forms an insulation layer causing an increase in the gas-side surface temperature. As the surface temperature continuously rises it eventually reaches a temperature where no new deposits form, and the performance stabilizes.
- The removal mechanisms, explained in the proceeding section, are proportional to the total deposit mass such that the rate of mass removal increases with the mass of total deposits. With time, the rate of deposit mass is equal to the rate of mass removal resulting in stabilization as shown in Figure 2.7.

Cooler recovery is defined as the sudden improvement in thermal performance (i.e. cooler effectiveness). Mulenga et al. [13] reported recovery characteristics of different EGR cooler designs implemented on a medium duty diesel engine. They noticed an increase in effectiveness when the engine load was rapidly increased after a 30 minute cold soak shut down period. The authors believe that during the cooling period, condensed exhaust forms on the cooler wall surfaces and during rapid transient heat up, the abrasive high gas speeds crack the deposits facilitating cooler recovery.

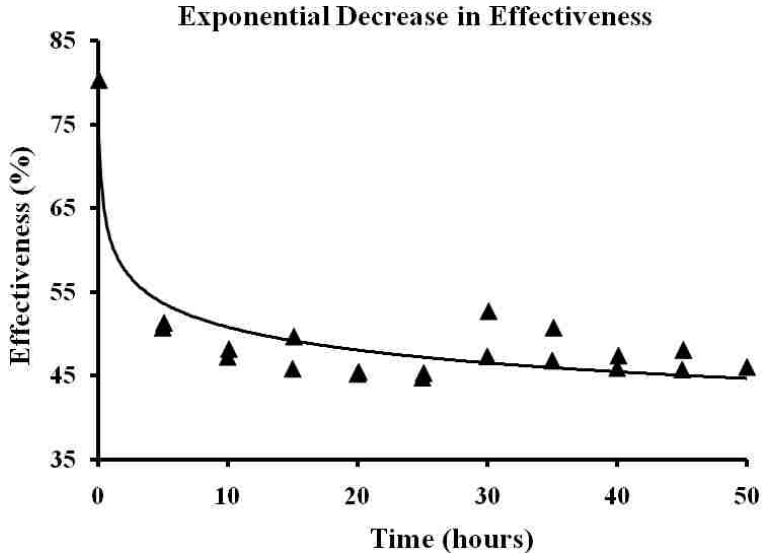

Figure 2.7: Stabilization of effectiveness

CHAPTER III

3 EXPERIMENTAL DESIGN & MEHTODOLOGY

Outlined in the following sections are concepts and methodologies used to streamline an experimental setup for testing the fouling behaviour of various EGR cooler designs in addition to examining the critical factors that contribute to the fouling process.

3.1 Determination of Test Parameters

In order to standardize a fouling test for comparing EGR cooler designs, it was necessary to establish the important test parameters that needed to be harmonized. The following wishbone diagram summarizes the major causes of EGR cooler fouling. Using Figure 3.1, an experimental setup was designed to investigate the significance of specific parameters on the fouling of EGR coolers. The main focus of this study was to compare various cooler designs on a common fouling test; thus, the different causes of fouling illustrated below needed to be consistent between experiments.

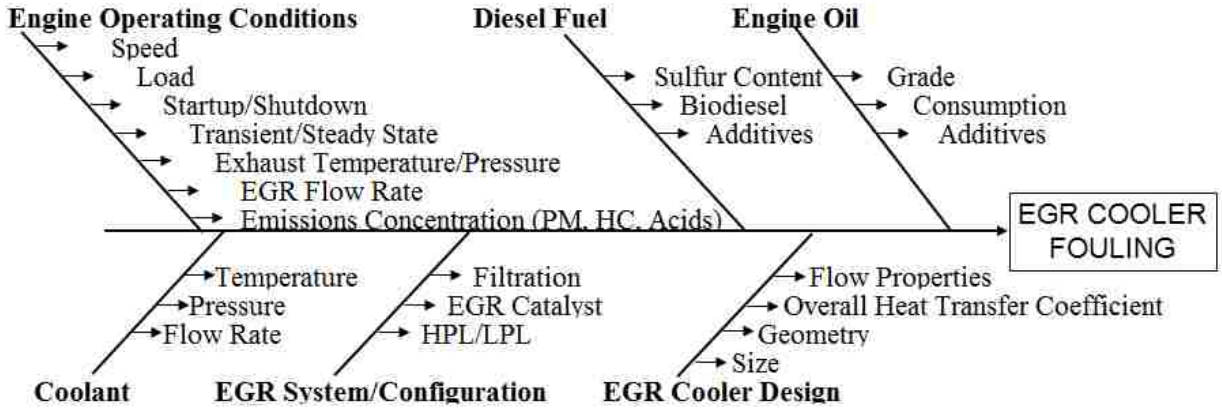

Figure 3.1: Causes of EGR cooler fouling

A summary of target values for specific experimental conditions are listed in the following table and derived from previous EGR cooler fouling experiments performed by the Ford research group at the Essex Engine Plant Powertrain Engineering Research and

Development Centre (PERDC). The methods by which these variables were controlled are discussed in the forthcoming sections.

Table 3.1: Experimental target values

					COOLANT PARAMETERS					
Speed	**BMEP**	**r_{EGR}**	**$\dot{m}_{EGR}$**	**Smoke**	**$T_{HT,IN}$**	**$T_{LT,IN}$**	**$P_{HT,IN}$**	**$P_{LT,IN}$**	**V_{HT}**	**V_{LT}**
(rpm)	(bar)	(%)	(kg/hr)	(FSN)	(°C)	(°C)	(psi)	(psi)	(L/min)	(L/min)
2280	8.2	30	200	1.5	85	35	30	20	75	35

3.2 Test Engine, Fuel, and Oil

A medium duty V8 turbocharged common rail direct injection diesel engine, with characteristics listed in Table 3.2, was instrumented and tested on an eddy current dynamometer. Commercially available ultra low sulfur diesel (ULSD) fuel was utilized with specifications found in Appendix A.1. Super-duty grade 15W-40 engine oil, meeting and/or exceeding API CJ-4, CI-4 PLUS, CG-4, CL and SL performance specifications, was employed.

Table 3.2: Engine characteristics

Test Engine	
Engine Type	Turbocharged V8 diesel, 4 cycle
Displacement	6.4 Litres
Bore & Stroke	98.2 x 105 mm
Compression Ratio	17.5:1
Application	Medium duty trucks
Combustion System	Direct injection
Injection System	Common-rail with piezo-electric injectors

DYNAMOMETER CALIBRATION – Prior to conducting any experiments, a calibration of the Dynamometer load cell was required. The calibration was conducted using a moment arm, 1 meter in length, along with several masses weighing 100 Newtons in force each.

The first sequence of the calibration involved adding weights consecutively to the moment arm and comparing the input torque values to the dynamometer load cell readings. The next sequence involved removing the weights one after the other and comparing the input torque values with the load cell readings again. The results of the calibration check as well as the dynamometer relative error are illustrated in the following figure.

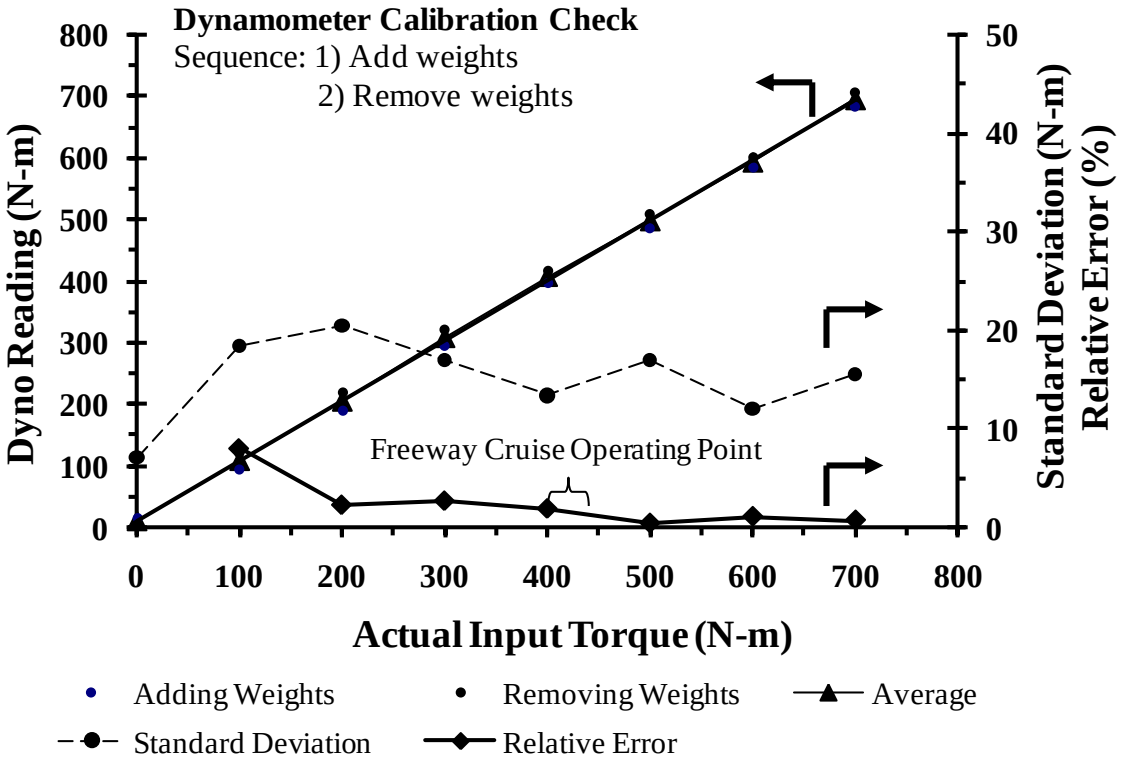

Figure 3.2: Dynamometer calibration check (relative error)

3.3 Operating Conditions

SPEED and LOAD - A steady state freeway cruise condition was employed as illustrated in Figure 3.3. This condition (referred to as B50) has been used in previous studies by the Ford group and was selected as the standard for cooler design testing based on its combination of high EGR inlet temperature and EGR mass flow [27]. The 'B' denotes the engine speed (i.e. 2280 rpm) and the '50' indicates the percentage of torque (i.e. 50% of full throttle).

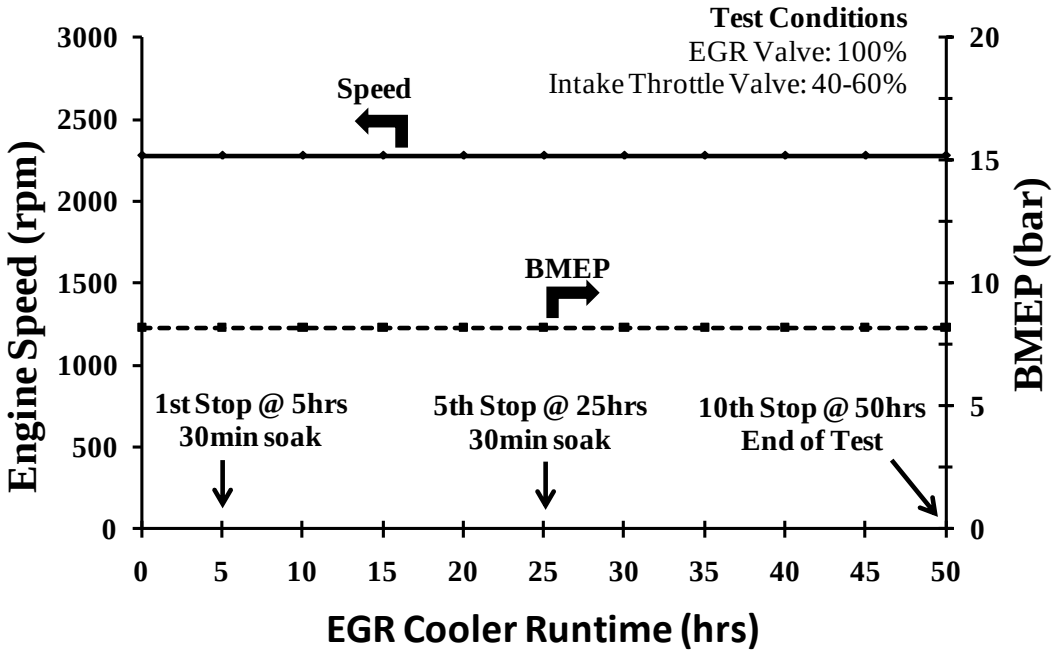

Figure 3.3: B50 freeway cruise condition

STARTUP and SHUTDOWN - After an initial engine warm up to the appropriate operating temperature (i.e. 85 – 90 °C oil temperature), the engine speed and Brake Mean Effective Pressure (BMEP) were set to 2280 RPM and 8.2 bar respectively. The engine warm up ensured a constant EGR temperature. At this point, the EGR mass flow rate and smoke levels were simultaneously matched to the target values in Table 3.1 via EGR valve opening and intake valve throttling. In order to achieve a desired flow rate 200 kg/hr, the EGR valve needed to be fully opened (i.e. 100%) and the engine intake needed to be throttled to raise the pressure differential in the EGR loop. With an increase in intake throttle position, lower air-to-fuel ratios were witnessed, resulting in higher smoke levels. Thus, control of the initial startup of the experiments was extremely important for achieving standardized conditions throughout the different tests. Once the proper EGR rate and smoke levels were obtained the engine operated under the steady state conditions for 5 hours followed by a 30 minute shut down (soak) period. After the 30 minute soak period, tests were resumed with fixed positions of EGR valve, intake throttle, and backpressure valves as established at 0 hours. This sequence was repeated until 50 hours of runtime was accumulated on the EGR coolers.

EVALUATION OF EGR – In order to utilize the reduced equation for effectiveness as defined in Equation 2.8, the mass flow of exhaust gas must be held constant. Assuming negligible piston blow-by and reasonably constant intake manifold pressures and temperatures, the EGR ratio r_{EGR}, may be approximated from the fresh charge mass air flow (MAF) sensor readings as shown in Equation 3.1, where MAF, MAF_{TOTAL}, and $\dot{m}_{EGR}$ are illustrated in Figure 3.4 [1,13,25].

$$r_{EGR} = \frac{\dot{m}_{EGR}}{MAF_{TOTAL}} = 1 - \frac{MAF}{MAF_{TOTAL}} \qquad \text{Equation 3.1}$$

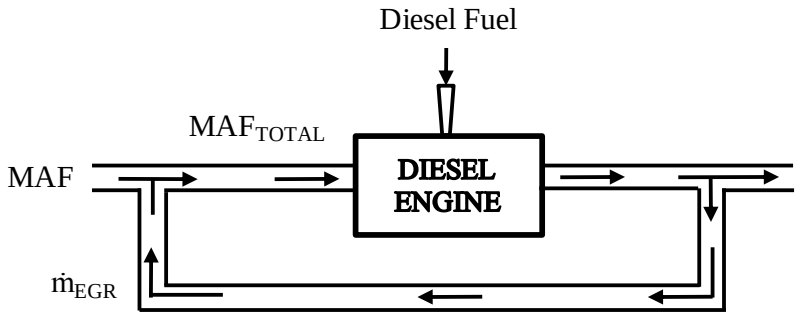

Figure 3.4: Schematic for calculating EGR ratio

The fresh intake charge contains negligible levels of CO_2 as compared to recycled combustion gases. Thus, a practical approximation of EGR ratio is established using intake and exhaust concentrations of CO_2 [1]:

$$r_{EGR} \approx \frac{[CO_2]_{\text{int}}}{[CO_2]_{exh}} \qquad \text{Equation 3.2}$$

A comparison of the MAF-based and CO_2-based EGR ratio calculations is illustrated in Figure 3.5 at steady state operation [13].

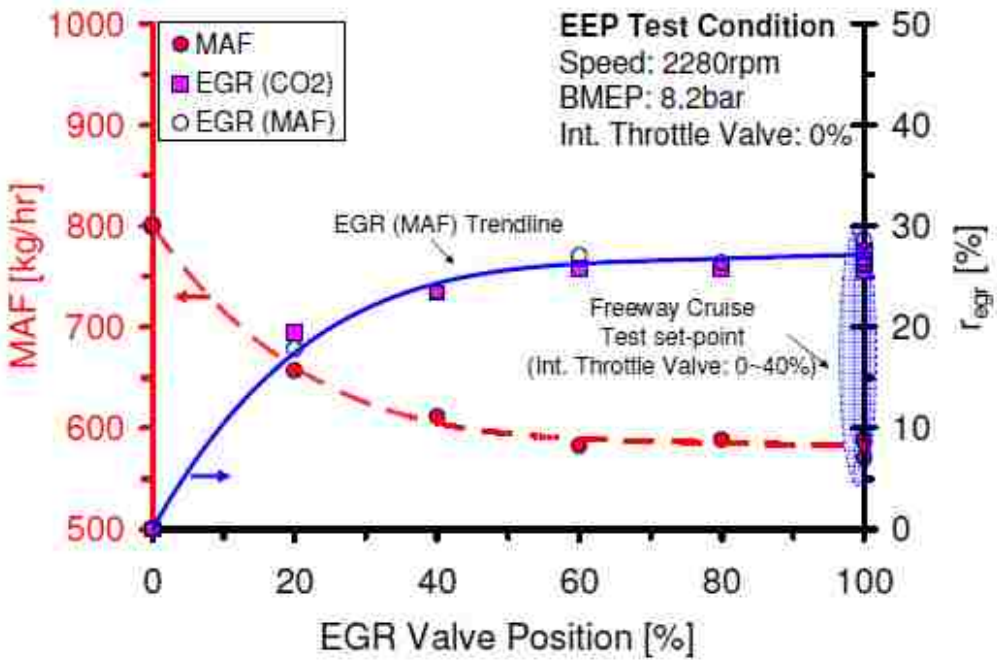

Figure 3.5: Comparing MAF- and CO_2-based EGR ratios [13]

If the EGR ratio (r_{EGR}) can be closely approximated, as in Equation 3.2, than the EGR mass flow rate ($\dot{m}_{EGR}$) can be expressed in terms of EGR ratio. The total mass air flow into the engine can be expressed as follows:

$$MAF_{TOTAL} = MAF + \dot{m}_{EGR} \qquad \text{Equation 3.3}$$

Combining equations Equation 3.1 and Equation 3.3, the EGR mass flow rate is expressed as:

$$\dot{m}_{EGR} = MAF \times \left[\frac{r_{EGR}}{1 - r_{EGR}} \right] \qquad \text{Equation 3.4}$$

EVALUATING PM – Previous works have shown, through chemical analysis (i.e. thermal gravimetric analysis), that EGR cooler deposits consist of mostly carbonaceous soot particles [26,27]. Furthermore, it is not practical to continuously measure PM for the entire test period. Instead, the use of smoke number has been recommended in literature

[2,35] as it provides a qualitative indication of the PM emissions and is more convenient to measure. Stone [35] gives the following correlation which allows one to deduce the mass of particulates from a smoke number and unburned hydrocarbon reading [33].

$$PM\ [g/m^3] = 1.024 \times Smoke[g/m^3] + 0.505 \times HC[g/m^3] \qquad \text{Equation 3.5}$$

To validate the strong correlation between soot and PM, an empirical correlation was made and presented in Figure 3.6.

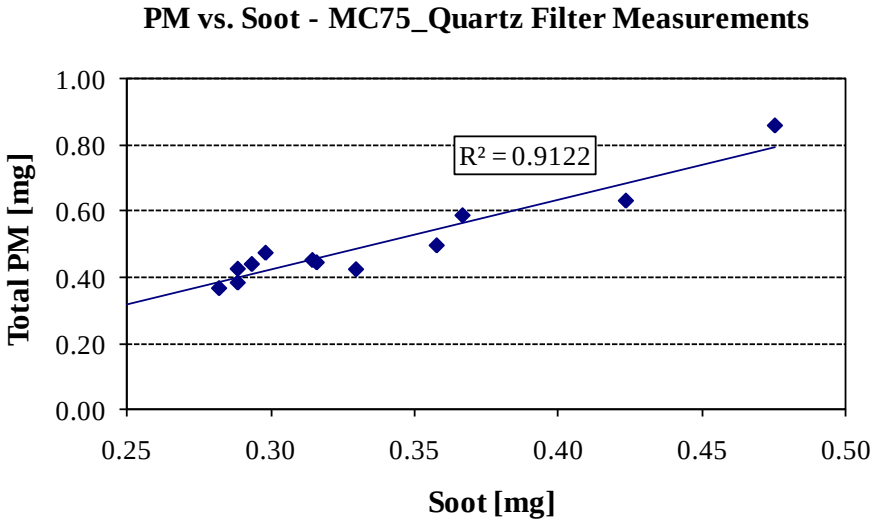

Figure 3.6: Correlation of soot and total particulate matter [33]

The mass of PM was determined using the MEXA-1370PM instrument and the quartz filter technique as described in a previous study by Chang et al. [33]. The soot values were evaluated using Equation 3.6, where the filter smoke number (FSN) was measured using a variable sampling smoke meter with details outlined in Table 3.7. Due to the high proportionality constant, soot rather than PM was monitored in the experimentation and will be used for developing trends with EGR cooler performance. The initial soot concentration target for the experiments was 1.5 FSN as summarized in Table 3.1.

$$Soot\,[mg/m^3] = \frac{1}{0.405} \times 5.32 \times FSN \times \exp(0.31 \times FSN) \qquad \text{Equation 3.6}$$

3.4 EGR System Configuration

A schematic representation of the cooler setup is given in Figure 3.7 showing the EGR flow control valve along with the high and low temperature coolant counter-flow configuration. A parrallel flow configuration was also used and easily achieved by simply reversing the flow of coolant through the high temperature (HT) and low temperature (LT) coolers such that the coolant and EGR flows were in the same direction (NOTE: the parallel flow configuration is not shown in the schematic diagram). It should also be noted that the EGR system was a high pressure loop system as the exhust gases are taken upstream of the turbocharger.

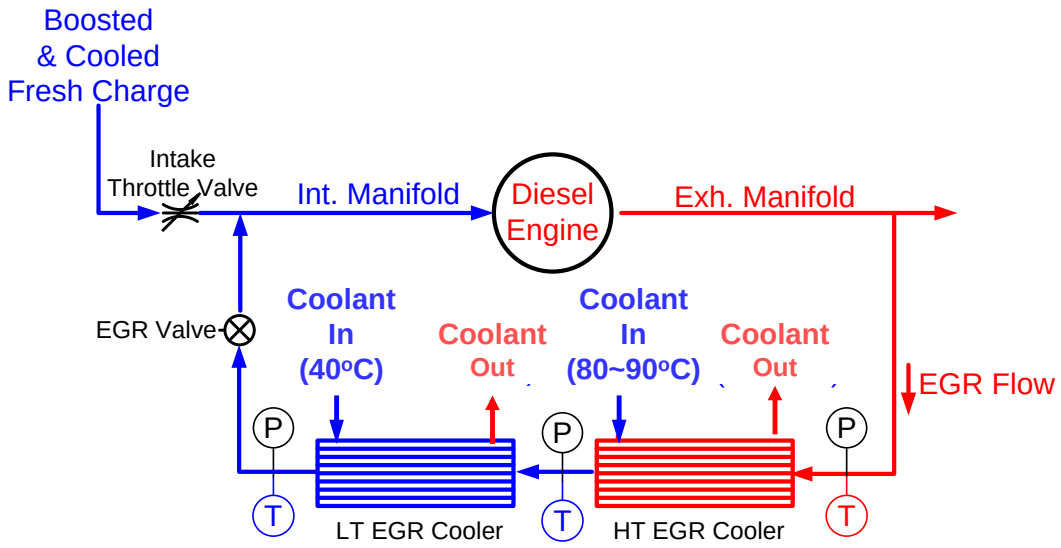

Figure 3.7: Schematic of EGR cooler setup [33]

CONTROL OF COOLANT – Important parameters to be standardized and controlled during experimentation are the coolant temperatures, pressures and flowrates.

Honeywell temperature controllers were used to regulate the inlet coolant temperatures into the HT and LT coolers (i.e. coolant temperature into each cooler was used for

feedback control). The coolant was directed through a liquid-to-liquid heat exchanger where it was cooled with cold process water. Depending on the measured feedback temperature (at the cooler inlet), a water control valve would open (if coolant temperature was too high) or close (if coolant temperature was too low), increasing or decreasing the water flowrate through the heat exchanger providing more or less cooling of the coolant.

The HT and LT coolant streams were pressurized using compressed air. Supply air pressure was regulated to 30 psi and 20 psi for the HT and LT circuits respectively and applied to the separate coolant towers. Target values of coolant temperature and pressure are listed in Table 3.1.

The coolant flowrates were measured using Bürkert inline paddle wheel design fluid flow meters with characteristics listed in Table 3.3 (data provided by Bürkert). Mechanical flow restrictors were implemented in the coolant circuit to control the flow of coolant through the EGR cooler.

Table 3.3: Characteristics of Bürkert fluid flow meter

General Data	
Pipe diameter	DN06 up to DN65
Measurement range	0.5 up to 200 l/min
Flow velocity	0.3 up to 10 m/s
Accuracy	±0.5% of F.S + 2.5% of Reading
Linearity	±0.5% of F.S.* (at 10 m/s)
Repeatability	±0.4% of Reading*

3.5 EGR Cooler Design Details

Table 3.4 summarizes specific characteristics of the different EGR cooler designs under investigation. Designs A, B, C, and D were considered as competitive designs based on their compactness and cost. More detailed information about the individual coolers is available in Appendix A.4.

Table 3.4: EGR cooler design documentation

Cooler	Classification	Characteristics	FPI	Number of Exhaust Gas Passages
A	Shell and Tube	Centred gas side diffusers at inlet and exit	N/A	36
B	Plate Fin (Wavy)	Angled gas diffuser at outlet and curved runner inlet	9	9
C	Plate Fin (Staggered/Offset)	Centred straight gas-side diffusers at cooler inlet and exit	11	7
D	Plate Fin (Wavy)	Centred gas diffusers at cooler inlet and exit	9	7
F, G, H	Plate Fin (Wavy)	F – 270 mm in length G – 285 mm in length H – 315 mm in length	7	6
J, K, L	Plate Fin (Wavy)	Centred gas diffuser at HT inlet with U shaped housing for HT and LT	J – 9 K – 11 L – 14	7

3.6 Diesel Particulate Filtration

To examine the effects of particulate filtration on EGR cooler performance, diesel particulate filters (DPFs) of different filtration efficiencies were employed. The wall-flow DPFs implemented for this study had an extremely low space velocity in comparison to the original engine manufacturer (OEM) diesel oxidation catalyst (DOC) normally used on the 6.4L diesel engine. The size difference between the OEM DOC and the DPF used in this study can be seen in Figure 3.8. The low space velocity reduces the pressure drop of the flow through the DPF so that the performance of the EGR coolers can be compared with minimum DPF pressure drop influence.

Figure 3.8: Comparison of diesel particulate filter to original diesel oxidation catalyst [33]

3.7 Temperature and Pressure Measurements

The temperature measurements were acquired at various locations in the experimental setup using Omega K-type thermocouples with specifications shown in Table 3.5. The locations of some important thermocouples are shown in Figure 3.7. Although the K-type thermocouples have a slow response time relative to other temperature measurement devices such as Thermistor Elements and Resistance Temperature Detectors (RTDs), the steady state operating condition of the experiments justifies their application.

Table 3.5: Characteristics of Omega K-type thermocouples

General Data	
Temperature Range (°C)	-200 to 1250
Standard Error	Greater of 2.2°C or 0.75%
Probe Diameter	1/16”

The pressure readings were also measured at the same locations as temperature. Ametek SPT Series pressure transducers were selected for the experiments and the specifications are listed below [36]. The excitation voltage input to the pressure transducer was supplied by the data acquisition module (ETAS ES611 Module). The ETAS module is

capable of supplying the required power to the transducer while acquiring the analog output signal.

Table 3.6: Characteristics of Ametek SPT Series pressure transducer

General Data	
Model	SPT0050X140
Range	0-50 psig (0-345 kPa)
Voltage Output	1 to 6 VDC
Input Excitation	8 to 15 VDC
Accuracy	±0.25% F.S.O
Response	< 20 ms
Connection Type	1/8" Male NPT Connection

3.8 Emissions Analyzers

The concentrations of regulated exhaust gas species were measured using emissions analyzers as outlined in Table 3.7.

Table 3.7: Exhaust gas analyzer descriptions

Measuring Principle	Species	Measured Unit	Manufacturer & Model No.
Non-Dispersive Infra-Red (NDIR) Analyzer	CO	ppm	Horiba MEXA-9100EGR AIA-120
	CO_2	%	Horiba MEXA-9100EGR AIA-110
Chemiluminescent Analyzer	NO	ppm	Horiba MEXA-9100EGR CLA-150
	NO_2	ppm	
Heated Flame Ionization Detector (H-FID)	THC	ppm C1	CAI Model 600-HFID Digital Horiba MEXA-9100EGR FMA-120
Variable sampling smoke meter	Smoke (Dry Soot)	FSN (mg/m^3)	AVL Model 415S G002
PM measurement	Soot, SOF, Sulfate	mg	Pallflex Membrane Quartz Filter with Horiba MEXA-1370PM Analyzer

3.9 Data Acquisition

The output information from the various measurement devices was collected and organized using ETAS modules along with INCA's graphical user interface which provides the functionality for data acquisition and evaluation. The flow of information is schematically shown in Figure 3.9.

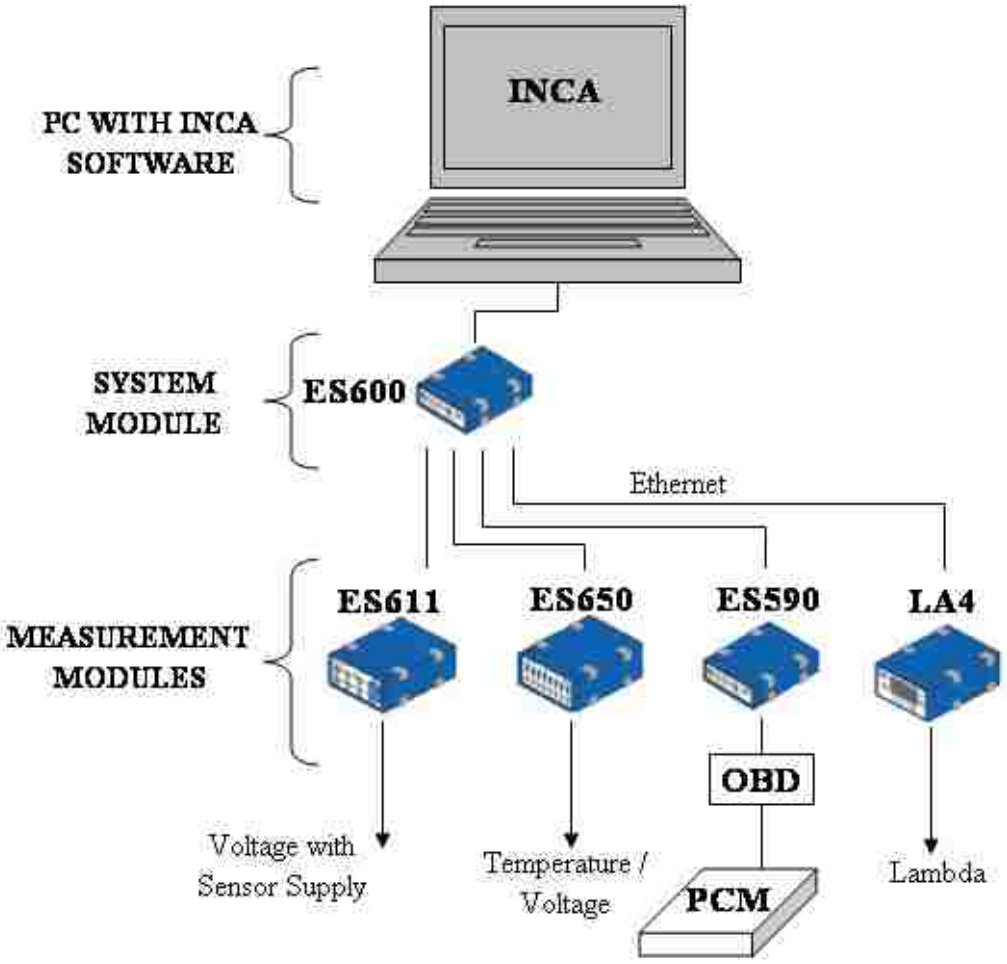

Figure 3.9: Schematic diagram of data acquisition system

A summary of technical specifications for the different modules is found in Appendix A.3. ES650 A/D Thermo Modules were used to collect temperature measurements as well as analog signals from emissions analyzers and flow meters. ES611 A/D Modules were utilized for pressure measurements due to their capability in supplying the pressure

sensor with the necessary input excitation voltage. An LA4 Lambda Meter was implemented in conjunction with a Robert Bosch LSU Broadband Lambda sensor (LSU) for precise measurement of exhaust oxygen content. Finally, the ES590 ETK, CAN Module made it possible to communicate and transfer data between the Powertrain Control Module (PCM) and the calibration software (INCA) on the host PC. This data transfer was accomplished through the On-Board Diagnostic (OBD) port of the engine harness. Each module was powered by the ES600 Network Module which connects the measurement modules to a host PC, enabling the data exchange through a common Ethernet cable. The host PC uses INCA software to organize and acquire the desired information.

CHAPTER IV

4 A DEFINITION OF METRICS

In this chapter, the measures used to evaluate and compare EGR cooler fouling performance are established. In addition to this, some quantitative metrics are defined based on previous EGR development tests performed at Ford Motor Company.

4.1 Effectiveness ε and Fouling Factor R_f

The measure of heat exchanger effectiveness has been defined previously in Chapter 2 and will be used to compare cooler performance. EGR cooler effectiveness (ε) was evaluated using the measured gas inlet temperatures ($T_{gas\ in}$), outlet temperatures ($T_{gas\ out}$), and coolant temperatures ($T_{coolant}$) as in Equation 4.1. It should be noted that the inlet coolant temperature was used for the value of $T_{coolant}$.

$$\varepsilon = \frac{T_{gasin} - T_{gasout}}{T_{gasin} - T_{coolant}} \qquad \text{Equation 4.1}$$

The absolute degradation in effectiveness ($\Delta\varepsilon_{abs}$) will also be evaluated for the design comparison and is defined as in Equation 4.2.

$$\Delta\varepsilon_{abs} = \frac{\varepsilon_{initial} - \varepsilon_{steadystate}}{\varepsilon_{initial}} \qquad \text{Equation 4.2}$$

Since effectiveness is dependent on heat transfer surface area, it is desirable to introduce the concepts of the fouling factor (R_f). The fouling factor represents the thermal resistance of the deposit layer and can be used to compare the EGR cooler performance independent of the heat transfer surface area. The equations used to compute the fouling factor are outlined in Shah and Sekulic [22] and summarized in this section.

$$R_f = \frac{1}{U_f} - \frac{1}{U_c} \qquad \text{Equation 4.3}$$

Where U_f, and U_c are the overall heat transfer coefficients of the fouled and clean cooler respectively. These quantities are determined by rearranging Equation 2.3.

$$U = \frac{q_c}{A \times \Delta T_m} \qquad \text{Equation 4.4}$$

The heat transfer rate to the coolant stream (q_c) was determined using Equation 2.5 where the mass flow rate of coolant was calculated using the product of measured volume flowrate and density. The fluid properties of the coolant can be found in Appendix B.1. The log mean temperature difference, ΔT_m, was determined for the parallel flow (PF) and counter flow (CF) configurations.

$$\Delta T_{m,PF} = LMTD_{PF} = \left(\frac{T_{h,in} - T_{h,out} + T_{c,out} - T_{c,in}}{\ln\left(\frac{T_{h,in} - T_{c,in}}{T_{h,out} - T_{c,out}} \right)} \right) \qquad \text{Equation 4.5}$$

$$\Delta T_{m,CF} = LMTD_{CF} = \left(\frac{T_{h,in} - T_{h,out} + T_{c,in} - T_{c,out}}{\ln\left(\frac{T_{h,in} - T_{c,out}}{T_{h,out} - T_{c,in}} \right)} \right) \qquad \text{Equation 4.6}$$

Inlet and outlet temperature measurements of the exhaust and coolant streams provide enough information to compute the LMTD. Given the heat transfer surface area of the respective coolers, the overall heat transfer coefficient can be determined for the clean case (i.e. @ 0 hour condition) and the fouled case (i.e. @ any time t).

Results of previous studies by the Ford group provide a maximum allowable target of 30% absolute degradation in effectiveness and maximum outlet temperature of 125 °C. These targets will be used to evaluate the performance of the competitive cooler designs.

4.2 Pressure Drop Δp and Friction Factor f

The increase of pressure drop through the cooler core section will be used to evaluate the fouling behaviour of the competitive designs tested. However, similar to the effectiveness measure, the cooler pressure drop metric does not normalize for different cross sectional areas. Consequently, a non dimensional presentation of the pressure drop data was considered. The most common representation of pressure drop data exists in the form of the Fanning friction factor defined as [22]:

$$f = \frac{1}{2}\frac{\Delta p}{\rho V^2}\frac{D_h}{L} \qquad \text{Equation 4.7}$$

It should be noted that the pressure drop (Δp) was measured across the core of the heat exchangers such that the friction factor of Equation 4.7 represents the core blockage of flow. The geometrical hydraulic diameter (D_h) and characteristic length (L) of the individual coolers were given and the mean velocity of the gas stream (V_{EGR}) was evaluated using EGR mass flow rate and density (ρ_{EGR}). The properties used for the diesel exhaust stream are presented in Appendix B.1.

The previous works established a target maximum pressure drop of 15 kPa which will be considered.

4.3 EGR Flow Rate $\dot{m}_{EGR}$

The ability of a cooler design to maintain EGR flow rate over time is crucial for consistent NOx reduction. For this reason, the EGR flow rate will be used to compare the various designs for flow capabilities. The EGR mass flow rate calculations have been discussed previously in Chapter 3.

CHAPTER V

5 DISCUSSION OF RESULTS

An analysis of the empirical investigations has been conducted and the results are discussed in the following sections of the document.

5.1 Basic Descriptive Statistics - Repeatability and Uncertainty

Several fouling tests were repeated so that a statistical analysis of repeatability could be conducted. The tests outlined in the following table were used to quantify the variations between experiments. Due to dynamometer cell availability and cost restraints, a total of two repeat tests were conducted for cooler designs A, B, and C.

Table 5.1: Test conditions for repeatability study

Cooler Design	Operating Condition	r_{EGR} (%)	Number of Replicates
A	B50	30	2
B	B50	30	2
C	B50	25	2

The important experimental parameters controlled for standardization of the test methods were compared for repeatability and summarized as in Table 5.2. The statistical summary was based on data from the 6 tests mentioned in Table 5.1 with the exception of EGR flow rate and smoke parameters due to the different nominal EGR ratios. Repeatability of EGR flow rate and smoke was based on the 4 tests with the same nominal EGR percentage (i.e. r_{EGR} = 30%). Each test included 600 data point recordings acquired over time.

The right-most column of Table 5.2 displays the uncertainty of the measurements for the repeated experiments. The results indicate that there were significant variations in EGR flow rate and smoke levels between tests and that there is a need for improvement in controlling these variables.

Table 5.2: Repeatability of experimental parameters

Parameter	Units	Min	Max	Mean	Standard Deviation	Uncertainty (%)
Speed	rpm	2280.883	2280.997	2280.933	0.039	0.002
Torque	N-m	419.685	422.831	421.041	1.909	0.454
EGR Flow Rate	kg/hr	146.059	183.966	158.731	12.952	8.172
Smoke	FSN	0.785	1.708	1.099	0.272	**24.970**
$T_{HT\ Gas\ In}$	°C	403.007	423.928	415.554	14.406	3.476
$T_{HT\ Coolant\ In}$	°C	85.547	87.063	85.999	0.660	0.767
HT Coolant Flow	L/min	76.225	77.745	77.291	2.957	3.825
$T_{LT\ Coolant\ In}$	°C	32.512	34.618	33.737	2.114	6.269
LT Coolant Flow	L/min	35.115	36.072	35.961	1.551	4.314

Additionally, it is of interest to compare the results of cooler performance from the repeated experiments to further qualify the repeatability of the experimental setup. The following basic statistics were computed using Minitab statistical software.

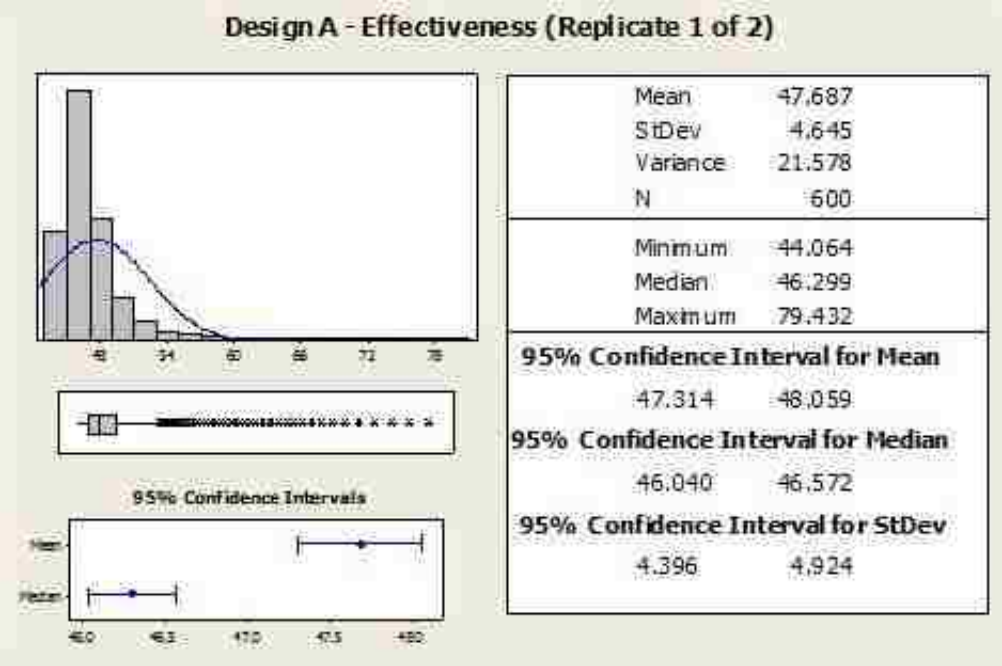

Figure 5.1: Statistical summary for design A effectiveness results of test 1 of 2

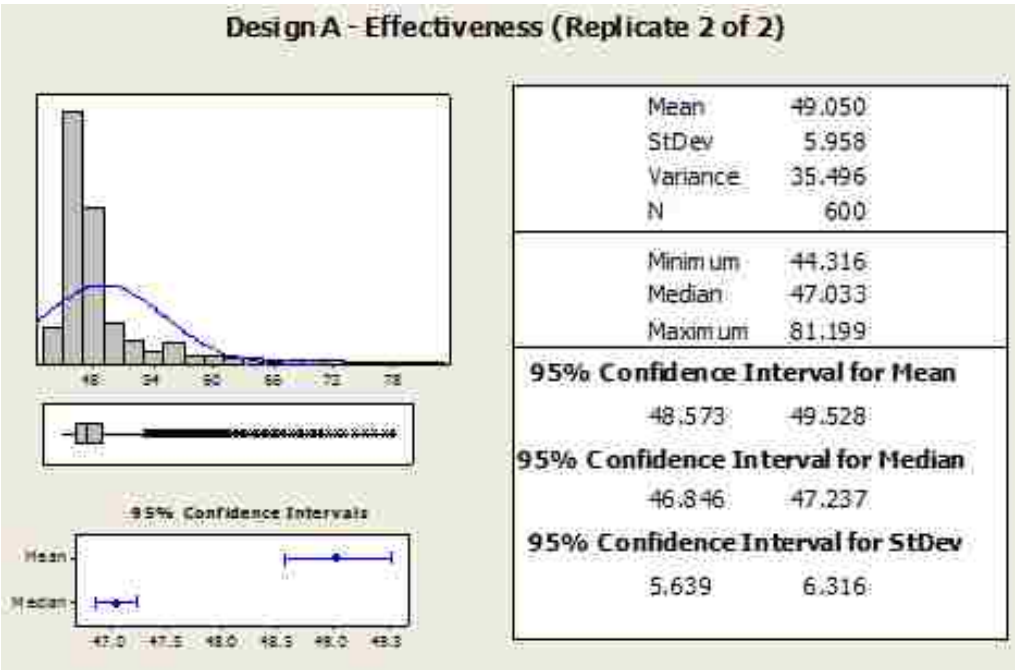

Figure 5.2: Statistical summary for design A effectiveness results of test 2 of 2

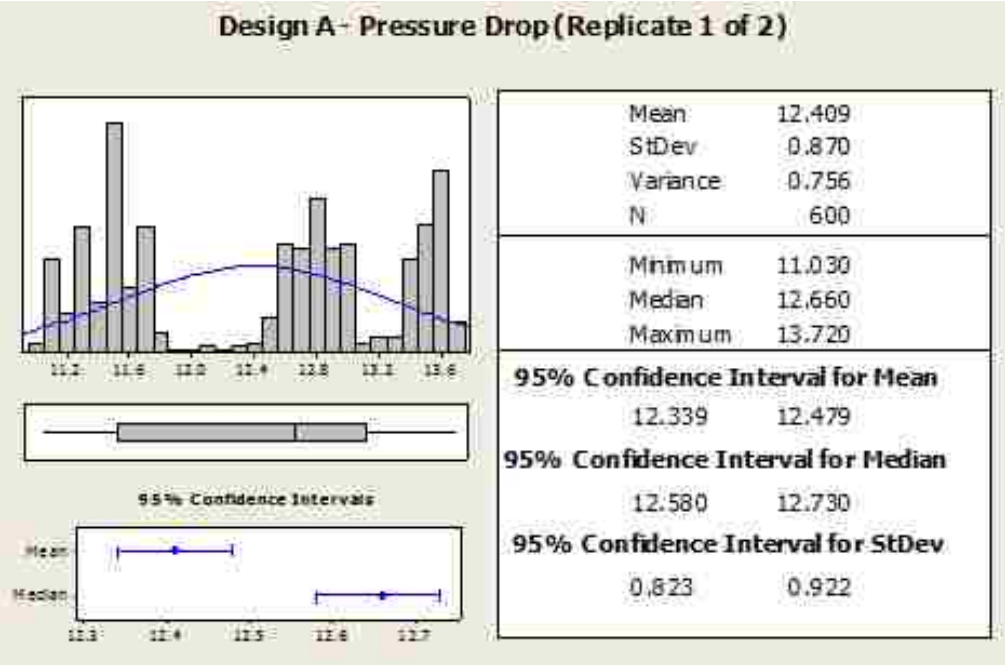

Figure 5.3: Statistical summary for design A pressure drop results of test 1 of 2

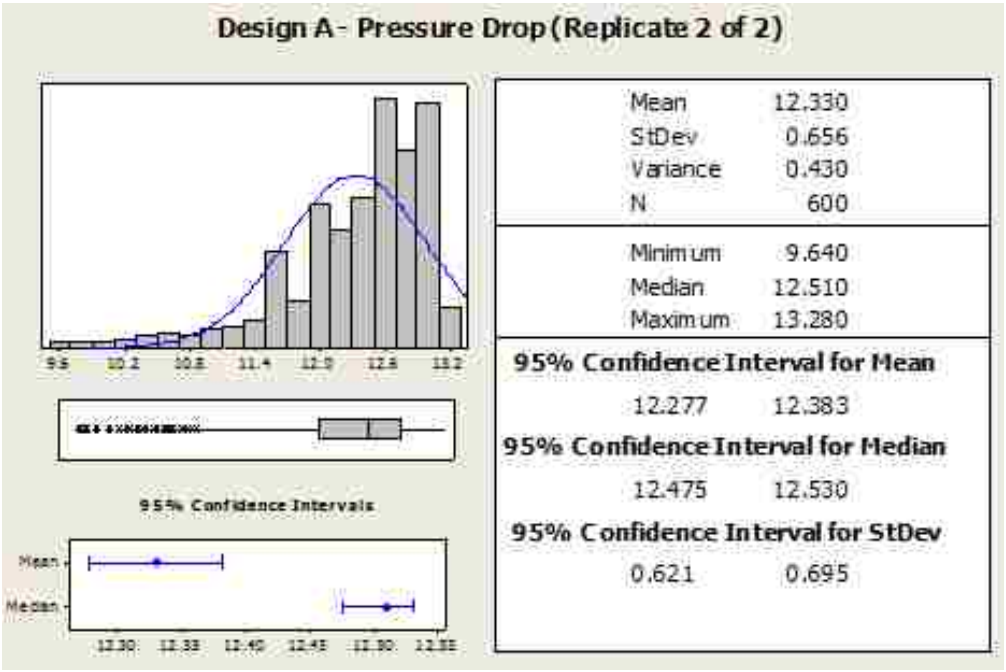

Figure 5.4: Statistical summary for design A pressure drop results of test 2 of 2

From Figure 5.1, the mean effectiveness of design A was determined to be 47.687 ± 4.645 %. Likewise, from Figure 5.2, the mean effectiveness for the replicated test was found to be 49.050 ± 5.958 %. A comparison of these results indicates that there is an agreement with the repeated experiments since the intervals of uncertainty of the means overlap. Similar results were found with pressure drop data as shown in Figure 5.3 and Figure 5.4. Design A pressure drop results of repeat tests 1 and 2 were 12.409 ± 0.870 kPa and 12.330 ± 0.656 kPa respectively. Once again the intervals of uncertainty in the means overlap indicating a good agreement in experimental repeatability.

The same analysis was conducted for designs B and C and the results are summarized in Table 5.3. It can be concluded that there was good agreement between the results of the repeated experiments.

Table 5.3: Summary of effectiveness and pressure drop repeatability results

	Replicate 1	Replicate 2	Replicate 1	Replicate 2
Cooler Design	Mean $\varepsilon \pm \sigma_\varepsilon$ (%)	Mean $\varepsilon \pm \sigma_\varepsilon$ (%)	Mean $\Delta p \pm \sigma_{\Delta p}$ (kPa)	Mean $\Delta p \pm \sigma_{\Delta p}$ (kPa)
A	47.687 ± 4.645	49.050 ± 5.958	12.409 ± 0.870	12.330 ± 0.656
B	75.343 ± 4.727	74.739 ± 3.492	10.726 ± 1.383	12.968 ± 1.634
C	65.165 ± 5.372	62.886 ± 2.951	11.515 ± 1.588	14.326 ± 1.279

5.2 Comparison of Competitive EGR Cooler Designs

5.2.1 Methodology

Competitive EGR cooler designs A, B, C, and D, as described in section 3.5, were tested using the standardized experimental setup detailed in Chapter 3. Table 5.4 is a test matrix that summarizes the initial conditions for each experiment. Each cooler design was tested twice under the B50 engine operating condition with EGR ratios of 25 and 30 %. A simple naming convention is employed to assign a test name for each experiment for future reference. The first letter in the test name represents the cooler design (i.e. A-

D) and the two-digit number following the hyphen represents the nominal EGR ratio used (i.e. 25 or 30 %).

Table 5.4: Test matrix of experiments conducted for design comparison

				Initial (0hr) Conditions					
Design	**Case**	**Test Name**	**r_{EGR} (%)**	**$\dot{m}_{EGR}$ (kg/hr)**	**Smoke (FSN)**	**T_{HT} Coolant In (°C)**	**T_{LT} Coolant In (°C)**	**V_{HT} (L/min)**	**V_{LT} (L/min)**
A	**(a)**	***A-25***	25	166	1.36	86	35	75	36
	(b)	***A-30***	30	210	2.44	85	32	75	39
B	**(a)**	***B-25***	25	176	1.77	86	35	69	37
	(b)	***B-30***	30	203	1.86	86	32	71	32
C	**(a)**	***C-25***	25	165	1.42	86	30	59	33
	(b)	***C-30***	30	215	2.23	86	34	70	36
D	**(a)**	***D-25***	25	160	2.28	87	35	76	34
	(b)	***D-30***	30	207	2.71	85	31	77	41

5.2.2 Detailed Operating Conditions

In order to thoroughly understand and interpret the results of the experiments, various operating conditions must be considered. With the aid of Figure 5.5, the measured fluid temperatures, pressures and flowrates at numerous locations of the experimental setup may be presented clearly. The following sets of figures illustrate the significant operating parameters that may have an effect on the EGR cooler performance measures.

Engine speed and load were maintained extremely well between experiments as indicated by the low measurement uncertainty (<1%). Some slight discrepancies were evident in the air to fuel ratios that were observed for case (a) as shown in Figure 5.6. Test ***C-25*** exhibited a leaner engine operating condition with an average air to fuel ratio of 26 to 1 as compared to 23 to 1 for the other tests ***A-25***, ***B-25***, and ***D-25***.

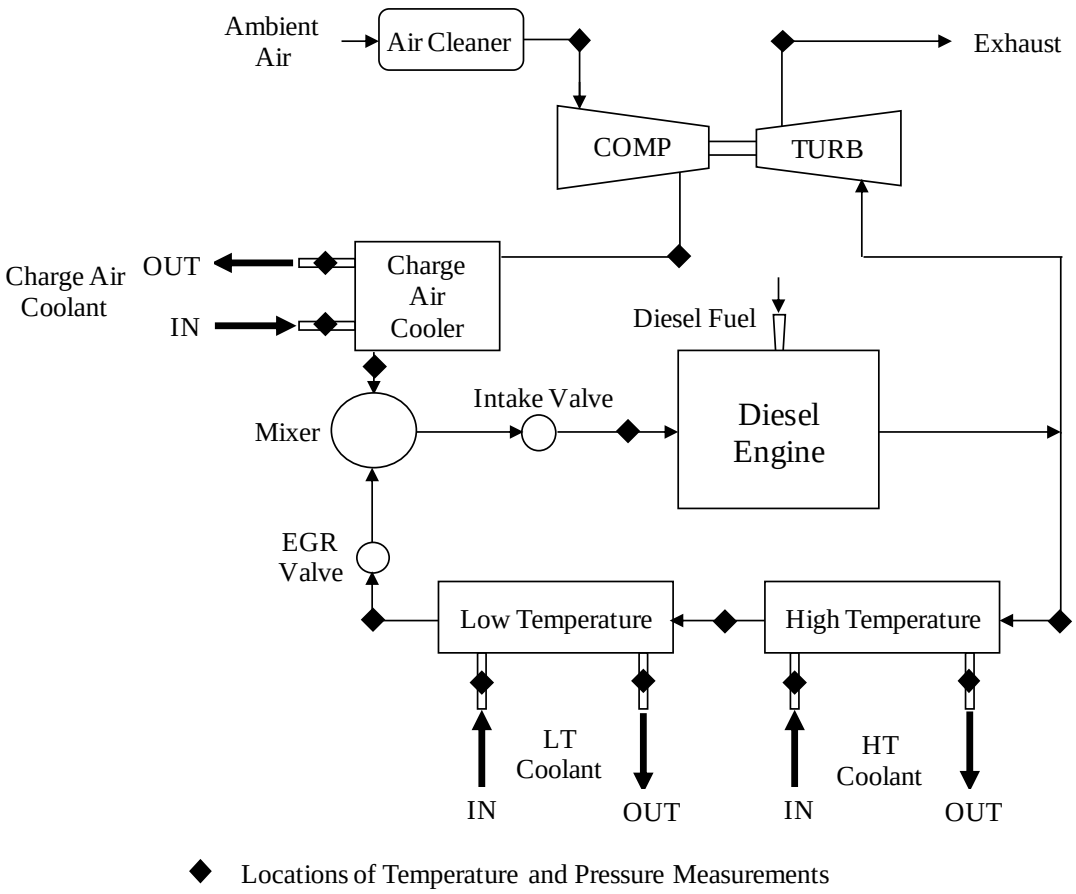

Figure 5.5: Schematic of fluid temperature, pressure and flow measurements

The measured temperatures of the charge air at the pre and post charge air cooler (CAC) locations are presented in Figure 5.7. The data suggests that the air temperature at the outlet of the charge air cooler was relatively consistent among the various experiments ranging between 42°C and 52°C. After leaving the charge air cooler, the fresh charge mixes with the recirculated exhaust gases coming from the low temperature EGR cooler before entering the intake manifold. Gas temperatures at the LT EGR cooler exit and intake manifold are presented in Figure 5.8 and Figure 5.9 respectively.

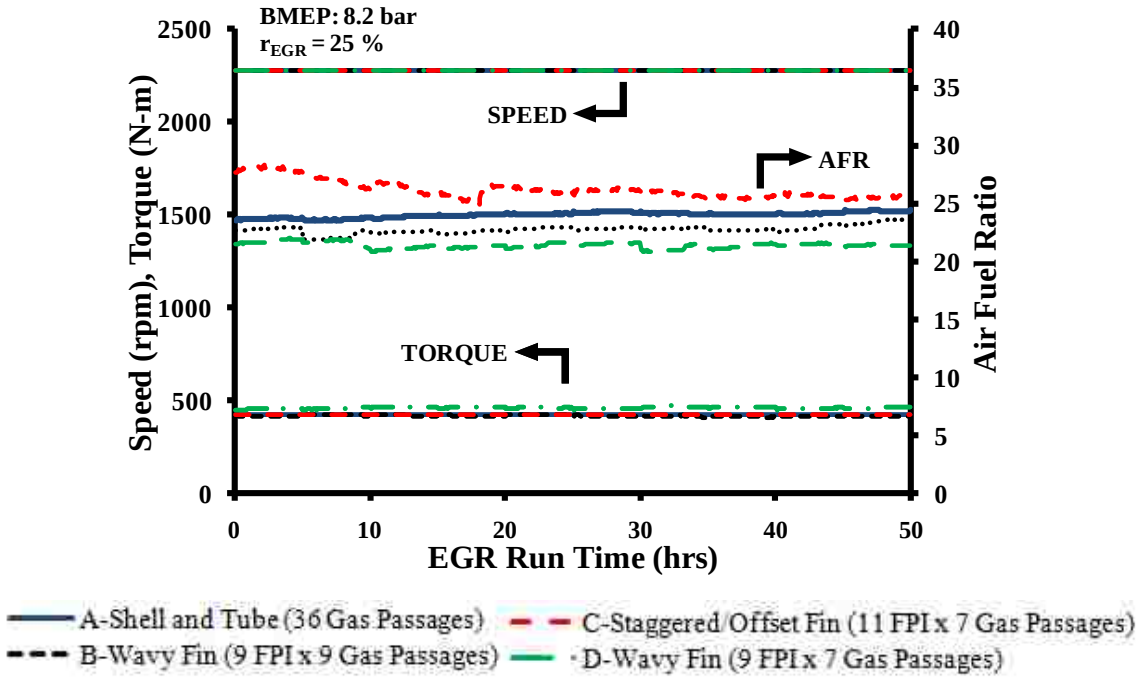

(a) r_{EGR} = 25%

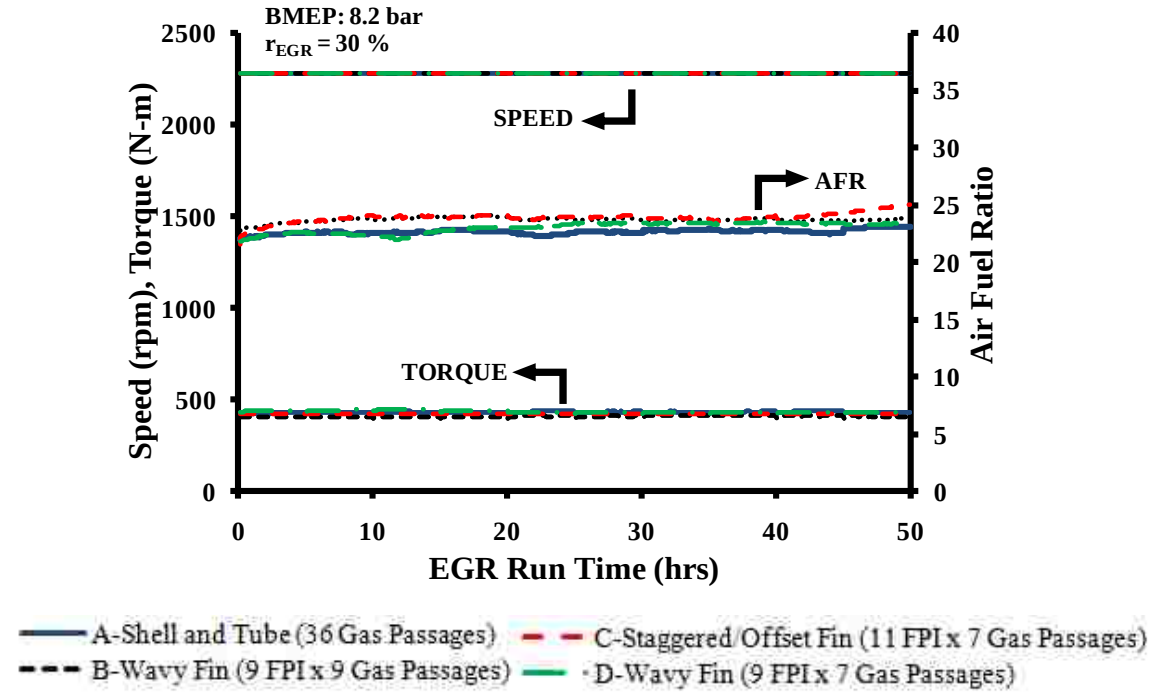

(b) r_{EGR} = 30%

Figure 5.6: Engine speed, torque and air fuel ratio

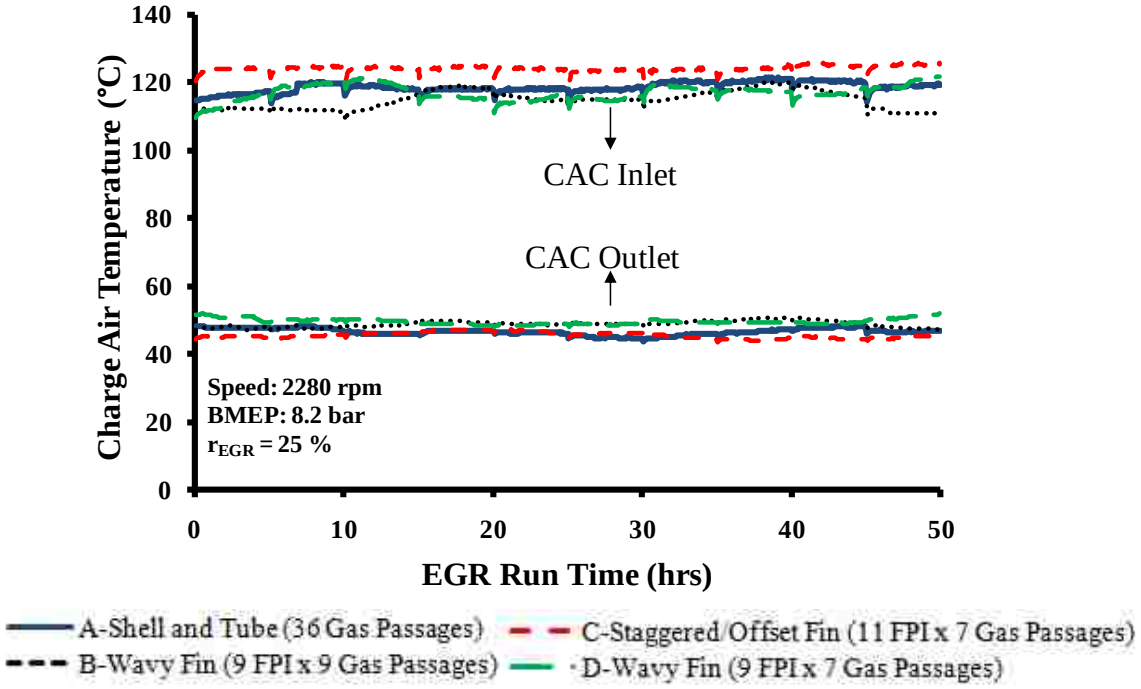

(a) r_{EGR} = 25%

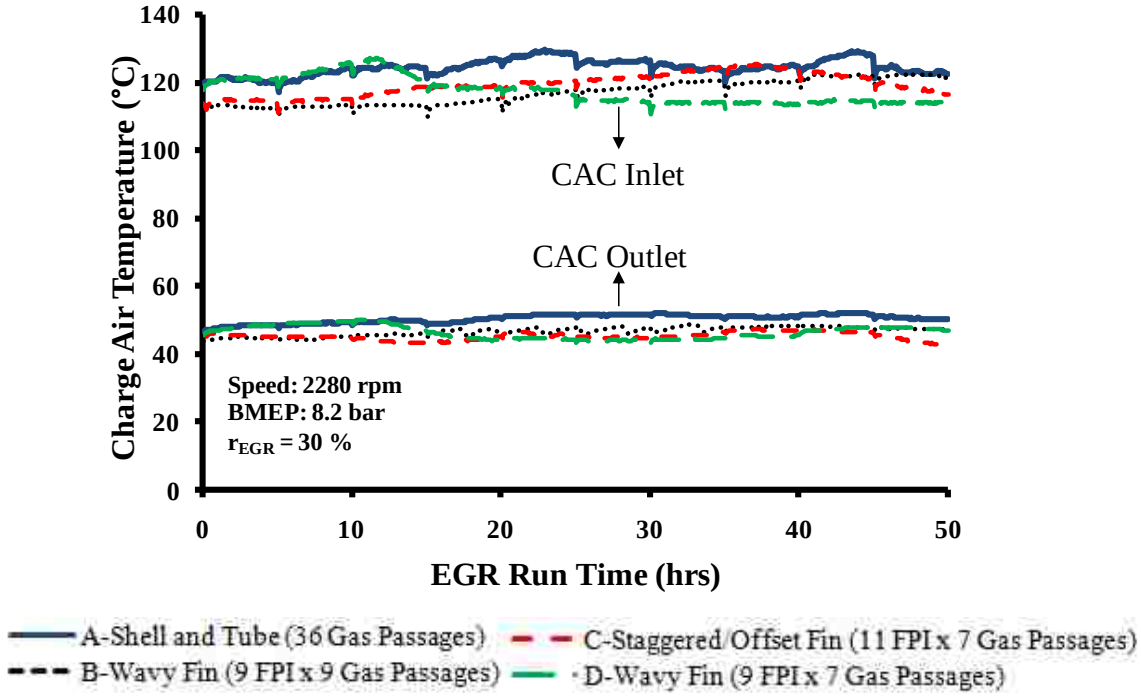

(b) r_{EGR} = 30%

Figure 5.7: Charge air temperatures at inlet and outlet of charge air cooler

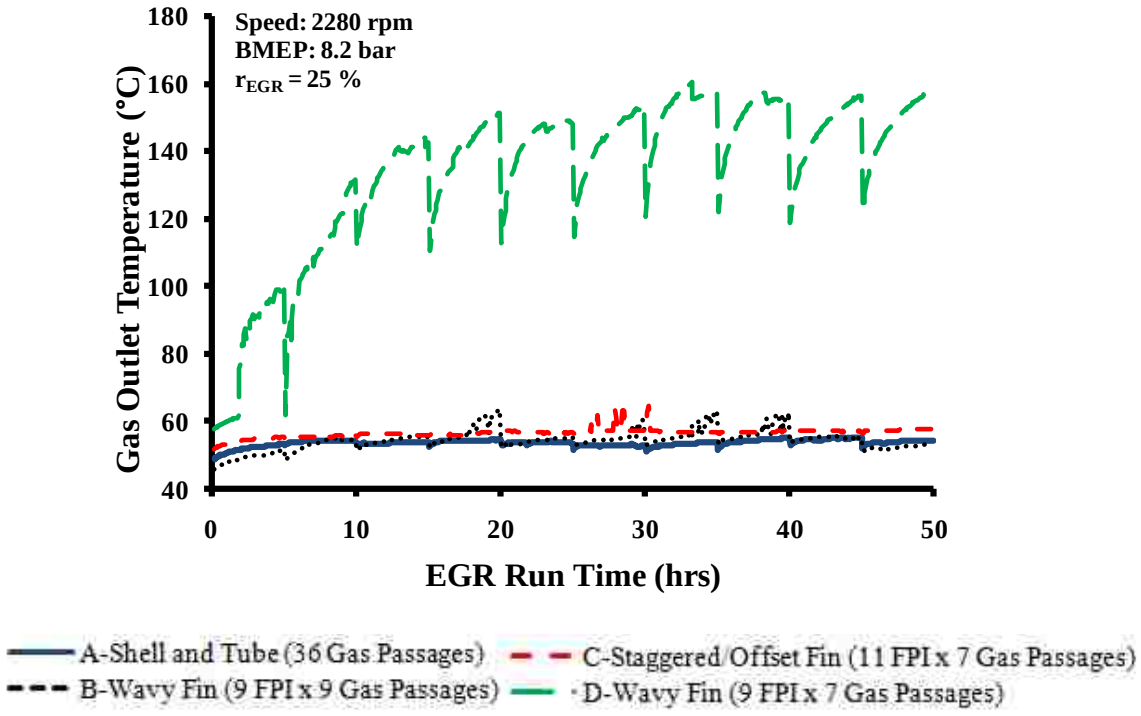

(a) r_{EGR} = 25%

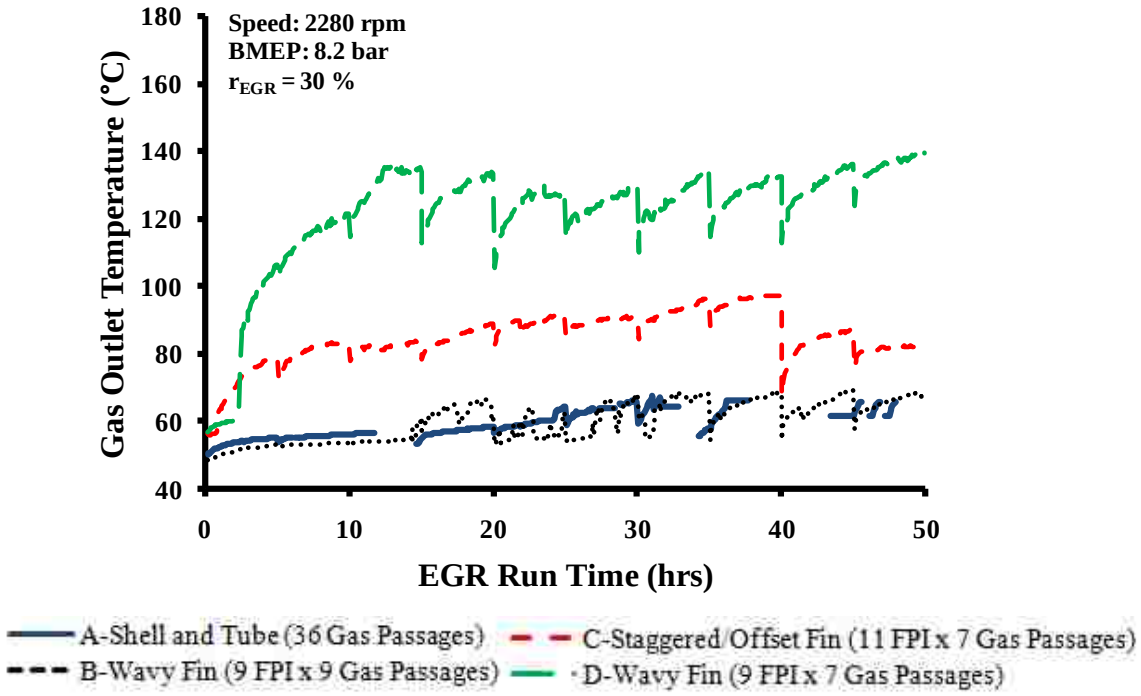

(b) r_{EGR} = 30%

Figure 5.8: Gas temperatures at LT EGR cooler exit

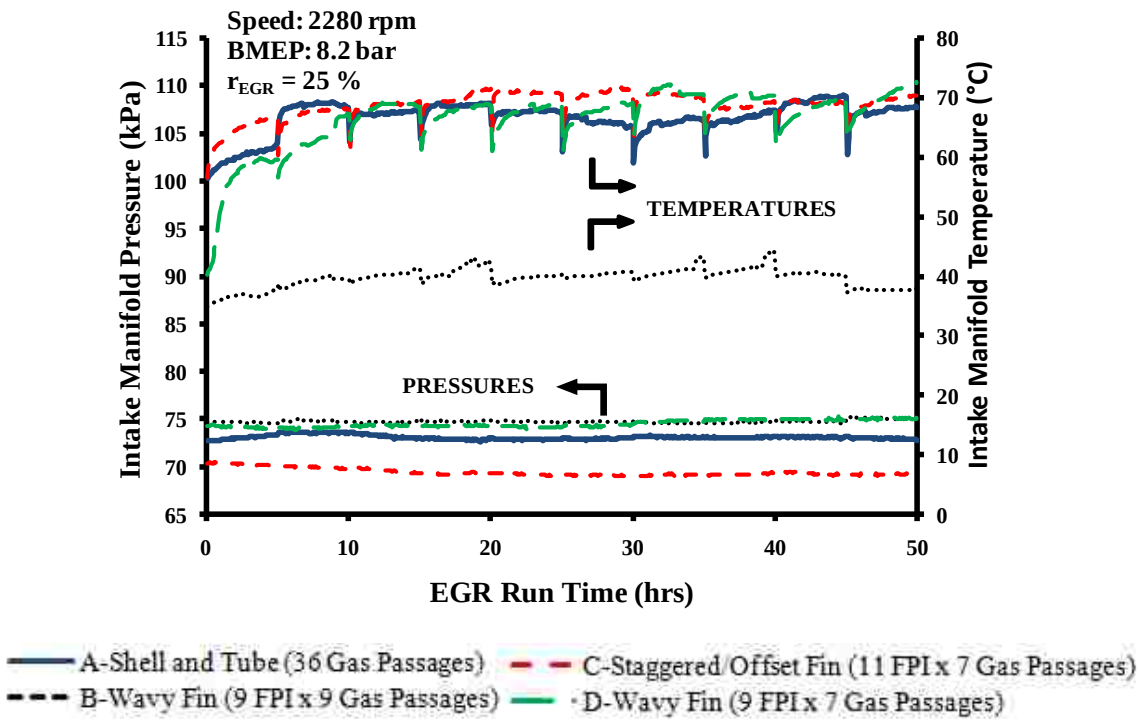

(a) r_{EGR} = 25%

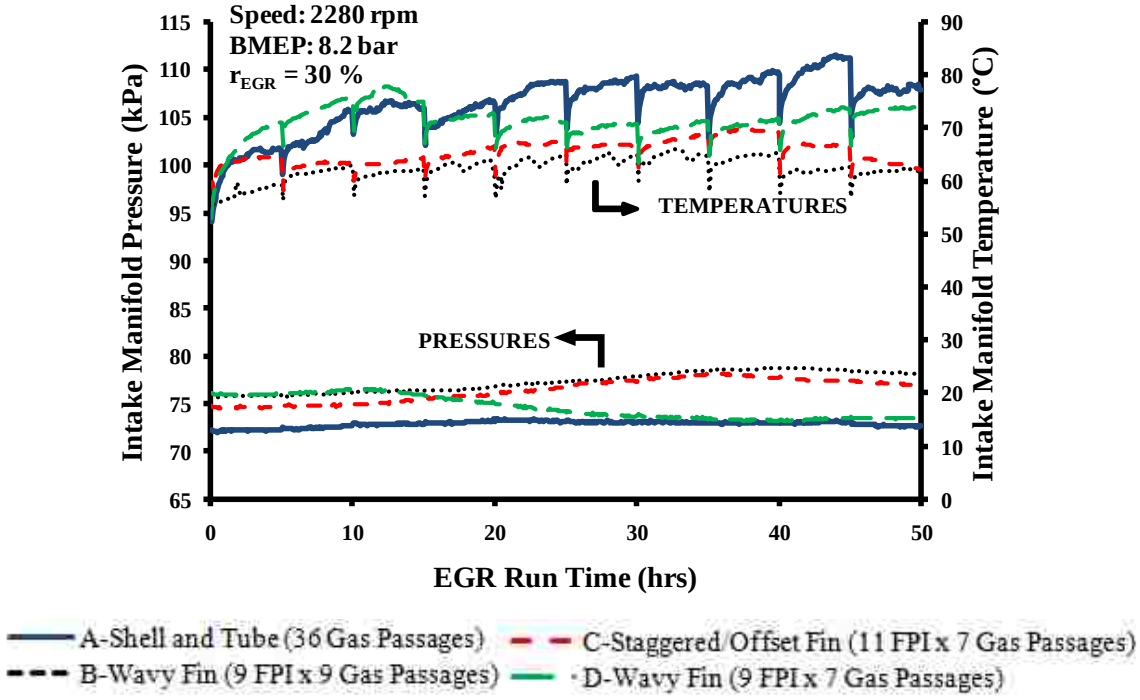

(b) r_{EGR} = 30%

Figure 5.9: Intake manifold temperature and pressure of charge air mass

The variations observed in Figure 5.8 were a result of the differences in EGR cooling performance between the competitive designs. In other words, the most effective EGR coolers provided the lowest gas temperatures at the LT cooler exit. Furthermore, as the recirculated exhaust gases mixed with the fresh intake charge, the temperature variations in the exhaust gas stream caused slight discrepancies in the intake manifold temperatures.

As established previously, the most significant soot deposition mechanism involves thermophoretic influences. Thus, it is important to highlight the temperature profiles of the exhaust gas and coolant streams entering the HT EGR cooler. The differential temperature between the exhaust gas and coolant stream may significantly affect the fouling characteristics and performance of the EGR cooler. The results of differential temperatures in Figure 5.10 indicate some disparity between experiments and need to be considered when evaluating EGR cooler fouling performance.

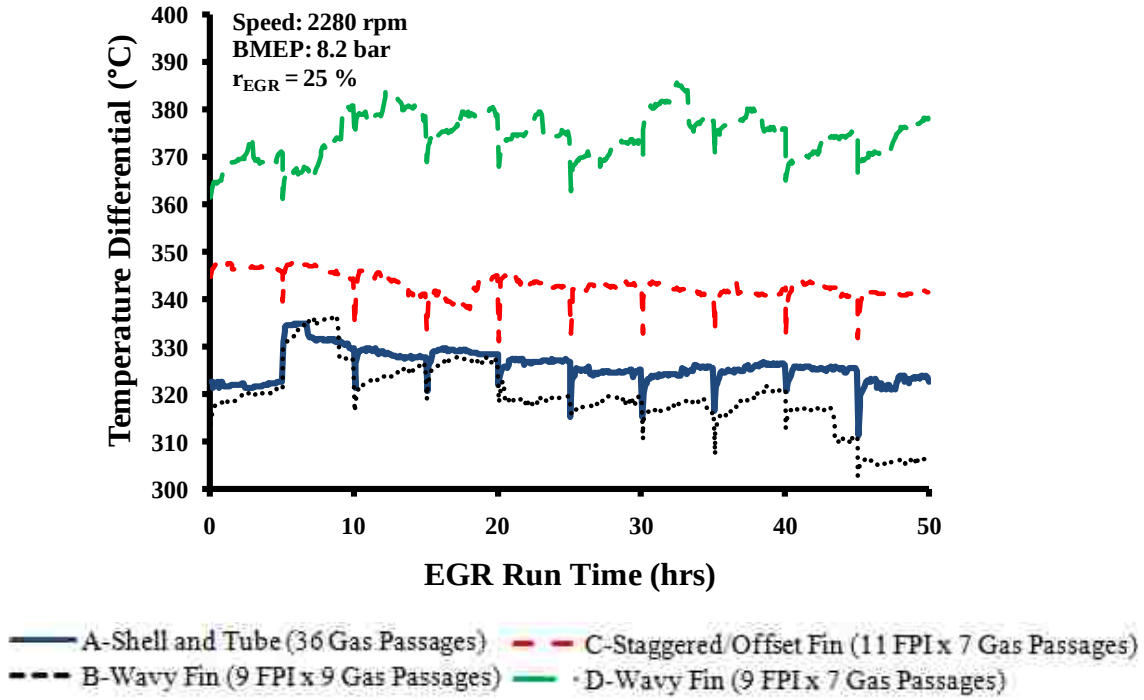

(a) r_{EGR} = 25%

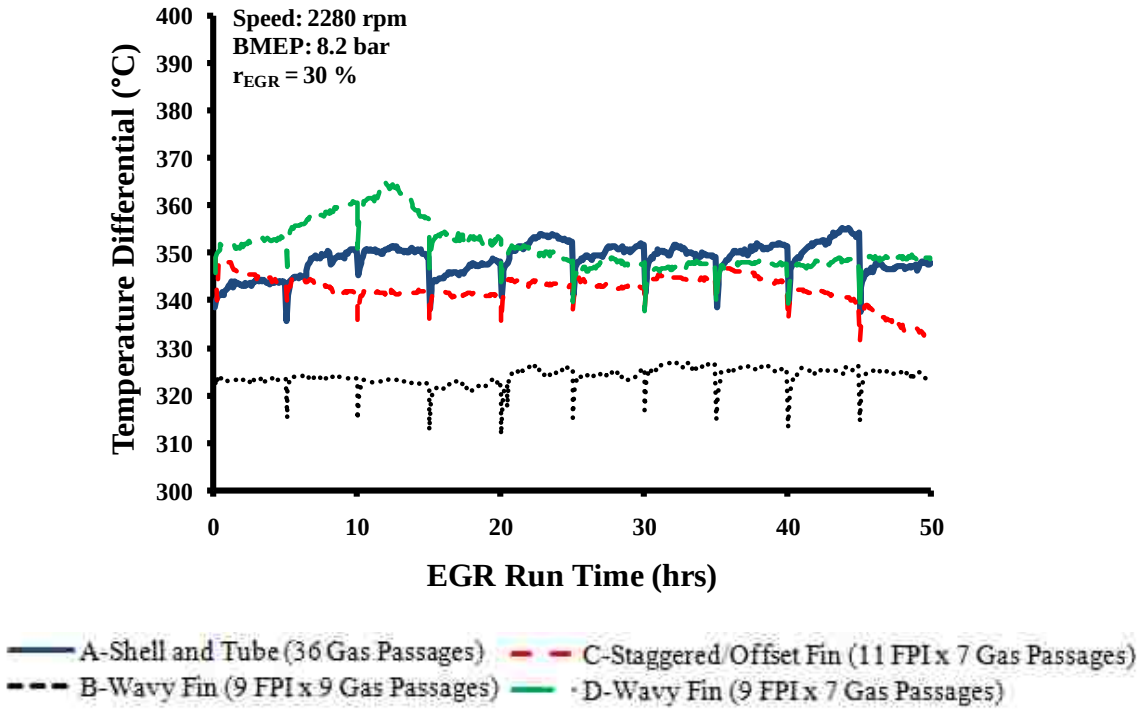

(b) r_{EGR} = 30%

Figure 5.10: ΔT between EGR and coolant streams at HT cooler inlet

5.2.3 Effectiveness – Comparison of Cooler Designs

High temperature (HT) cooler effectiveness results from all experiments listed in Table 5.4 are presented below in Figure 5.11. All curves exhibited an exponential characteristic with heavy degradation within the first 5-10 hours of run time followed by a slow decay in effectiveness as steady state was reached. The decrease in effectiveness after the first 5 hours of run time, for case (a) tests, is illustrated in the bar chart of Figure 5.13.

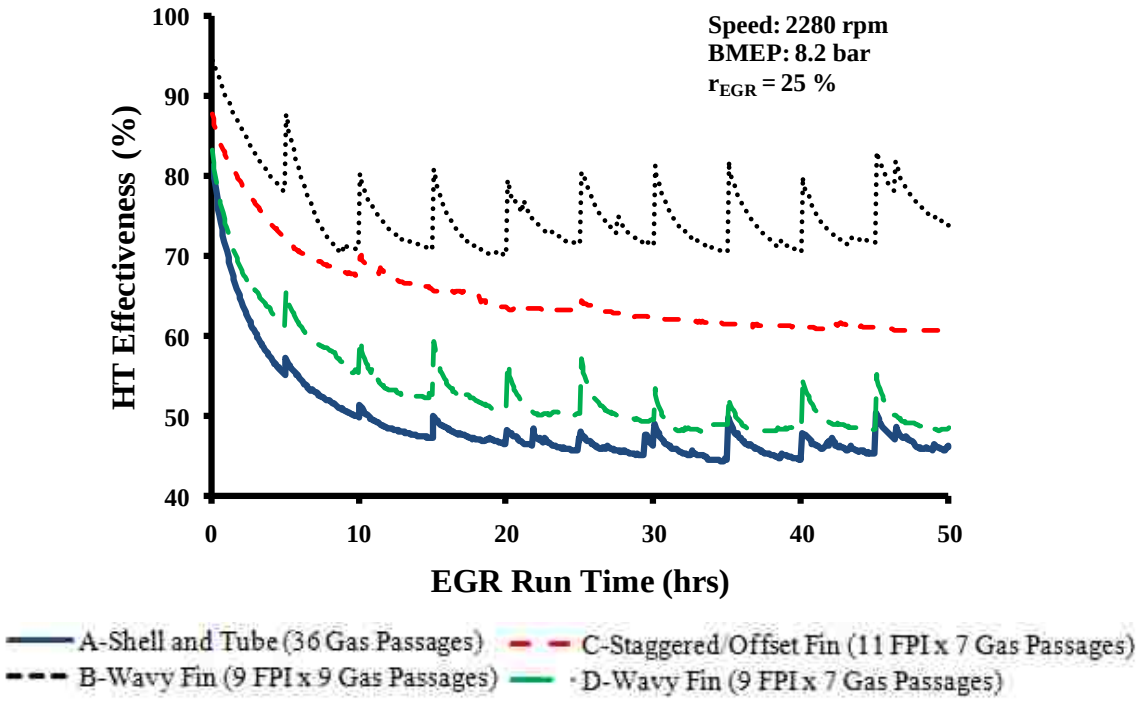

(a) r_{EGR} = 25%

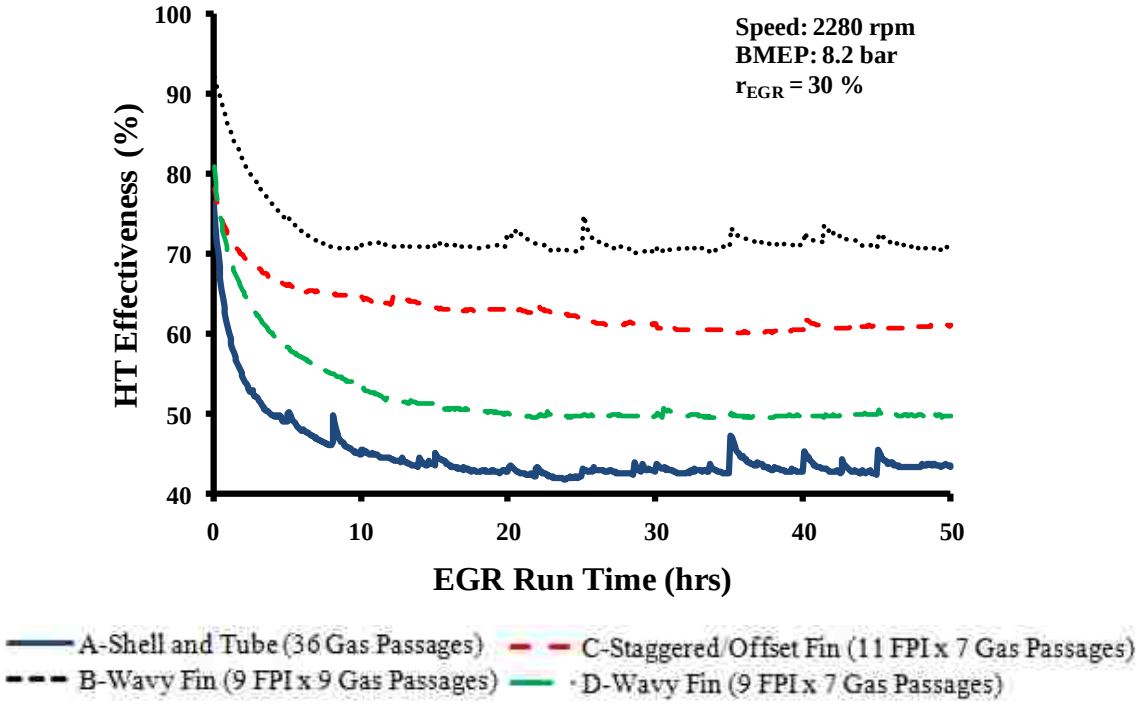

(b) r_{EGR} = 30%

Figure 5.11: HT cooler effectiveness trends with time - comparison of designs

An obvious observation to be made from Figure 5.11 is that, for both cases (a) and (b), cooler B (wavy fin) was most effective in reducing exhaust gas temperature followed by design C (staggered/offset fin), D (wavy fin) and A (shell and tube). Choosing design A as the baseline, a comparison of the remaining designs B, C, and D can be made relative to the baseline such as in Equation 5.1. The differences in effectiveness performance of each respective cooler design relative to the baseline (i.e. results of Equation 5.1) are graphed in Figure 5.12.

$$\Delta\varepsilon_{from\,baseline} = \frac{\varepsilon_{cooler} - \varepsilon_{baseline}}{\varepsilon_{baseline}} \times 100\% \qquad \text{Equation 5.1}$$

Moreover, design B showed the least absolute degradation over EGR run time as summarized in Table 5.5 and that only designs B and C met the target of 30% maximum allowable degradation. It should also be noted that regardless of initial (0 hour) effectiveness each design seemed to approach the same final (steady state) value for each case (a) and (b). In other words, design A will always approach a steady state effectiveness value of approximately 41%, design B approaches ε_{50HR} = 70%, C approaches ε_{50HR} = 60%, and D approaches ε_{50HR} = 50%.

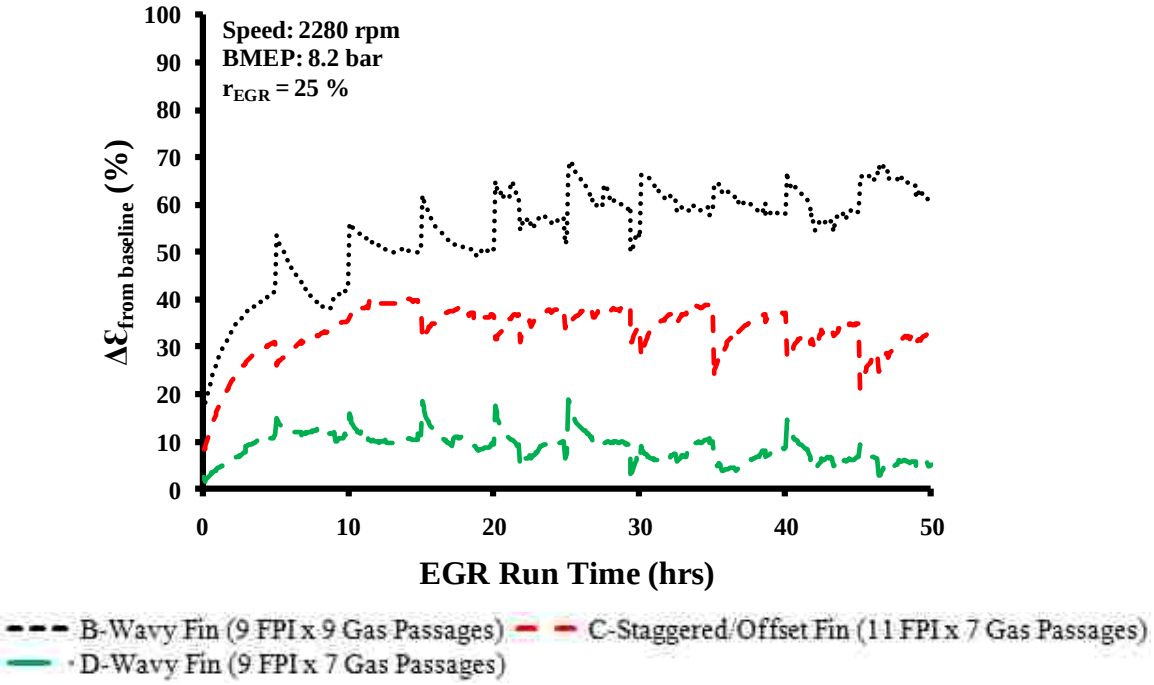

(a) r_{EGR} = 25%

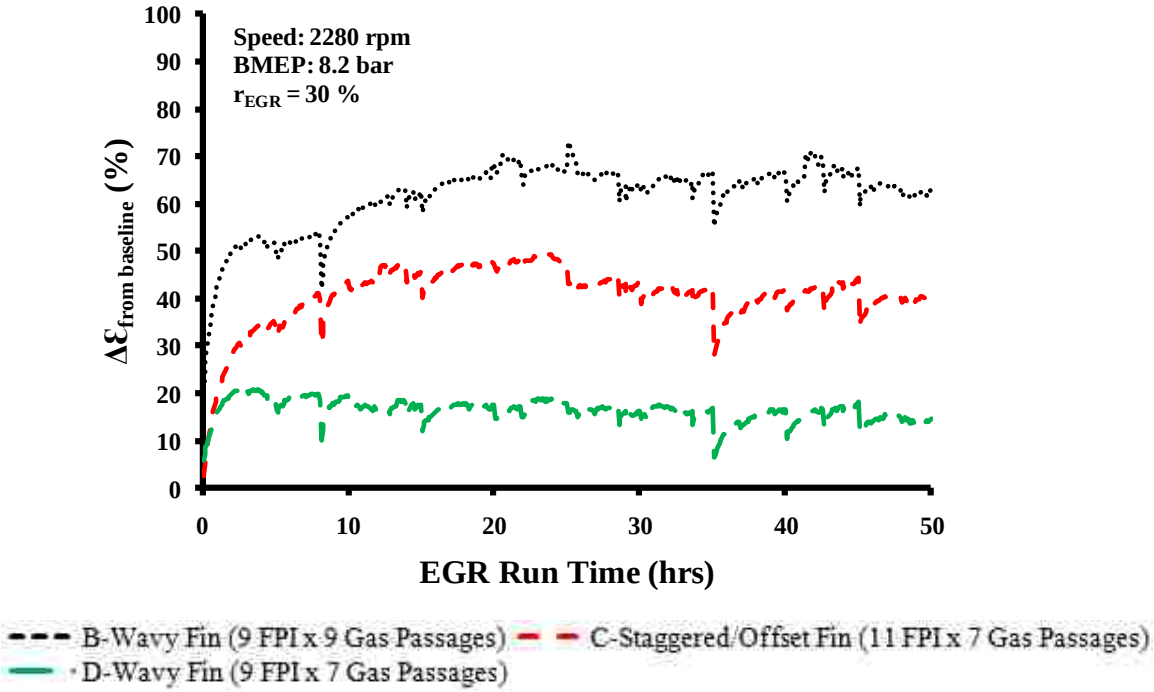

(b) r_{EGR} = 30%

Figure 5.12: Effectiveness performance relative to baseline design A

Table 5.5: Absolute degradation of high temperature cooler effectiveness comparison

Design	A		B		C		D	
r_{EGR} (%)	**25**	**30**	**25**	**30**	**25**	**30**	**25**	**30**
ε_{0HR} (%)	81	76	95	92	88	78	83	81
ε_{50HR} (%)	44	41	70	70	61	60	48	49
ε_{abs} (%)	***43***	***43***	22	23	30	22	***42***	***39***

Values bolded and italicized do not meet the target for absolute degradation

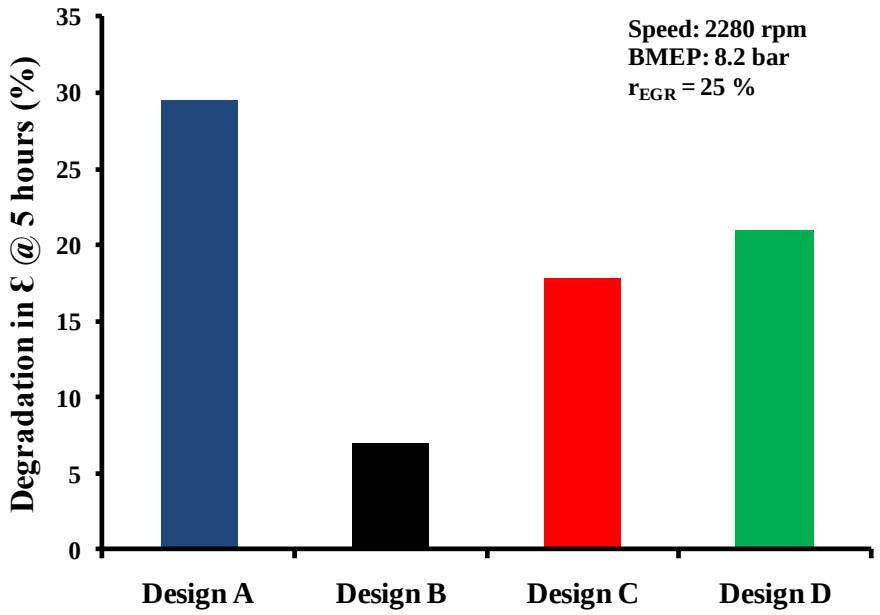

Figure 5.13: HT cooler effectiveness degradation after initial 5 hours

Figure 5.14 presents the cooler fouling factor which, by definition, is normalized with respect to heat transfer surface area. Results of fouling factor suggest that design B was least effected by fouling, followed by design C, which defends the observations made in Table 5.5 that designs B and C suffered the least degradation in effectiveness over run time.

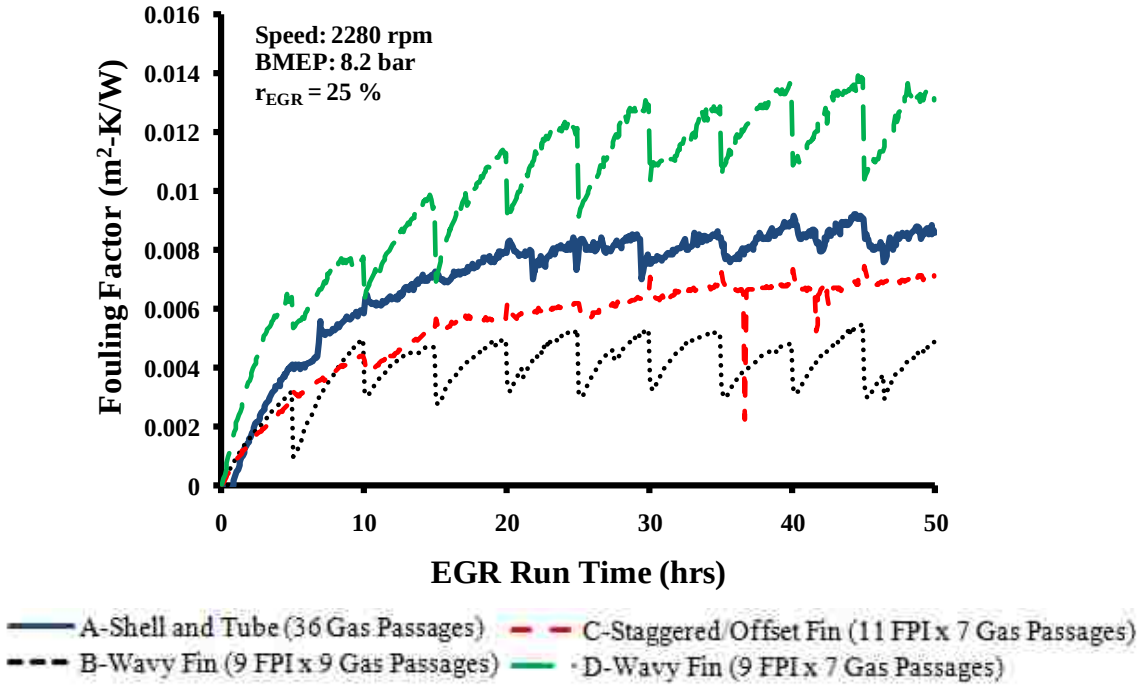

(a) r_{EGR} = 25%

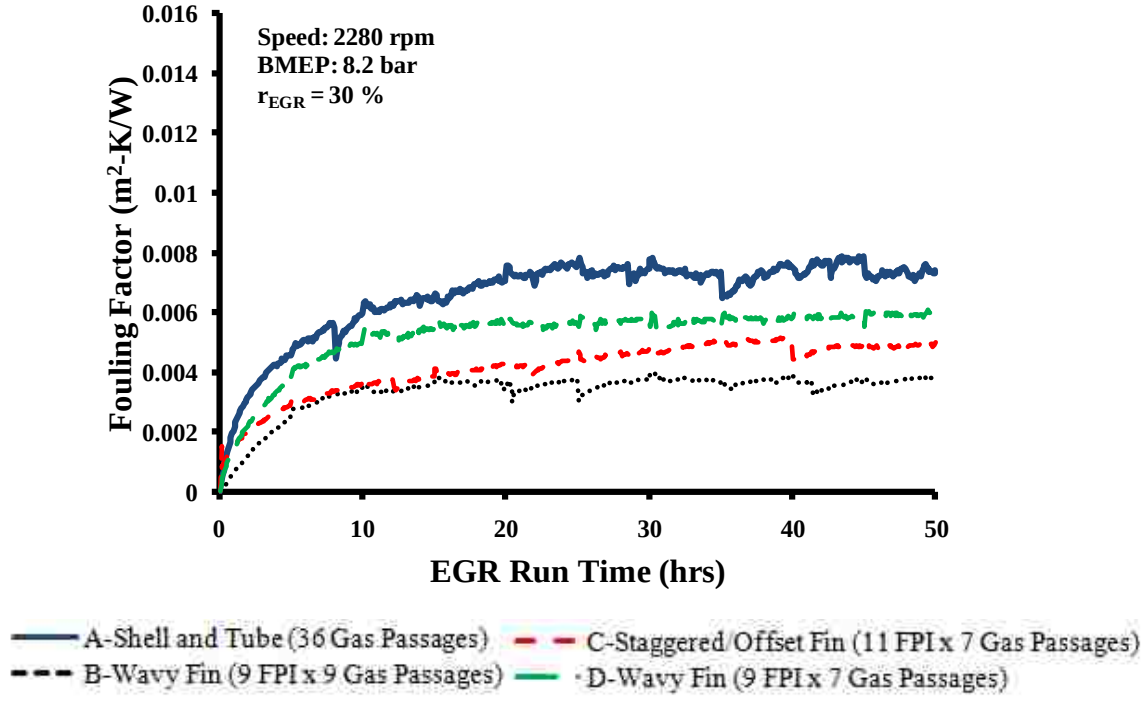

(b) r_{EGR} = 30%

Figure 5.14: HT cooler fouling factor (R_f) trends with time - comparison of designs

Another interesting result observed was the difference in fouling factor for design D between tests D-25 and D-30. The possible causes of this behaviour are explained through consideration of smoke levels and EGR flow rates. From Table 5.4, test D-30 had a slightly higher initial smoke level compared to D-25. This observation alone would suggest that test D-30 should exhibit higher fouling behaviour. However, the smoke levels need to be considered in parallel with the EGR flow rates of the experiments. Although, D-30 experienced slightly higher smoke levels, the EGR flow rate was significantly higher for D-30 in comparison to D-25 (i.e. 207 kg/hr compared to 160 kg/hr). The higher flow rate through the coolers is believed to enhance the deposit removal mechanisms within the cooler and provide less fouling behaviour.

The end goal of the EGR cooling process is to meet the target outlet gas temperature necessary to provide adequate in-cylinder NOx reduction. From Figure 5.15, the cooler performance degradation was too great and the target was not achieved. Clearly a secondary pass or low temperature cooler is required for meeting the target requirements.

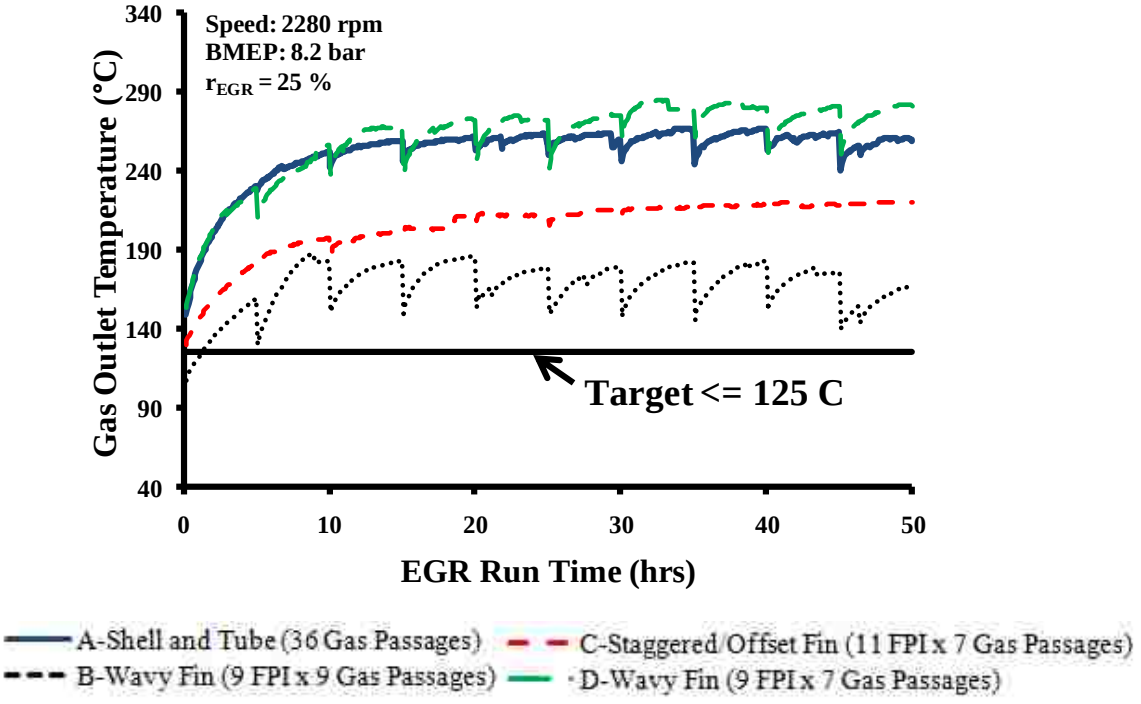

Figure 5.15: Outlet gas temperature compared to target

Based on the presented results of HT effectiveness and fouling factor, the plate fin type cooler design B outperformed the competitive designs A, C, and D. Further analysis of cooler performance characteristics is required before any type of conclusion can be suggested.

5.2.4 Pressure Drop – Comparison of Cooler Designs

Pressure drop data is presented in Figure 5.16 below. Similar to the trends of effectiveness discussed previously, the pressure drop across the coolers increased exponentially with time, more particularly for the fin type coolers. The shell and tube design A on the other hand, showed the most intriguing pressure drop characteristic. Although initially high, the pressure drop did not change much over the 50 hour test cycle for design A in both cases (a) and (b). These results are due to the inherently larger flow passages of the shell and tube cooler design compared to the fin type designs.

In a comparison of case (a) with case (b) one would expect higher pressure drops across the coolers when being exposed to higher levels of particulate matter such as in case (b). This assumption holds true for designs A and C, but not for B and D. The reason for this outcome can be explained by considering the average smoke levels for each test. Notice from Table 5.4, that the initial values of smoke for all case (b) tests (i.e. $r_{EGR} = 30\%$) were greater than that of case (a) for each specific cooler design. However, the average values for smoke over the 50 hour test cycle do not maintain this pattern. From the summarized data in Table 5.6, the average smoke levels for test B-30 was less than B-25. Likewise average smoke level of test D-30 was less than D-25. The lower overall exposure to particulate matter, coupled with the higher EGR flow rates through the coolers would explain the lower pressure drops witnessed in case (b) for designs B and D. This result not only identifies the difficulties encountered in controlling smoke levels, but also highlights the strong dependence of fouling build up on soot concentration.

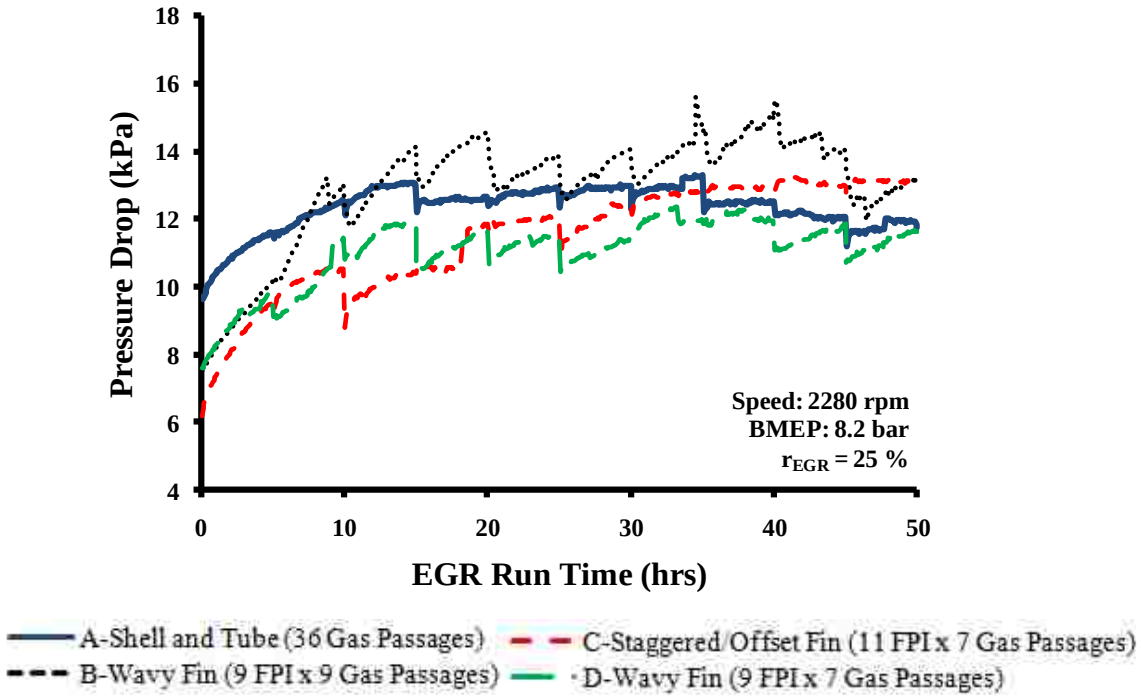

(a) r_{EGR} = 25%

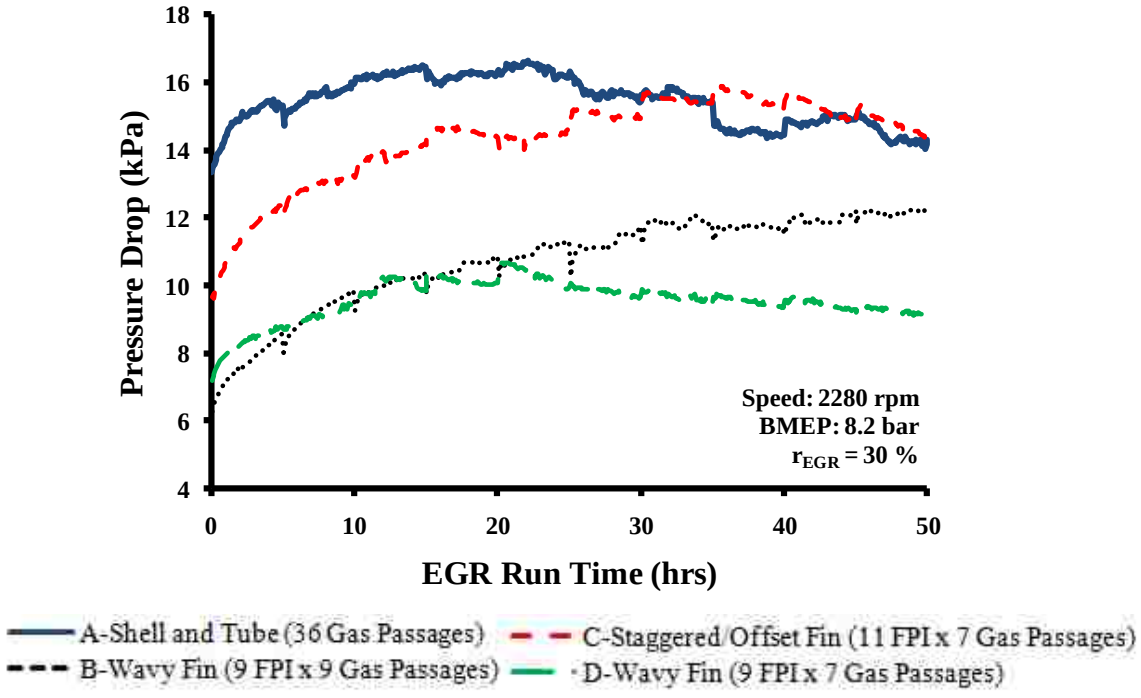

(b) r_{EGR} = 30%

Figure 5.16: HT cooler pressure drop trends with time - comparison of designs

Table 5.6: Summary of HT pressure drop performance

Design	A		B		C		D	
r_{EGR} (%)	25	30	25	30	25	30	25	30
Mean Smoke (FSN)	0.97	1.52	1.58	1.14	0.87	1.07	1.85	1.43
Mean $\dot{m}_{EGR}$ (kg/hr)	148	165	158	170	134	168	137	163
Δp_{avg} (kPa)	12.33	15.45	12.97	10.73	11.52	14.33	11.06	9.56

Unlike the results of effectiveness, no specific cooler significantly out-performed the other designs with respect to pressure drop. The major noteworthy observation was that the shell and tube type design A showed the least pressure drop increase over time, but was the only cooler that did not meet the 15 kPa target for case (b). This is more clearly illustrated using the non-dimensional representation of pressure drop data (friction factor) as seen in Figure 5.17.

In general, shell and tube designs are turbulence dominated as compared to fin type coolers which are surface area dominated. Consequently, for the same EGR mass flow rate ($\dot{m}_{EGR}$), the gas velocity (V) through shell and tube design A will be greater than that of fin type designs B, C, and D. Furthermore, as seen in Equation 4.7 the dimensionless friction factor (f) is inversely proportional to the square of the gas velocity (V^2) and so increasing gas velocity leads to significant reduction in friction factor. As a result, design A simultaneously showed highest levels of pressure drop with lowest friction factor.

The effects of increasing gas velocity can also be seen by comparing the friction factors of the respective designs across the two cases (a) and (b). The higher gas velocities experienced in case (b) cause lower friction factors as compared to case (a). The relationship between exhaust gas mass flow rate and pressure drop is illustrated in Figure 5.18. A weak correlation is evident that indicates a decrease in pressure drop with increasing EGR flow rate.

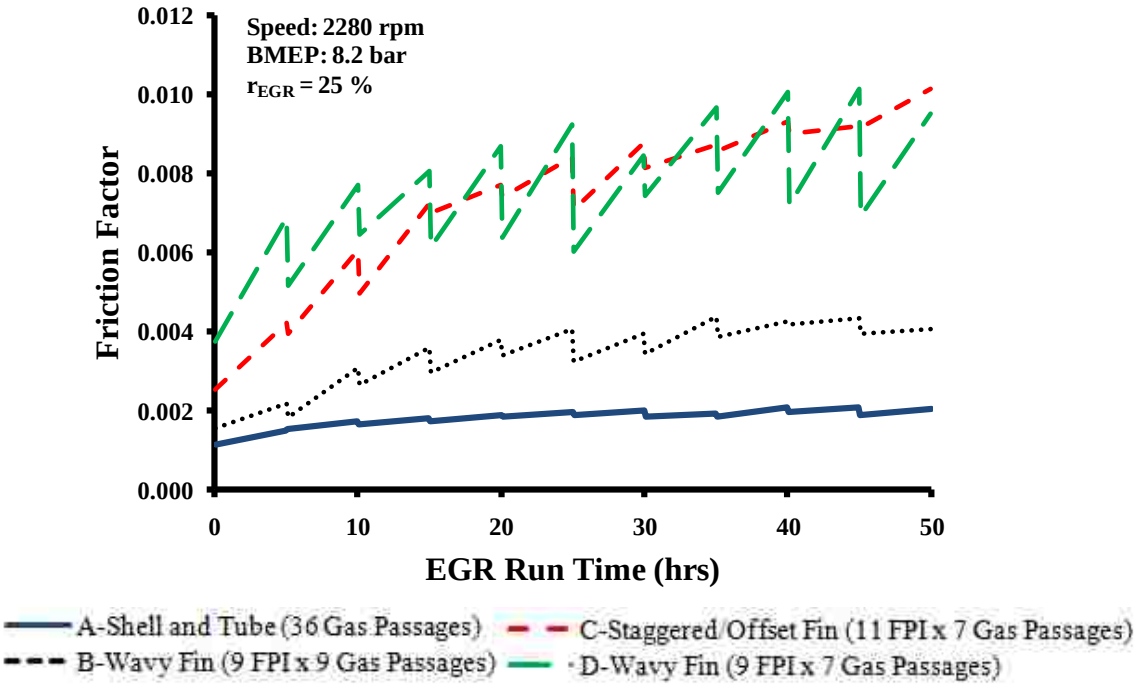

(a) r_{EGR} = 25%

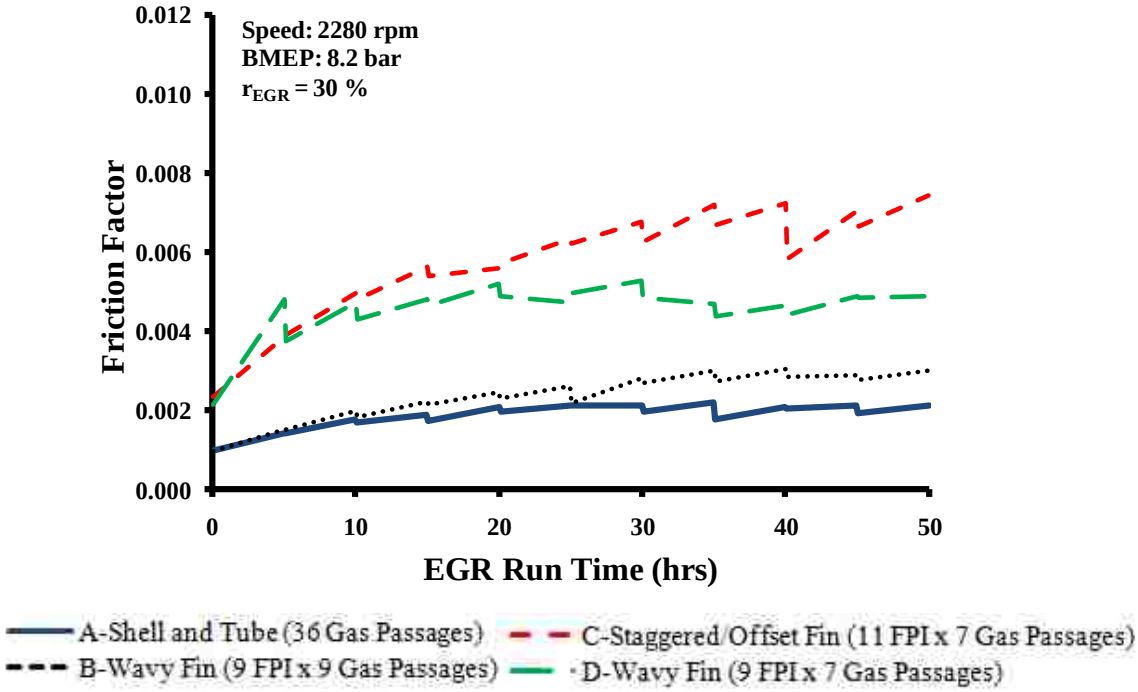

(b) r_{EGR} = 30%

Figure 5.17: Non-dimensional friction factor comparison for HT EGR coolers

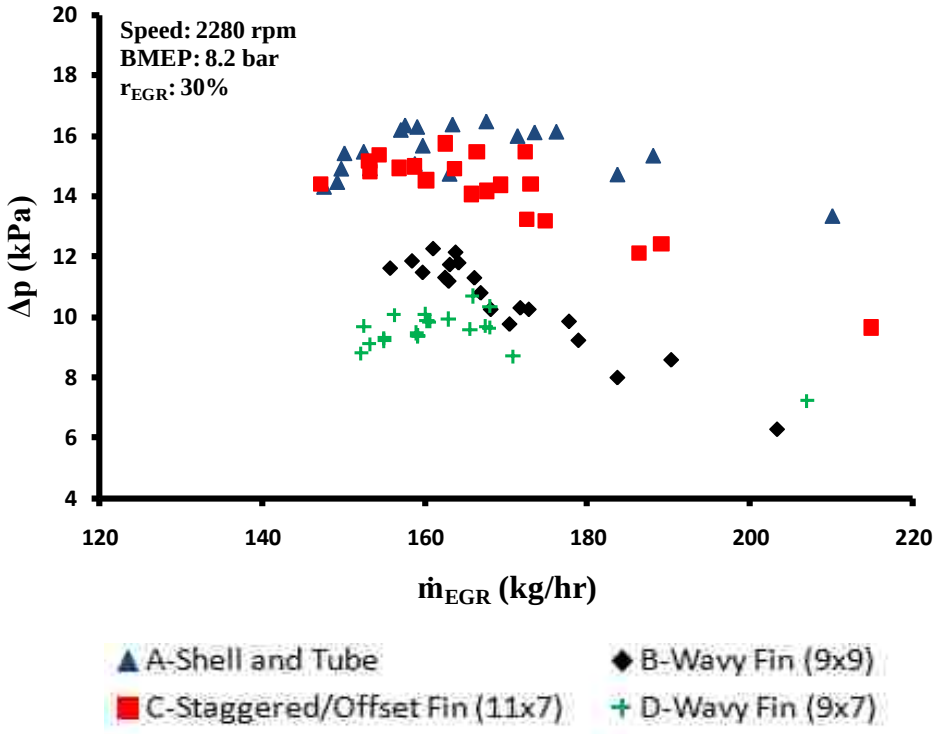

Figure 5.18: Relationship of pressure drop vs. EGR mass flowrate

5.2.5 EGR Mass Flow Rate – Comparison of Cooler Designs

As explained in the previous discussions, the exhaust gas mass flow rate through the EGR coolers is an important factor in the fouling process and the results are presented in Figure 5.19. Some differences in the initial EGR flow rates are evident in the results of tests from case (a). As described in Chapter 3, standardized procedures were utilized at the start of each test to match the initial conditions with the predefined target values. However, the methods of controlling EGR flow rate used in this investigation may need to be improved for future testing. In other words, EGR valve and intake throttle position need to be controlled in addition to other parameters effecting EGR flow such as EGR loop differential pressure, intake and exhaust temperatures, and turbo vane position for variable geometry turbochargers (VGT).

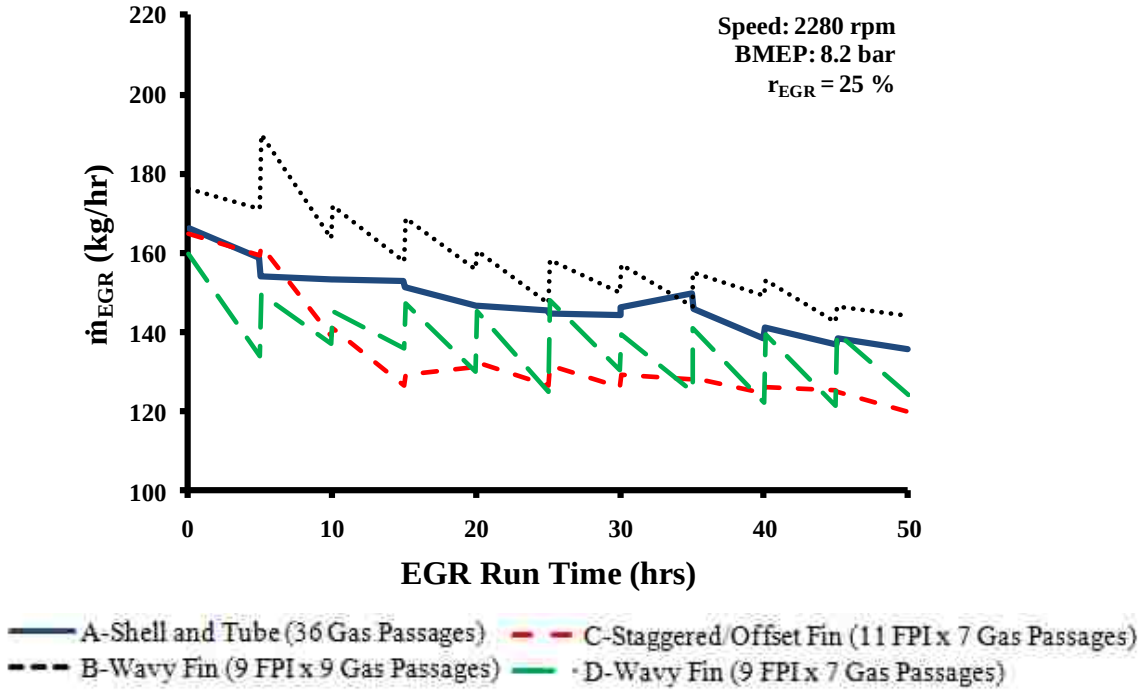

(a) r_{EGR} = 25%

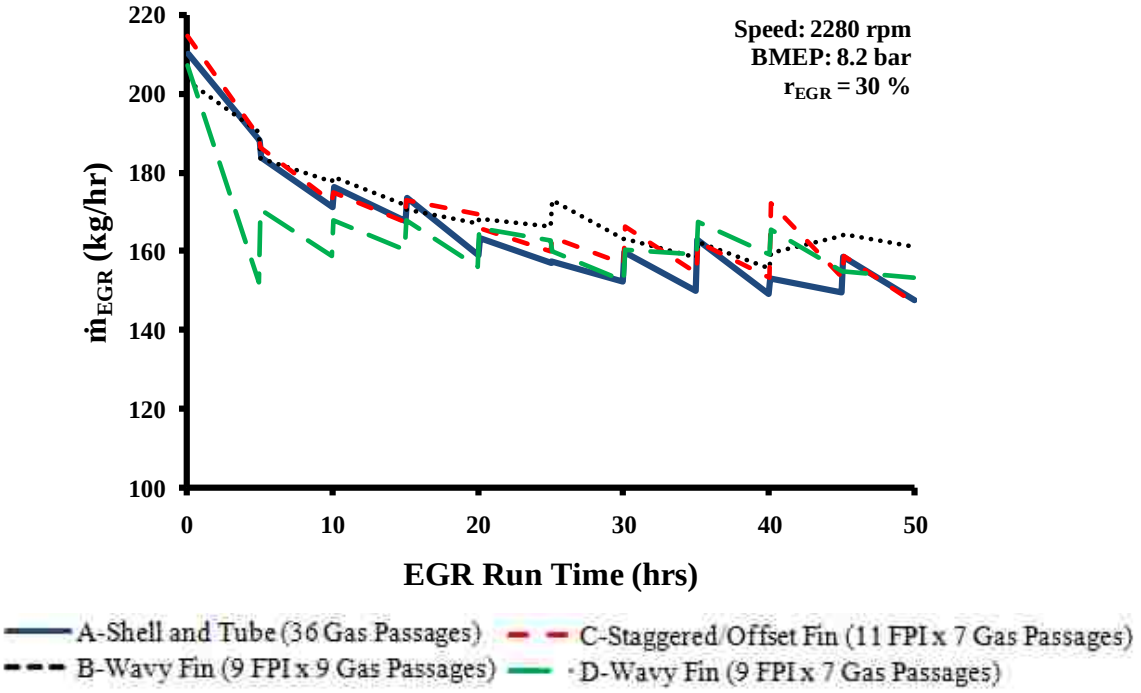

(b) r_{EGR} = 30%

Figure 5.19: Exhaust gas mass flow rate ($\dot{m}_{EGR}$) trends with EGR run time

Well designed EGR coolers should maintain sufficient flow rates even under fouled conditions. An evaluation of the percentage decrease in $\dot{m}_{EGR}$ from the initial value gives a good indication of the individual cooler performance with respect to maintaining adequate EGR flow rates during fouling. The decrease in flow rate over time is presented in Figure 5.20. From these results, design B displayed the least performance loss in terms of maintaining EGR mass flow rate. Design B averaged a 19% decrease in flow rate between the two tests (B-25 and B-30) whereas the other designs A, C, and D averaged 24%, 29%, and 24% drops in flow rate respectively.

A comparison of the percentage decrease in $\dot{m}_{EGR}$ with the average smoke levels yields an interesting result. Although the summary of Table 5.7 suggests that designs B, and D were exposed to the highest average levels of smoke, these designs maintained mass flow rate relatively better than the competitive shell and tube design A and staggered offset fin type design C. These observations suggest that the wavy fin type design may be superior to fouling resistance compared to other designs.

Table 5.7: Summary of decrease in $\dot{m}_{EGR}$ with respect to smoke levels

Design	**A**		**B**		**C**		**D**	
r_{EGR} (%)	**25**	**30**	**25**	**30**	**25**	**30**	**25**	**30**
Mean Smoke (FSN)	0.97	1.52	1.58	1.14	0.87	1.07	1.85	1.43
Mean $\dot{m}_{EGR}$ (kg/hr)	148	165	158	170	134	168	137	163
Decrease in $\dot{m}_{EGR}$ from 0hr (%)	19	30	18	20	27	32	22	26

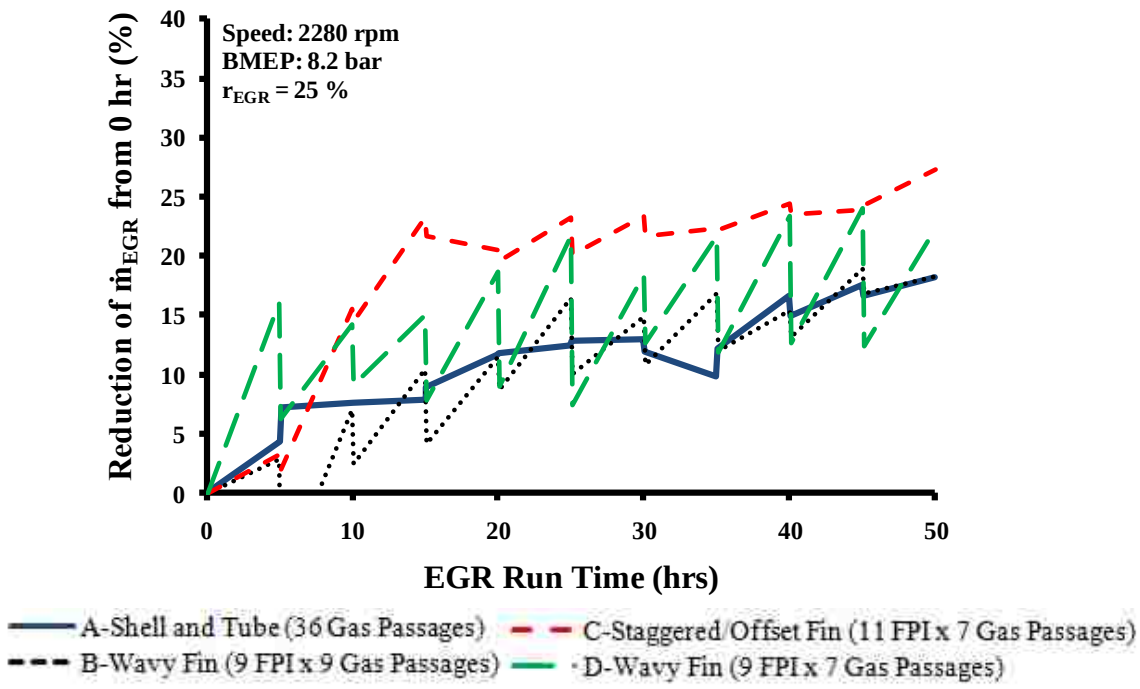

(a) r_{EGR} = 25%

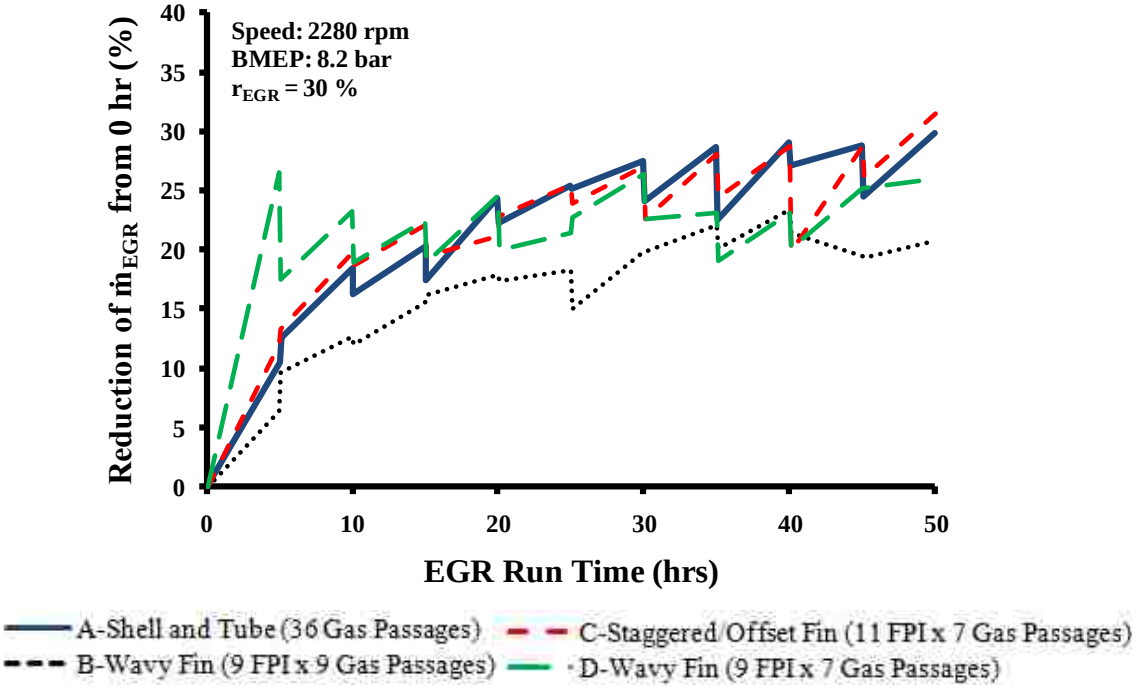

(b) r_{EGR} = 30%

Figure 5.20: Percentage decrease in $\dot{m}_{EGR}$ from initial (0 hr) condition

5.2.6 Engine-Out Emissions of Pollutant Species

PARTICULATE MATTER

As previously established, the particulate matter emissions were not directly measured in this investigation. Instead, smoke level measurements were used to represent the emissions of PM. Smoke level results are shown in Figure 5.21. The decrease in smoke level, over time, was caused by the diminishing EGR flow rates that resulted due to the fouling process. Reducing EGR flow decreases the displacement of intake oxygen charge and improves the soot oxidation rate hence reducing engine-out smoke emissions.

Also mentioned throughout the previous discussions were the difficulties encountered in consistently setting the initial smoke levels between tests. Although the procedures were standardized, there was a lack of control of the initial smoke levels which indicates an area of improvement for future EGR cooler fouling experiments.

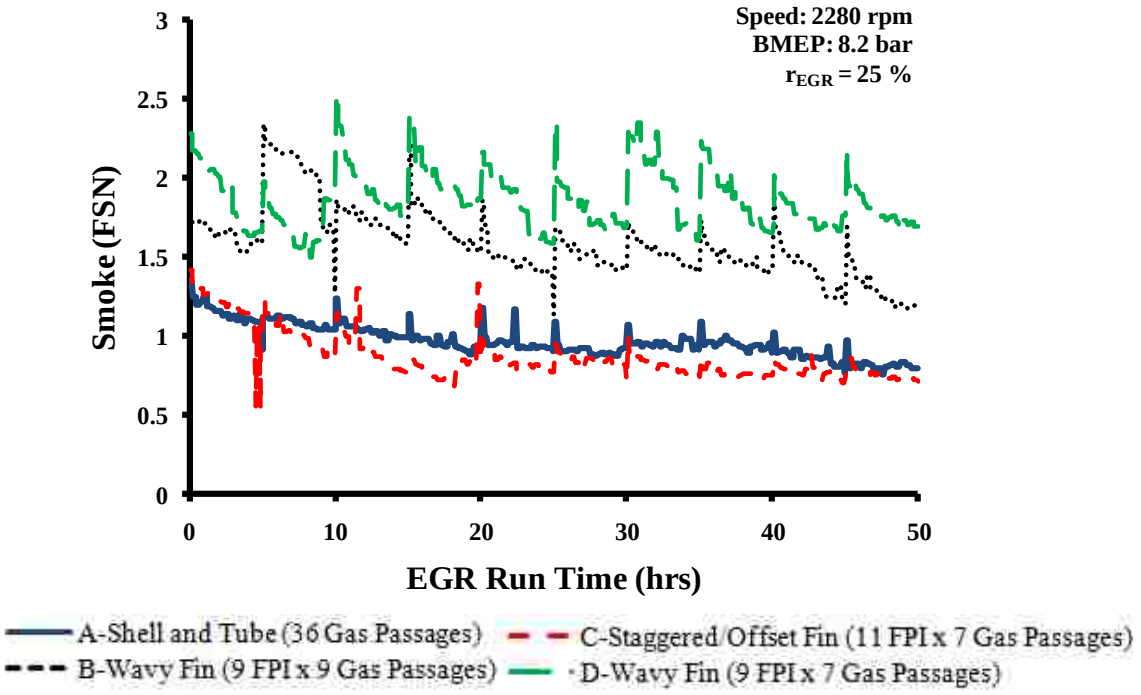

(a) r_{EGR} = 25%

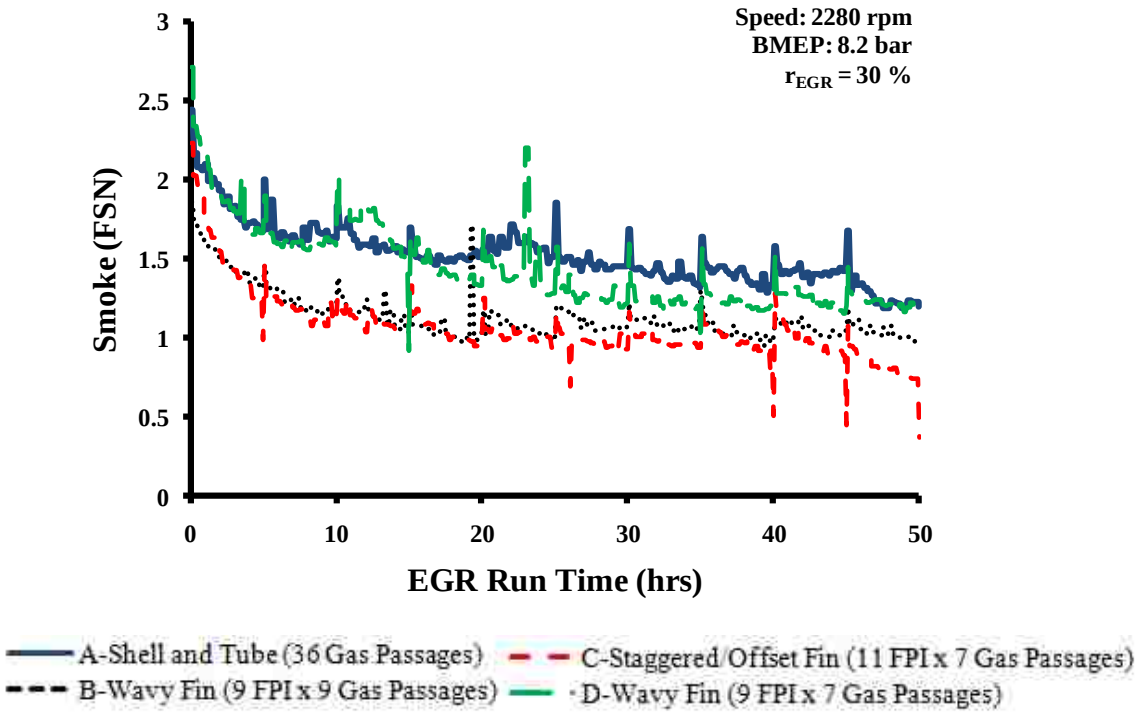

(b) r_{EGR} = 30%

Figure 5.21: Engine-out smoke emissions levels

OXIDES OF NITROGEN (NOx)

With cooler performance degradation over time, EGR flow rate decreased and EGR temperatures increased, weakening the dilution, thermal, and chemical effects of EGR on combustion. Accordingly, the NOx emissions levels increased with time as can be seen in Figure 5.22. A comparison of the designs using Figure 5.22 and Table 5.8 reveals that designs A and B were most effective in reducing and maintaining lowest relative NOx emissions levels.

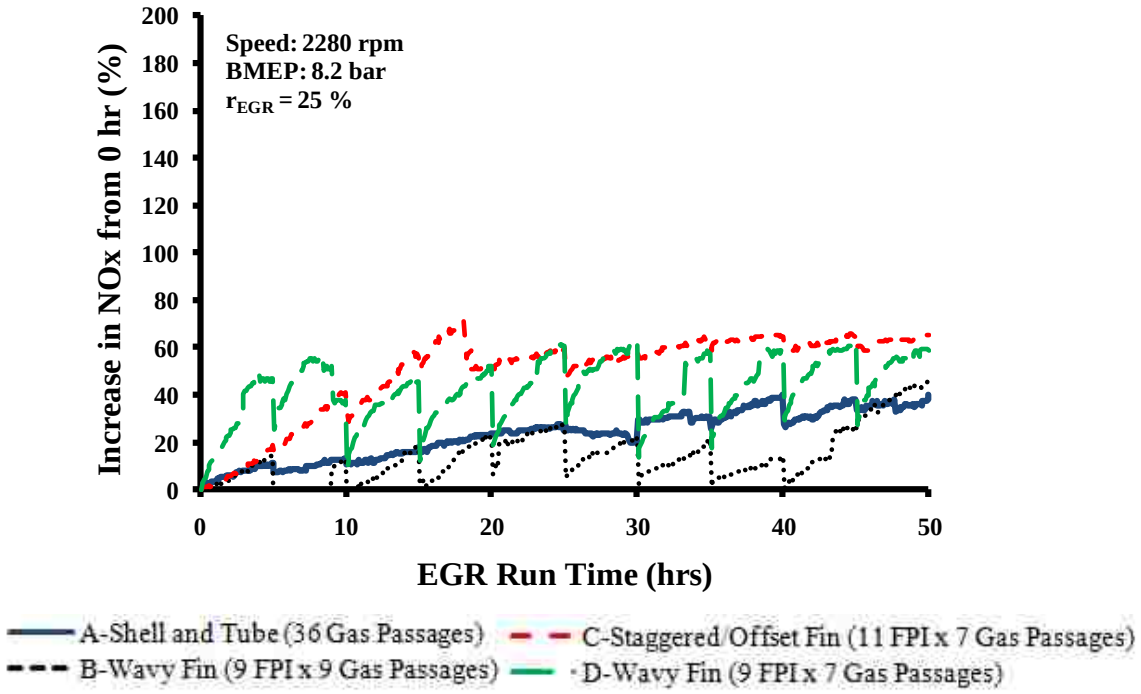

(a) r_{EGR} = 25%

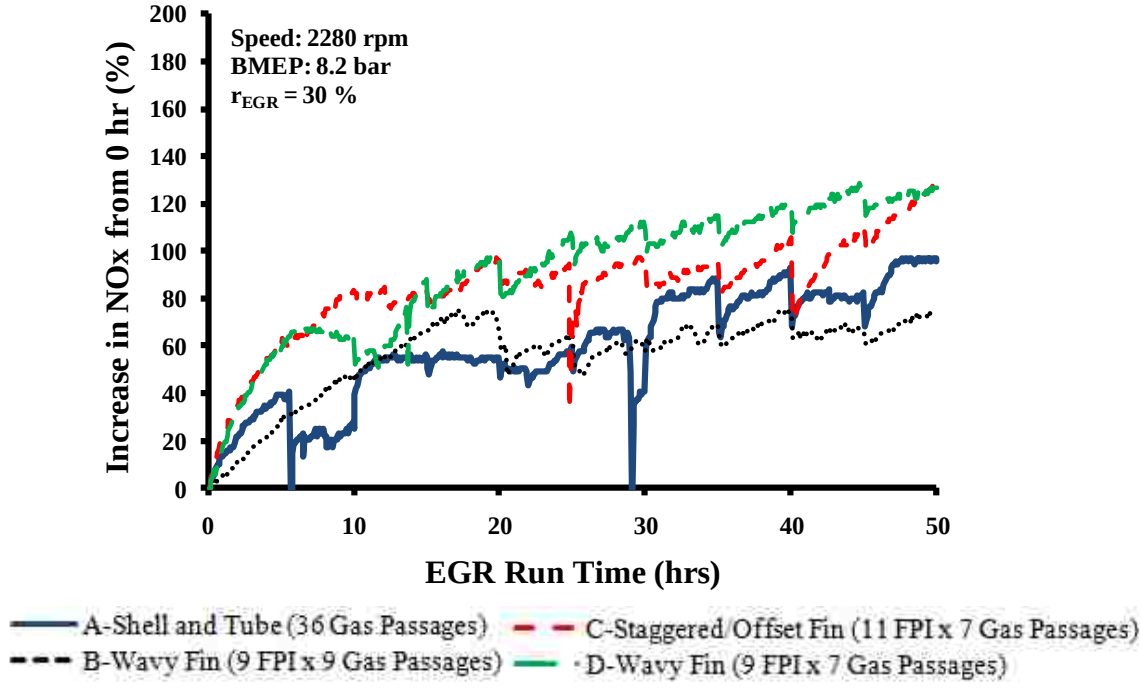

(b) r_{EGR} = 30%

Figure 5.22: Percent increase in engine-out NOx emissions from initial condition

Table 5.8: Summary of average NOx emissions and percentage increase from 0 hr

Design	A		B		C		D	
r_{EGR} (%)	25	30	25	30	25	30	25	30
Mean NOx (g/kW-hr)	1.39	1.10	0.87	1.15	1.68	1.35	1.37	1.28
Total Increase in NOx from 0 hr (%)	40	96	45	74	65	127	58	127

TOTAL HYDROCARBONS (THC)

Figure 5.23 shows the total hydrocarbon emissions measured over time. Although there was a slight decrease in THC emissions within the first 5 hours of the test cycle, the overall change in emissions was small. The reason for the slight decrease in THC emissions is the same as that for the decreasing PM trend previously explained. As the EGR flow rate decreases due to fouling, an improvement in engine combustion efficiency and hydrocarbon oxidation is witnessed, producing less unburned HC emissions. The difference in the THC emissions levels between tests was minimal as the values were in proximity of 0.1 g/kW-hr C_1 throughout the test cycle.

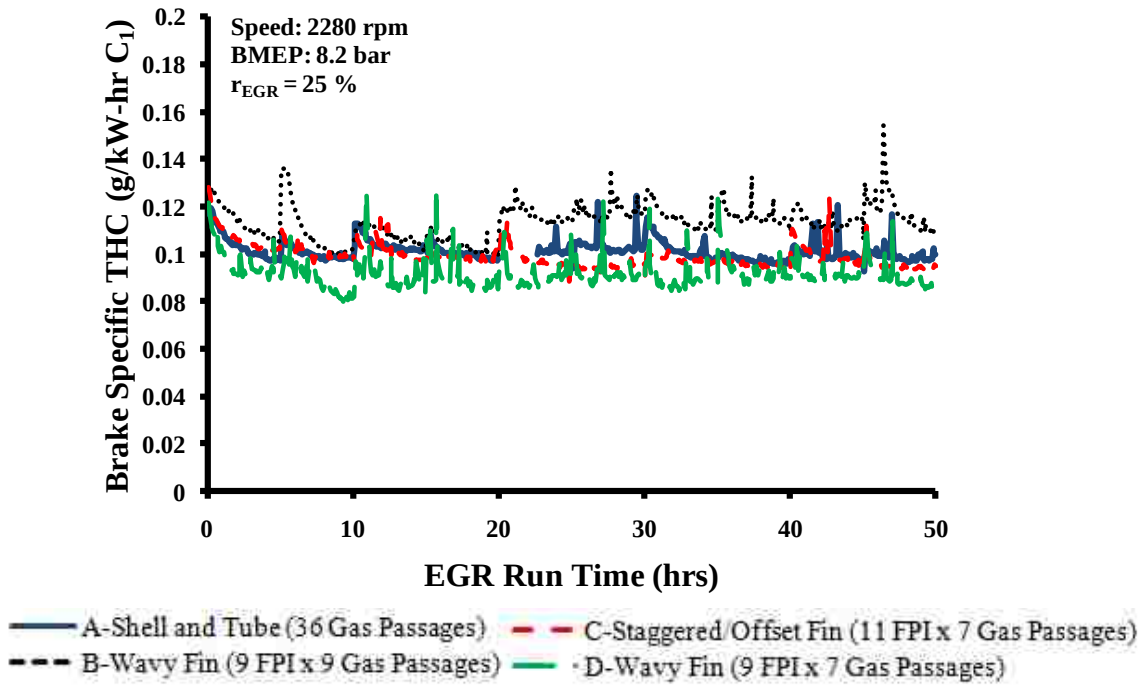

(a) r_{EGR} = 25%

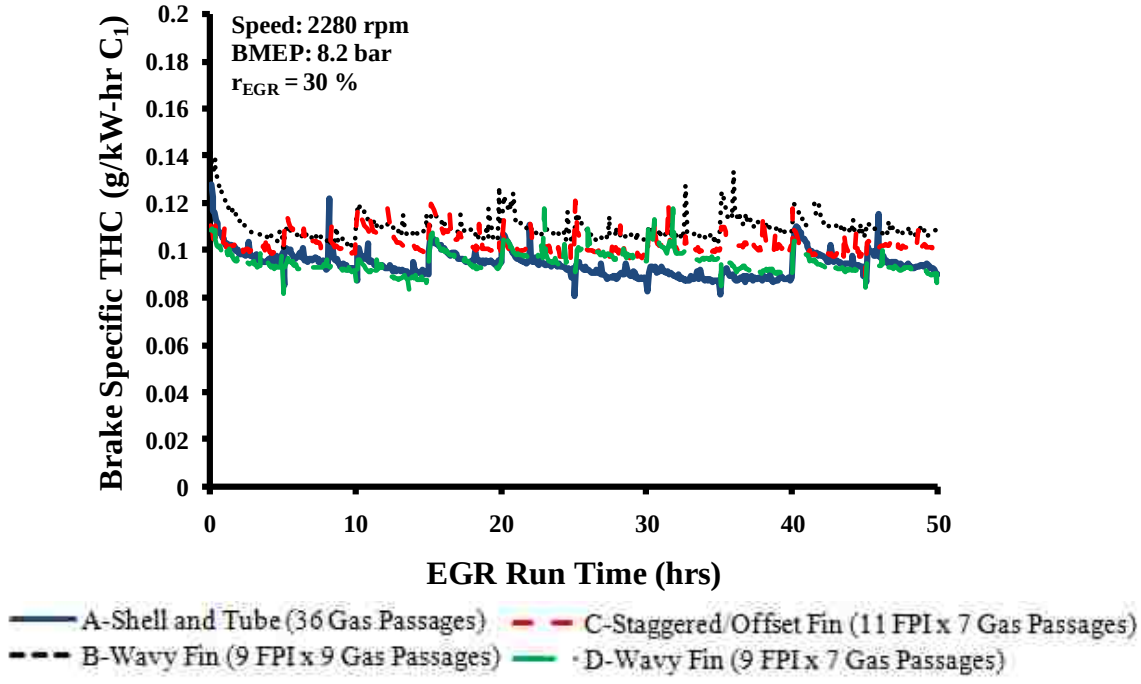

(b) r_{EGR} = 30%

Figure 5.23: Engine-out THC emissions

CARBON MONOXIDE (CO)

In similar fashion, the effects of EGR cooler performance deterioration can also be observed through the decrease in CO emissions levels over time as shown in Figure 5.24.

The presented results of the pollutant species indicate that the EGR cooler performance degradation can cause significant impacts on engine operation and emissions.

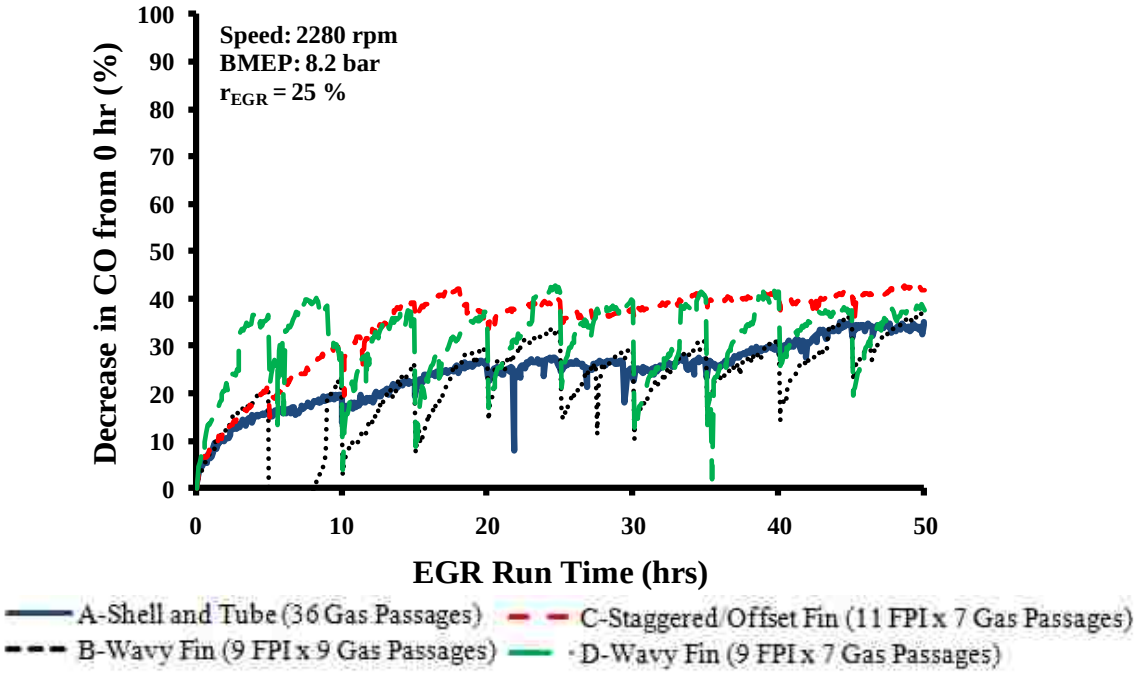

(a) r_{EGR} = 25%

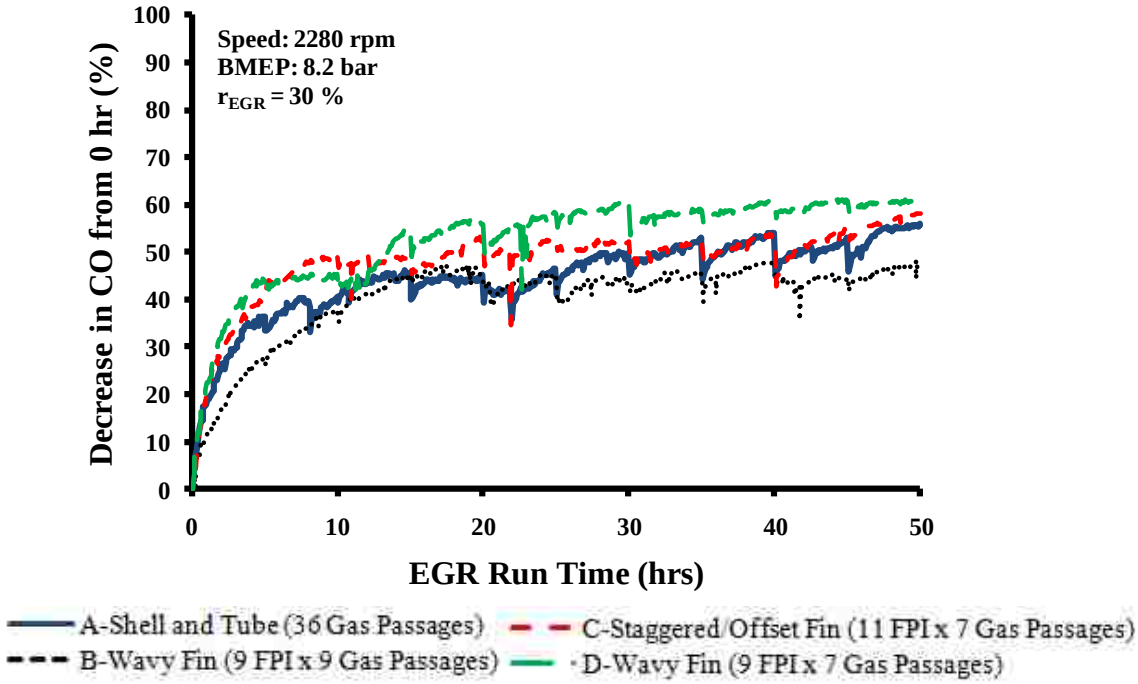

(b) r_{EGR} = 30%

Figure 5.24: Percent decrease in engine-out CO emissions from initial condition

5.2.7 The Need for a Secondary Low Temperature (LT) Cooler

Based on the analysis of the results presented in the previous sections of the report, design B demonstrated best performance in comparison to the other designs and was superior to fouling resistance. Thus, design B will be considered for the investigation of the usefulness of a low temperature cooler circuit.

Theoretically, the high temperature (HT) first pass EGR cooler acts as a filter, reducing the amount of fouling matter that passes through the low temperature (LT) EGR cooler. Thus, it would be expected that the LT cooler exhibit less degradation due to fouling and this argument was supported by the average results summarized in Table 5.9. For case (a), r_{EGR} = 25%, the HT effectiveness degradation and absolute increase in pressure drop were 22 % and 76 % respectively, compared to LT effectiveness degradation and absolute increase in pressure drop of 0 % and 52 %.

Table 5.9: Comparison of average HT and LT cooler performance characteristics

Design	r_{EGR} (%)	Mean ε_{HT} (%)	Mean ε_{LT} (%)	Mean Δp_{HT} (kPa)	Mean Δp_{LT} (kPa)	HT $\Delta\varepsilon_{abs}$ (%)	LT $\Delta\varepsilon_{abs}$ (%)	HT Δp_{abs} (%)	LT Δp_{abs} (%)
B	25	75	87	12.9	5.4	22	0	76	52
	30	72	82	10.7	5.3	23	4	96	59

The end goal of EGR cooling is to reduce the temperature of the exhaust gases as much as possible and it is desirable to quantify the contribution of each cooler (HT and LT) in the EGR circuit. The total reduction in gas temperature was calculated as the difference between HT inlet ($T_{HT,IN}$) and LT outlet ($T_{LT,OUT}$) and the individual contribution of each cooler as a percentage of the total reduction was determined as in Equation 5.2 and Equation 5.3.

$$\%\Delta T_{HT\ CONTRIBUTION} = \frac{T_{HT,IN} - T_{HT,OUT}}{T_{HT,IN} - T_{LT,OUT}} \times 100\% \qquad \text{Equation 5.2}$$

$$\%\Delta T_{LT\ CONTRIBUTION} = \frac{T_{LT,IN} - T_{LT,OUT}}{T_{HT,IN} - T_{LT,OUT}} \times 100\% \qquad \text{Equation 5.3}$$

The results of Figure 5.25 indicate that the contribution of the HT cooler in total gas temperature reduction was most significant throughout the 50 hour test period. However, as HT performance degrades with time, the LT cooler becomes more significant in overall temperature reduction and makes up for the lost performance in the HT cooler.

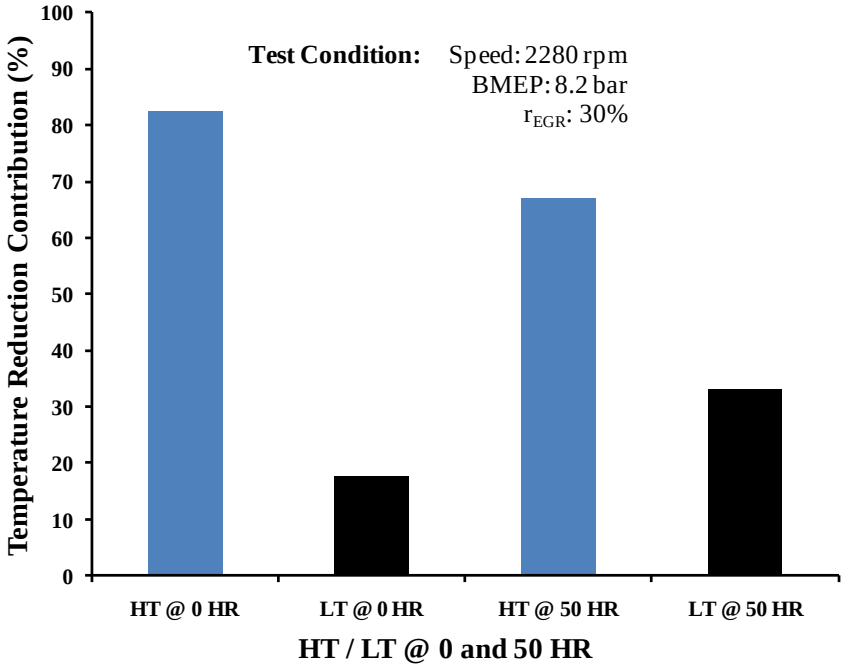

Figure 5.25: HT and LT contributions to total exhaust gas temperature reduction

Clearly illustrated in Figure 5.15, the performance of the HT cooler alone was not sufficient in meeting the pre-described gas outlet temperatures hence a secondary cooler would be necessary. The implementation of a secondary EGR cooler involves the design of a secondary coolant system/circuit on the engine. This would require more components such as a secondary water pump and the EGR cooler itself adding weight

and cost to the overall engine design making the secondary EGR cooler an arguably costly consideration.

5.2.8 Summary of Cooler Design Comparison

From the results of the standardized experiments it was evident that cooler design B (wavy fin type) displayed the best overall performance in comparison to the alternative designs. Although some difficulties were experienced in controlling initial conditions of Smoke and EGR mass flow rate, the average values were within reasonable limits for comparability with Smoke ranging from 1.07 to 1.52 FSN, and $\dot{m}_{EGR}$ between 163 and 170 kg/hr for case (b) tests. The following interval plots of Figure 5.26 summarize the findings of the investigation and show the overall superiority of Design B performance.

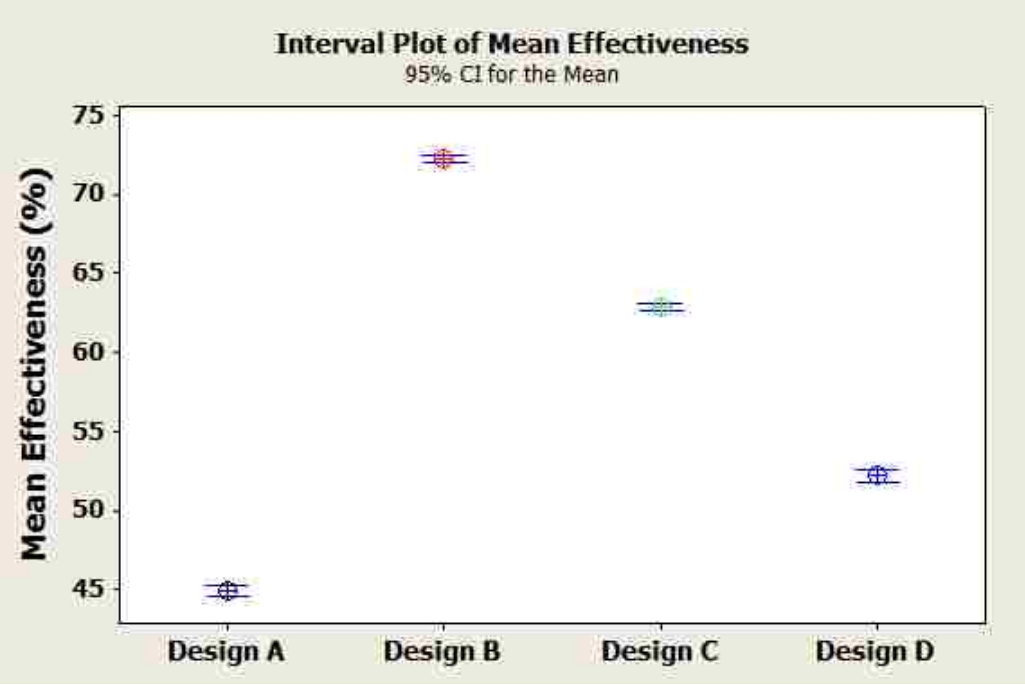

(a) Interval plot of mean effectiveness

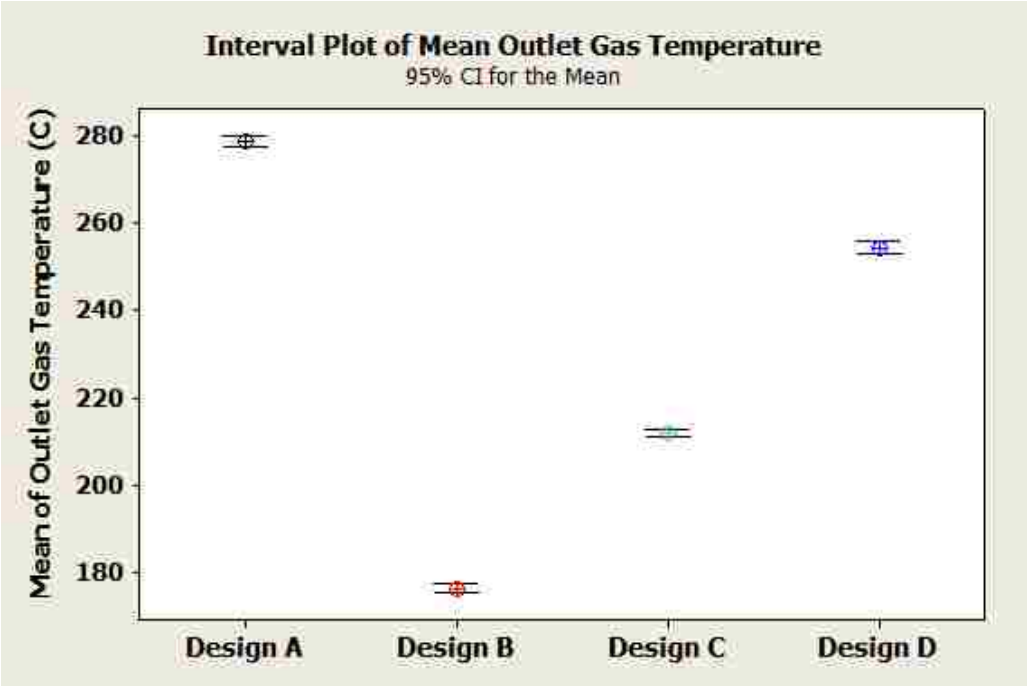

(b) Interval plot of mean outlet gas temperature

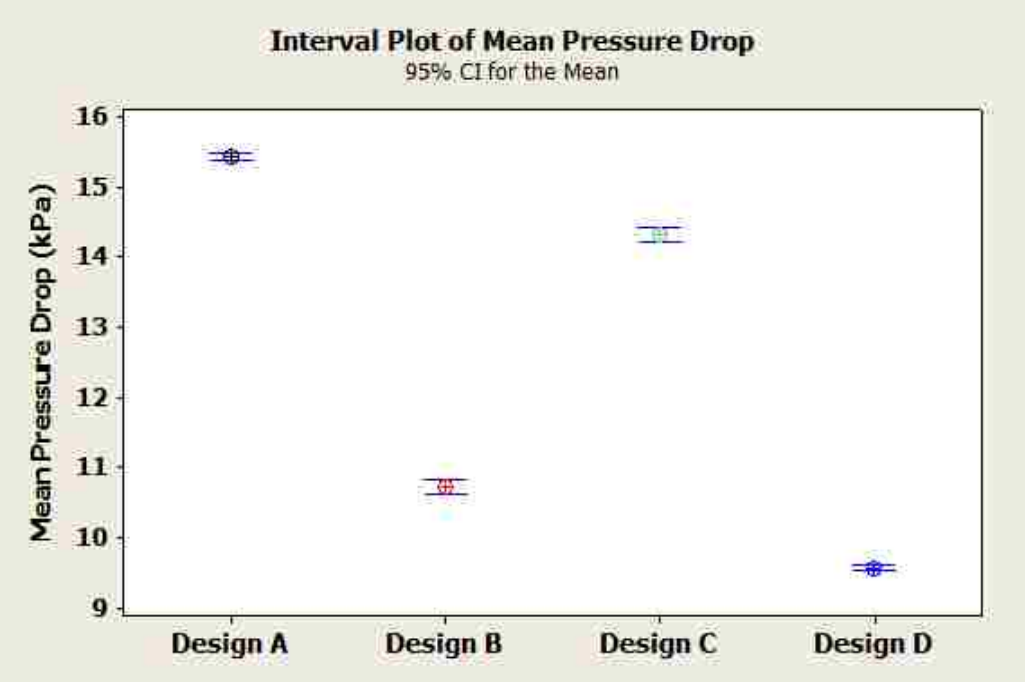

(c) Interval plot of mean pressure drop

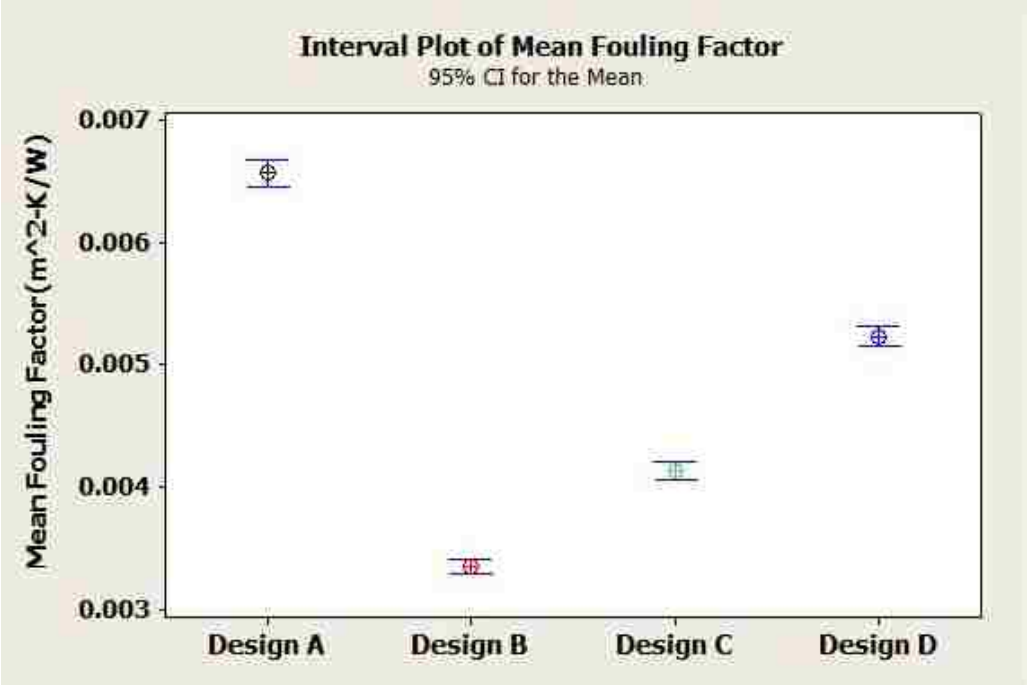

(d) Interval plot of mean fouling factor

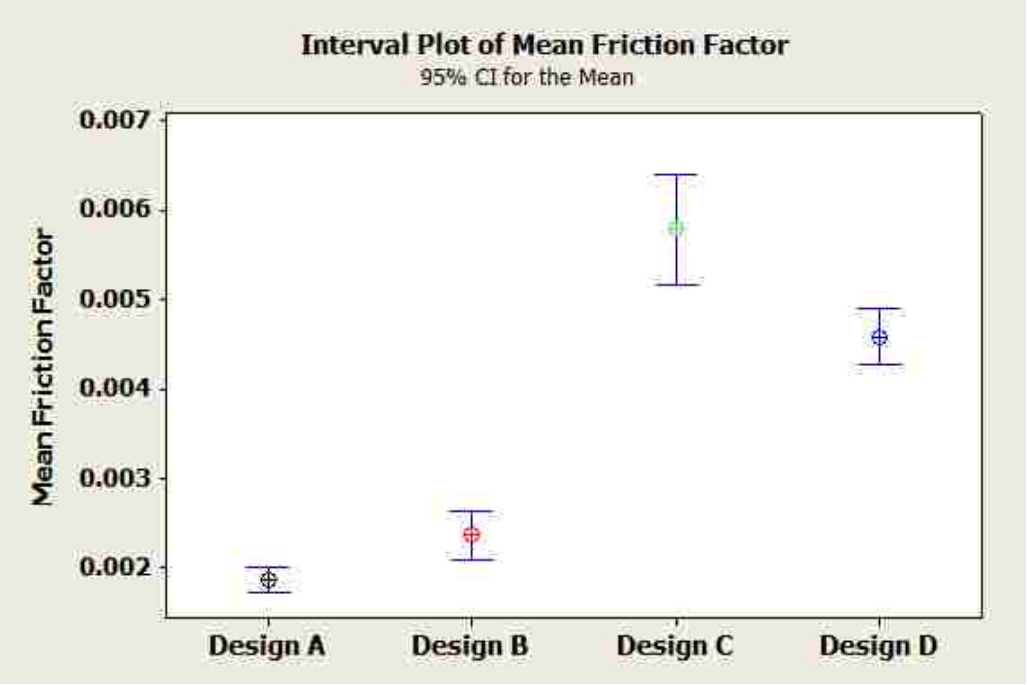

(e) Interval plot of mean friction factor

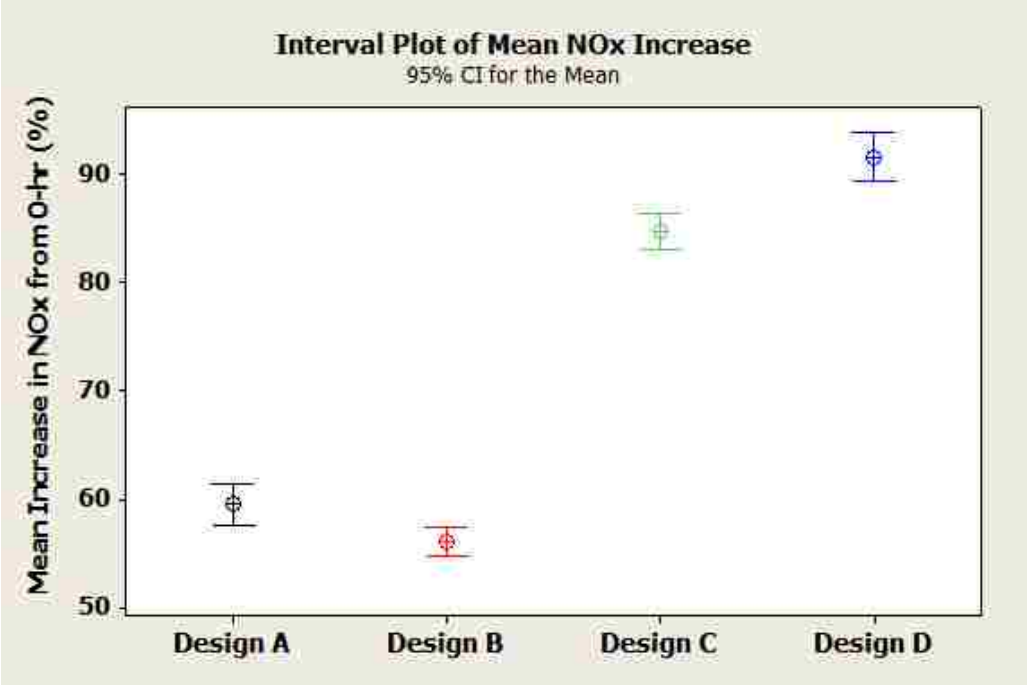

(f) Interval plot of mean NO_x increase

Figure 5.26: Summary of cooler design comparison study

5.3 Aspects of Coolant Flow Configuration on Fouling

5.3.1 Methodology

To study the effects of coolant flow configuration on fouling behaviour, designs F, G, and H with characteristics listed in Table A.2 were tested at the B50 operating condition with both counter flow and parallel flow setups. Table 5.10 summarizes the tests conducted for this investigation.

From Table 5.10, it can be seen that similar challenges were experienced in achieving the target test conditions as in the previous experiments. At the B50 operating condition with EGR valve fully opened (i.e. 100%) the EGR flow did not meet the desired value of 200 kg/hr. Thus, the engine intake was throttled to induce more flow of exhaust gases resulting in an increase in PM emissions. To achieve the desired flow, some tests required an intake throttle position greater than 60% which may be harmful to the engine operation. To prevent any detrimental engine damage, it was decided to limit the intake

throttling to 60% maximum. Ultimately, the most important factor with regards to experimentation was consistency and standardization of tests which would provide conclusive comparative results.

Table 5.10: Test matrix for coolant flow configuration study

			TARGET VALUES		
			r_{EGR} (%)	$\dot{m}_{EGR}$ (kg/hr)	Smoke (FSN)
			30	**200**	**1.5**
			ACTUAL (INITIAL) VALUES		
COOLER DESIGN	F	PF	25	176	2.22
		CF	29	201	2.44
	G	PF	27	177	2.54
		CF	30	206	2.84
	H	PF	27	177	2.37
		CF	30	198	2.56

PF – PARALLEL FLOW CONFIGURATION / CF – COUNTER FLOW CONFIGURATION

5.3.2 Comparing Parallel and Counter Flow Effectiveness

The results of effectiveness are shown in Figure 5.27. A noteworthy observation is that the tests with parallel flow configurations seemed to exhibit more significant and consistent recovery occurrences after every cold soak period in the test cycle as compared to the counter flow case. The recovery action provided sudden improvement in the cooler effectiveness, but quickly degraded within the 5 hour steady state interval. Further investigations are required to validate this observation and determine whether the parallel flow of coolant to exhaust can enhance the recovery of cooler performance.

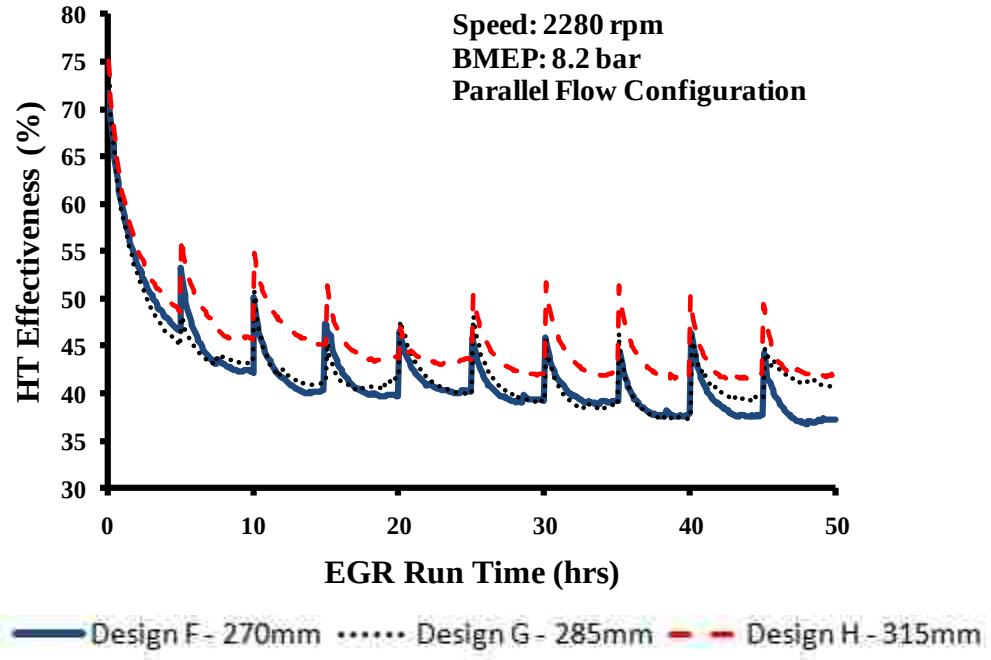

(a) Parallel Flow Configuration

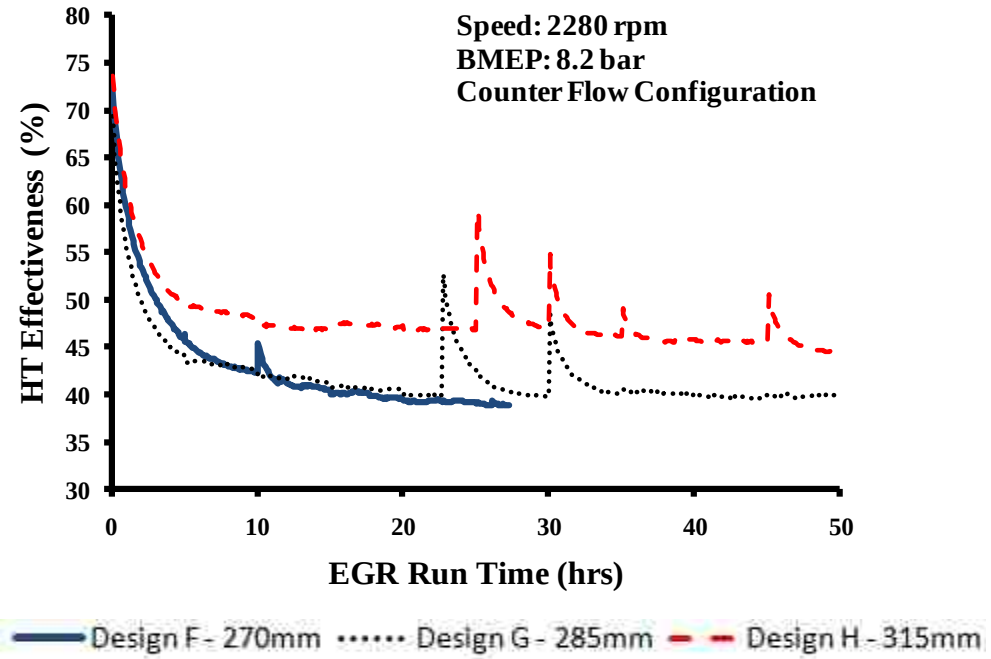

(b) Counter Flow Configuration

Figure 5.27: Comparing effectiveness of parallel flow and counter flow configurations

From the results of Table 5.11, it is evident that there was no significant difference between the parallel and counter flow configurations. Both, the absolute degradation in

effectiveness and average fouling factors for the PF configuration seemed to be slightly higher than the CF case. However, this trend is not believed to be related to the cooler configuration, rather a result of the variation in the initial operating conditions between experiments (i.e. $\dot{m}_{EGR}$). The effects of EGR mass flow rate on fouling are discussed in the next section.

Table 5.11: High temperature effectiveness - PF vs. CF

Design	F		G		H	
Configuration	**PF**	**CF**	**PF**	**CF**	**PF**	**CF**
ε_{0HR}	72	73	74	69	75	74
ε_{50HR}	37	39	37	39	41	44
$\Delta\varepsilon_{abs}$	48	47	45	42	44	40
R_f (m^2-K/W)	0.0151	0.0064	0.0135	0.0065	0.0100	0.0059

5.3.3 Comparing Parallel and Counter Flow Pressure Drop

A summary of the pressure drop and friction factor data is presented in Table 5.12. The percentage (absolute) increase of friction factor from initial conditions was also presented in Table 5.12 and was determined as in Equation 5.4.

$$\Delta f_{abs} = \frac{f_{steady\ state} - f_{initial}}{f_{initial}} \qquad \text{Equation 5.4}$$

Table 5.12: Summary of pressure drop for parallel and counter flow configuration

Design	F		G		H	
Configuration	**PF**	**CF**	**PF**	**CF**	**PF**	**CF**
Δp_{avg} (kPa)	8.15	9.23	7.46	9.25	9.54	10.51
f_{avg}	.000546	0.000487	0.000537	0.000529	0.000492	0.000537
Δf_{abs} (%)	128	125	159	110	118	113
$\dot{m}_{EGR}$ (kg/hr)	143	164	141	158	142	166

The results indicate that for each cooler design, the parallel flow configuration experienced slightly larger increases in fouling factor throughout the test cycle (i.e. larger values of Δf_{abs}). This outcome is believed to be due to the test conditions which were not controlled strictly enough. Figure 5.28 illustrates the mass flow rate and smoke levels for cooler design H tests with both parallel and counter flow configurations. From this graph, it is clear that the smoke levels between tests were held relatively close unlike the EGR mass flow rates. Higher EGR mass flow rates were witnessed in the counter flow configurations providing higher Reynolds numbers which are believed to enhance deposit removal mechanisms such as blow out, flaking, and wash out as explained in Chapter 2.

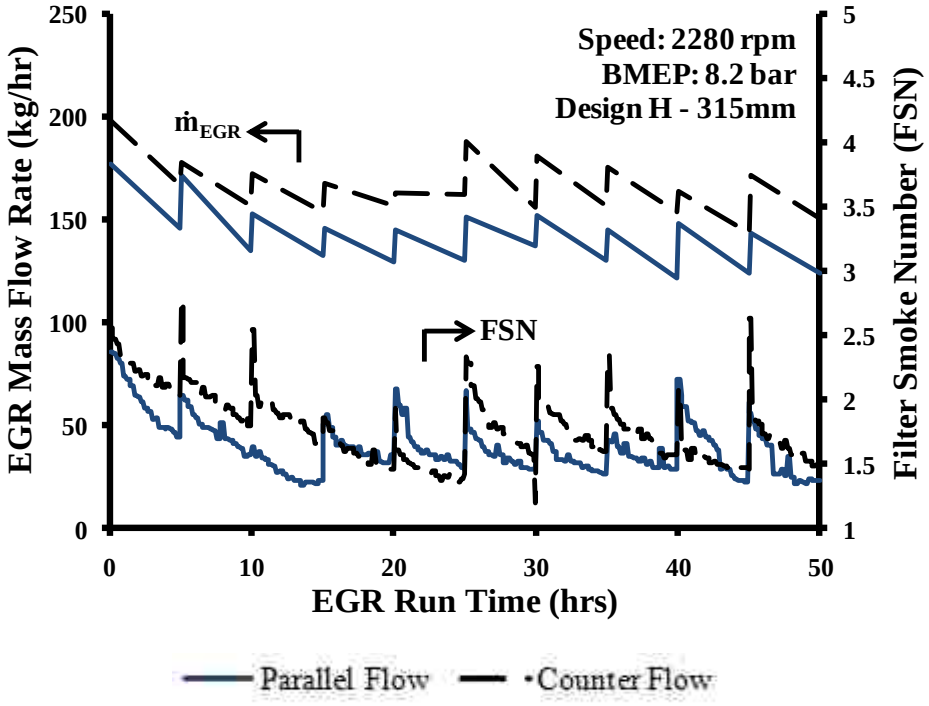

Figure 5.28: EGR mass flow rate and smoke levels for parallel and counter flow

5.3.4 Summary - Aspects of Coolant Flow Configuration on Fouling

Under the operating conditions chosen for the experiments, an interesting trend was observed in the findings of EGR cooler effectiveness. The cooler designs with parallel flow configurations displayed more prominent and consistent recovery actions during

engine startup after cold soak periods. This outcome requires further investigation for validation.

5.4 Effects of Cooler Fin Density

5.4.1 Methodology

To study the effects of cooler fin density on fouling behaviour, designs J (9FPI), K (11FPI), and L (14FPI), detailed in Appendix A.4, were tested at the B50 operating condition. Table 5.13 summarizes the tests conducted for this investigation.

Table 5.13: Test matrix for cooler fin density study

Design		**J**	**K**	**L**
Fin Density (FPI)		9	11	14
Initial Conditions	**$\dot{m}_{EGR}$ (kg/hr)**	276	265	292
	Smoke (FSN)	1.00	1.3	1.17
Averages	**$\dot{m}_{EGR}$ (kg/hr)**	262	261	270
	Smoke (FSN)	1.53	1.32	1.09

5.4.2 Effects of Fin Density on Effectiveness

The results of effectiveness for the high temperature EGR coolers are plotted in Figure 5.29. As expected, the higher fin density designs provided greatest reduction in EGR gas temperatures owing to the increased heat transfer surface area. However, the results also seem to indicate that the higher fin density cooler designs suffered the least degradation in heat transfer performance throughout the 50 hour test cycle. This outcome is inconsistent with previous studies performed by the group and requires further explanation. The absolute degradation and average fouling factors of the designs are summarized and presented in Table 5.14.

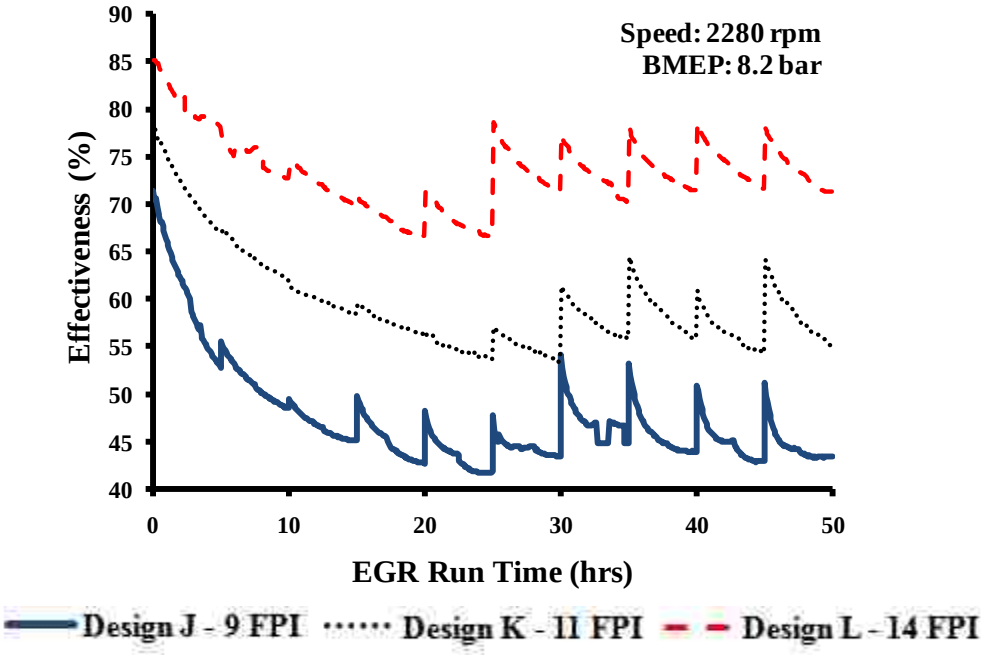

Figure 5.29: Effects of fin density on cooler effectiveness

The values of Table 5.14 alone suggest that the higher fin density designs were superior in heat transfer performance, though it should be noted that these values do not accurately describe the events that may have occurred during the experiments. For example, it is evident from Figure 5.29 that cooler design L (14 FPI) experienced a significant recovery action at the 25 hour point in the test cycle, causing a sudden 18% enhancement in effectiveness which improves the overall average performance of the cooler. Thus, more attention should be dedicated to the recovery actions and other performance behaviours throughout the test cycle.

Table 5.14: Summary of effectiveness trends with cooler fin density

Design	**J**	**K**	**L**
Fin Density (FPI)	**9**	**11**	**14**
ε_{0HR}	71	79	85
ε_{50HR}	43	55	71
$\Delta\varepsilon_{abs}$	39	30	16
R_f (m^2-K/W)	0.0041	0.0023	0.0018

Figure 5.30 identifies the recovery in effectiveness ($\varepsilon_{recovery}$), as defined in Equation 5.5, of each cooler design after the cold soak cycle was completed. It is apparent from Figure 5.30 that no distinct relationship exists between fin density and effectiveness performance recovery. Nevertheless, the recovery actions of the individual coolers became more significant with time, confirming theory that deposit removal mechanisms become more significant as fouling increases.

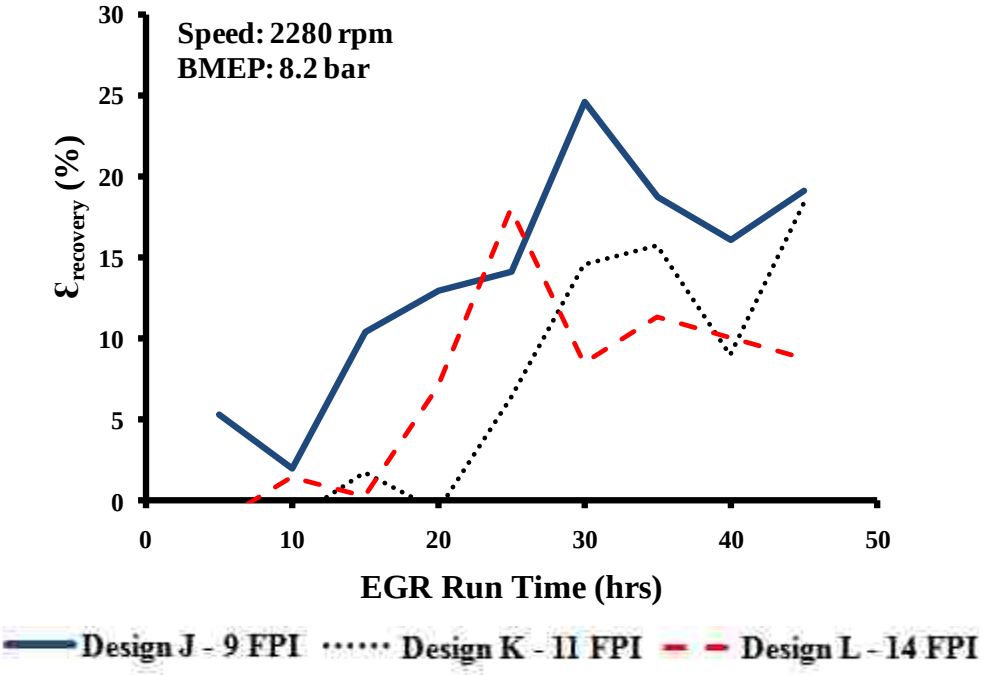

Figure 5.30: Recovery in effectiveness – a function of fin density

$$\varepsilon_{recovery} = \frac{\varepsilon_{after\,soak} - \varepsilon_{before\,soak}}{\varepsilon_{before\,soak}} \qquad \text{Equation 5.5}$$

The next section provides discussion of the pressure drop characteristics and trends witnessed in the experiments.

5.4.3 Effects of Fin Density on Pressure Drop

The pressure drop findings are shown in Figure 5.31. With increasing fin density, one would expect a higher resistance (or blockage) of flow as witnessed in Figure 5.31. Although design L (14 FPI) suffered from higher gas pressure drops through the cooler

core as compared to the other less dense designs, a non-dimensional analysis of the data clearly shows that design L was least effected by fouling.

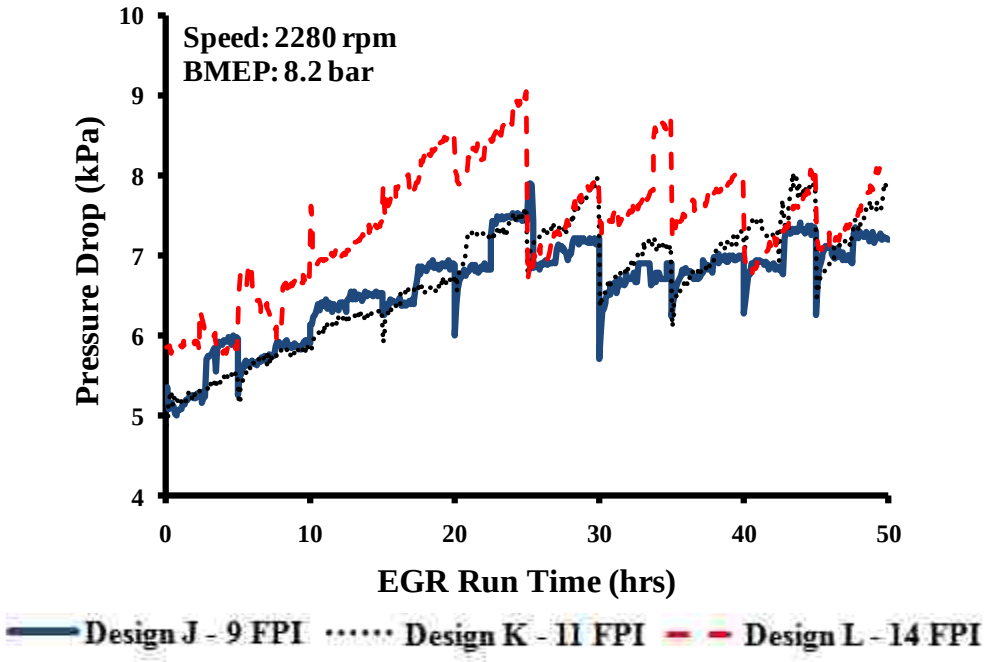

Figure 5.31: Effects of fin density on cooler pressure drop

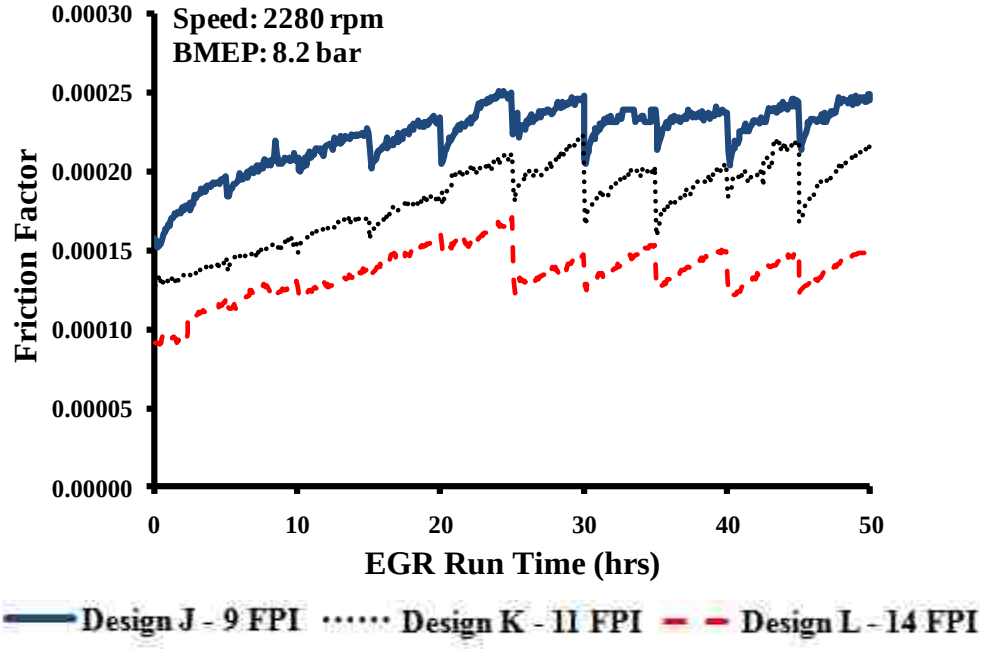

Figure 5.32: Relating fin density with non-dimensional friction factor

Figure 5.32 illustrates that reduction of fouling may be achieved with increasing fin density, but this outcome does not concur with previous work [26] and further analysis of other test parameters is necessary to determine the root cause of this trend.

The EGR mass flow rates and smoke levels are presented in Figure 5.33. The initial smoke levels were relatively close (within 0.3 FSN) between experiments, but diverged with time. The percentage increase of smoke levels from initial values for designs J, K, and L was 87, 45, and 0 % respectively. As discussed previously, soot is known to be the most significant constituent in diesel exhaust gas that contributes to cooler fouling. Accordingly, the increased fouling behaviours that were witnessed in the lower fin density designs may be attributed to the higher soot levels observed within these coolers and not a result of the fin density.

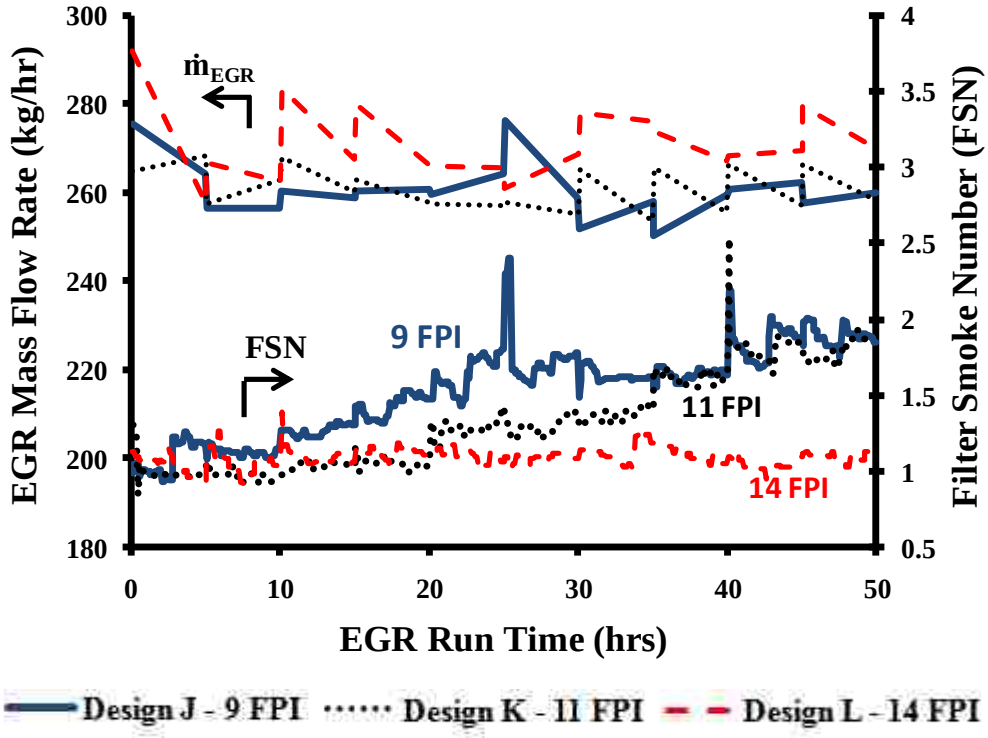

Figure 5.33: Differences in EGR mass flow rates and smoke levels

Furthermore, slight differences in the EGR mass flow rates between the tests were observed. From Figure 5.33, design L (14 FPI) maintained a higher EGR mass flow rate

throughout the majority of the test cycle which could have enhanced the deposit removal mechanisms and reduced the overall fouling of the cooler.

5.4.4 Summary - Aspects of Cooler Fin Density on Fouling

An increase in the fin density provided greater reduction in gas temperatures owing to the increased heat transfer surface area of the fins. Results of the experiment showed that increasing fin density reduced fouling and clogging risk. However the outcome conflicted with previous work [26] and through further investigation was attributed to differences in EGR mass flow rate and soot levels between tests. Ultimately, this particular investigation identified the importance of controlling and standardizing experimental parameters.

5.5 Effects of Particulate Filtration

5.5.1 Methodology

In order to establish the effects of particulate filtration on EGR cooler fouling, the following experiments summarized in Table 5.15 were conducted. Cooler design L (14 FPI) was tested with and without the implementation of a diesel particulate filter (DPF) upstream. Two DPFs of different filtration efficiencies (50% and 70%) were employed and will be referred to as DPF-50 and DPF-70 throughout the discussion. It should be noted that the smoke levels were measured in the diesel exhaust upstream of the diesel particulate filter and not at the cooler inlet.

Table 5.15: Test matrix for filtration effects on EGR cooler fouling investigation

DPF		**NO-DPF**	**DPF-50**	**DPF-70**
Filtration Efficiency (%)		0	50	70
Initial Conditions	**r_{EGR} (%)**	25	25	25
	$\dot{m}_{EGR}$ (kg/hr)	292	313	313
	Smoke (FSN)	1.13	1.15	1.52
Averages	**$\dot{m}_{EGR}$ (kg/hr)**	270	302	289
	Smoke (FSN)	1.09	1.11	1.71

5.5.2 Filtration Efficiency and EGR Cooler Effectiveness

The results of effectiveness for the aforementioned tests are presented in Figure 5.34. The initial effectiveness performance of the cooler was approximately 86% for all three cases and as expected the NO-DPF case suffered the largest degradation due to fouling. The degradation in effectiveness after 25 hours of EGR cooler runtime for the three cases NO-DPF, DPF-50, and DPF-70, were 22%, 9%, and 7% respective. During startup after the 30 minute soak period at the 25 hour mark, a significant 19% improvement in cooler effectiveness was witnessed for the NO-DPF case. From the literature survey of Chapter 2 it was mentioned that the deposit removal mechanisms are proportional to the deposit mass. Hence, it is believed that the soot accumulation in the cooler for the NO-DPF case was sufficient in promoting the removal of deposits and caused a sudden improvement in effectiveness performance.

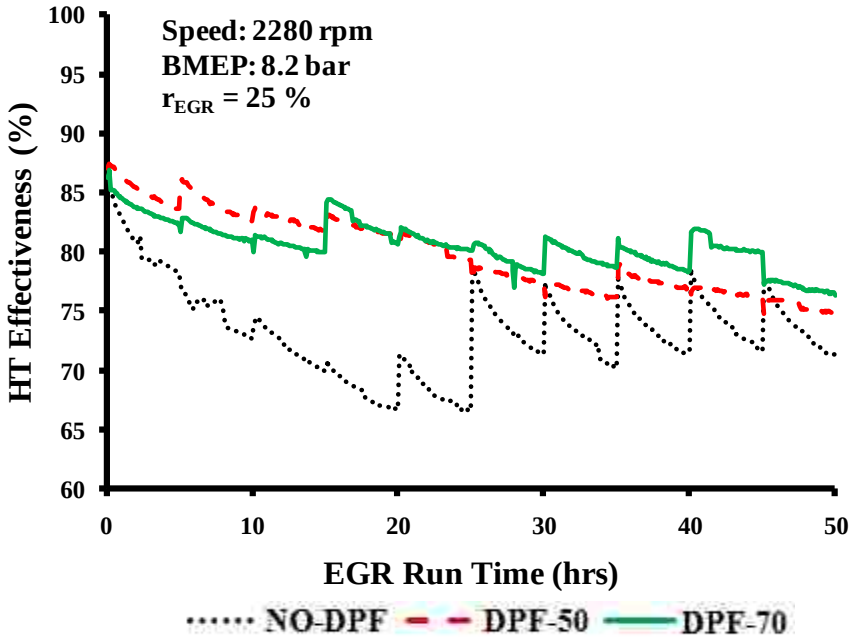

Figure 5.34: Improvement in effectiveness with particulate filtration

In addition to effectiveness, the results of fouling factor also signify the improvement in cooler fouling behaviour with particulate filtration.

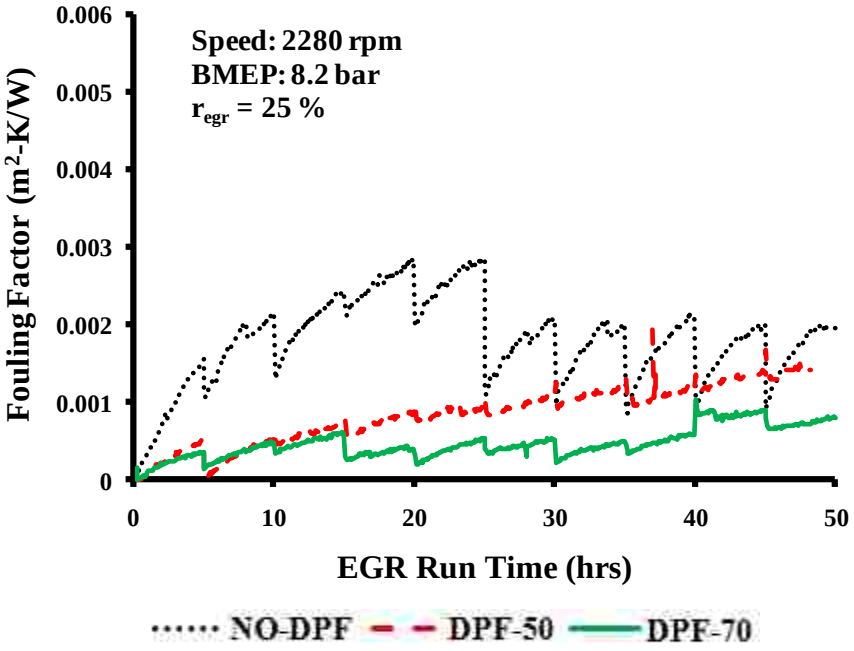

Figure 5.35: Improvement in fouling factor with particulate filtration

5.5.3 Filtration Efficiency and EGR Cooler Pressure Drop

Displayed in the following figure are results for the increase in pressure drop from the initial value. Again the trend suggests that the filtration of the particulate matter in the exhaust gas prevents the performance degradation of the EGR cooler. The absolute increase in the pressure drop of cooler design L with NO-DPF, DPF-50, and DPF-70 was 38%, 33%, and 24% respectively.

The increase in friction factor from initial (0 hour) conditions shows a significant difference in results between the filtered and un-filtered cases. Figure 5.37 shows that the fouling factor nearly doubled (increased by 85%) after 25 hours of EGR run time for the NO-DPF case as compared to a 20% increase seen in both the DPF-50 and DPF-70 scenarios.

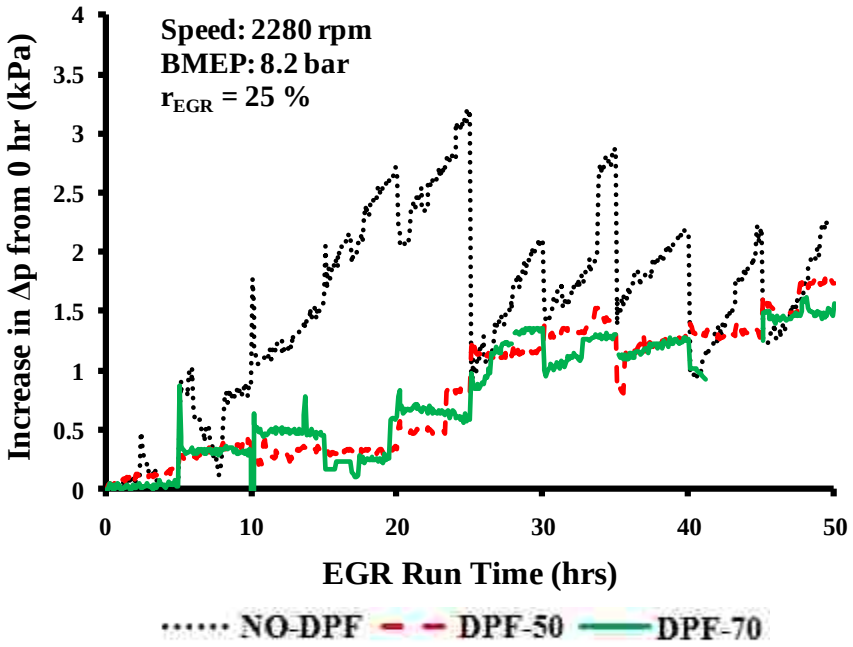

Figure 5.36: Effects of filtration on the increase in pressure drop with time

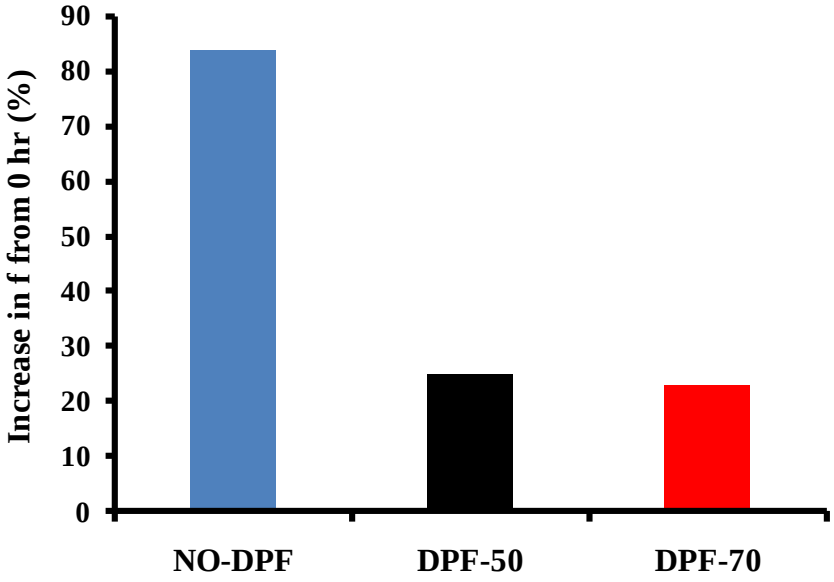

Figure 5.37: Increase in friction factor from initial value after 25 hours of run time

5.5.4 Summary - Aspects of Particulate Filtration on Fouling

From the observations of this study, the use of particulate filtration can be extremely effective in reducing the EGR cooler fouling process and maintaining cooler performance for longer operating times. Additionally, there was no significant difference in cooler

performance when comparing the DPF-50 and DPF-70 test results. It may be possible to determine an optimum filtration efficiency that would provide the most cost effective solution for implementation in production vehicles.

CHAPTER VI

6 CONCLUSIONS

With the completion of this investigation, the following conclusions were reached:

1. A standardized EGR cooler fouling experimental setup was developed for comparing various competitive EGR cooler designs. The experimental methods and test procedures were adapted from corporate test procedures for cooler fouling studies performed by Ford Motor Company.
2. The repeatability study showed good agreement in the results of the repeated tests. Thus, validating the design of the experiment.
3. A detailed performance comparison analysis of the various EGR coolers identified the advantage of cooler design B (wavy fin) in fouling resistance and stabilization characteristics. The analysis was based on standard performance measures such as effectiveness, fouling factor, pressure drop, friction factor, mass flow rate, and engine-out NOx emissions.
4. The EGR mass flow rate and soot levels in the exhaust stream were major factors contributing to the EGR cooler performance under fouling conditions. Increasing EGR mass flow rate reduces fouling factor and enhances deposition removal mechanisms. Increasing soot emissions results in more significant cooler degradation owing to the higher soot accumulation on the cooler surfaces.
5. The performance degradation due to fouling resulted in a 50% increase in engine-out NOx emissions over 50 hours of run time. The increase in NOx was attributed to the diminishing EGR flow rate that results due to cooler blockage from fouling.
6. The parallel and counter flow configurations did not show any significant differences in overall cooler performance. However, the parallel flow configuration did exhibit more consistent and significant cooler recovery actions after the shutdown periods, but further investigation is required to validate this outcome.

7. An increase in the fin density from 9 to 11 to 14 fins per inch provided progressively lower exhaust gas temperatures and lower susceptibility to fouling.

CHAPTER VII

7 RECOMMENDATIONS

The following recommendations are made for the future enhancement and development of EGR cooler fouling studies:

1. Improvements in the control of EGR mass flow rate and soot concentration are required for better consistency of the experiments.
2. Simultaneous measurements of intake and exhaust CO_2 should be used to provide more stable readings used to calculate EGR rate.
3. Measurements of soot concentration before and after the EGR cooler would be useful to correlate the performance degradation to accumulation of soot.
4. Monitoring parameters during engine shutdown period may provide more insight on cooler recovery behaviours.

REFERENCES

1. Zheng, M., Reader, G., Hawley, J. (2004). "Diesel Engine Exhaust Gas Recirculation - A Review on Advanced and Novel Concepts", *International Journal of Energy Conversion and Management*, *45*(6), 883-900.
2. Greeves, G., C.H.T. Wang., (1981). “Origins of Diesel Particulate Mass Emission", SAE Paper No. 810260.
3. Majewski, W.A., Khair, M.K. (2006). *Diesel emissions and their control*. Warrendale, Pa.: SAE International.
4. Zhao, H., Hu, J., Ladommatos, N., (2000). "In-Cylinder Studies of the Effects of CO2 in Exhaust Gas Recirculation on Diesel Combustion and Emissions", *Journal of Process Mechanical Engineering, Part D*, 214, 405-419.
5. Jacobs, T., D. Assanis., Z. Filipi., (2003). “The Impact of Exhaust Gas Recirculation on Performance and Emissions of a Heavy-Duty Diesel Engine", SAE Paper No. 2003-01-1068.
6. Idicheria, C.A., L.M. Pickett., (2005). “Soot Formation in Diesel Combustion under High-EGR Conditions", SAE Paper No. 2005-01-3834.
7. Ladommatos, N., S.M. Abdelhalim., H. Zhao., Z. Hu., (1996). “The Dilution, Chemical, and Thermal Effects of Exhaust Gas Recirculation on Diesel Engine Emissions – Part 1: Effect of Reducing Inlet Charge Oxygen”, SAE Paper No. 961165.
8. Ladommatos, N., S.M. Abdelhalim., H. Zhao., Z. Hu., (1996). “The Dilution, Chemical, and Thermal Effects of Exhaust Gas Recirculation on Diesel Engine Emissions – Part 2: Effects of Carbon Dioxide”, SAE Paper No. 961167.
9. Ladommatos, N., S.M. Abdelhalim., H. Zhao., Z. Hu., (1997). “The Dilution, Chemical, and Thermal Effects of Exhaust Gas Recirculation on Diesel Engine Emissions – Part 3: Effects of Water Vapour”, SAE Paper No. 971659.
10. Ladommatos, N., S.M. Abdelhalim., H. Zhao., Z. Hu., (1997). “The Dilution, Chemical, and Thermal Effects of Exhaust Gas Recirculation on Diesel Engine Emissions – Part 4: Effect of Carbon Dioxide and Water Vapour”, SAE Paper No. 971660.
11. Ladommatos, N., S.M. Abdelhalim., H. Zhao., Z. Hu., (1998). “The Effects on Diesel Combustion and Emissions of Reducing Inlet Charge Mass Due to Thermal Throttling with Hot EGR”, SAE Paper No. 980185.

12. Wagner, R.M., J.B. Green Jr., J.M. Storey., C.S. Daw., (2000). “Extending Exhaust Gas Recirculation Limits in Diesel Engines", AWMA 93rd Annual Conference and Exposition, Salt Lake City, UT, June 18-22, 2000, http://www-chaos.engr.utk.edu/pap/crg-awma2000.pdf
13. Mulenga, C.M., D.K. Chang., J.S. Tjong., D. Styles., (2009). “Diesel EGR Cooler Fouling at Freeway Cruise”, SAE Paper No. 2009-01-1840.
14. Tomazic, D., A. Pfeifer., (2002). “Cooled EGR – A Must or an Option for 2002/04”, SAE Paper No. 2002-01-0962.
15. van Aken, M., F. Willems., D.J. de Jong., (2007). “Appliance of High EGR Rates With a Short and Long Route EGR System on a Heavy Duty Diesel Engine", SAE Paper No. 2007-01-0906.
16. Mellow, J.P., A.M. Mellor., (1999). "NOx Emissions from Direct Injection Diesel Engines with Water/Steam Dilution", SAE Paper No. 1999-01-0836.
17. Broda, A., M. Rieping., P. Eilts., A. Elsäβer., M. Lau., (2008). “Advanced EGR Control for HD-Truck-Engines", SAE Paper No. 2008-01-1200.
18. Zheng, M., Reader, G., (1995). "Preliminary Investigation of Cycle to Cycle Variations in a Nonair-Breating Diesel Engine", *Journal of Energy Resources Technology*, 117(1), 24-29.
19. Zheng, M., Reader, G., (1993). "An Experimental Analysis of EGR on Operational Stabilities of Diesel Engines", *ASME ICE*, 36(1), 101-106B.
20. Bejan, A., Tsatsaronis, G., Moran, M. J. (1996). *Thermal design and optimization*. New York: Wiley.
21. Hesselgreaves, J. E. (2001). *Compact heat exchangers: selection, design, and operation*. Amsterdam: Pergamon.
22. Shah, R. K., Sekulić, D. P. (2003). *Fundamentals of heat exchanger design*. Hoboken, NJ: John Wiley & Sons.
23. Russell, T. W., Robinson, A. S., Wagner, N. J. (2008). *Mass and heat transfer: analysis of mass contactors and heat exchangers*. Cambridge: Cambridge University Press.
24. Murayama, T., M. Zheng., T. Chikahisa., Y.T. Oh., Y. Fujiwara., S. Tosaka., M. Yamashita., H. Yoshitake., (1995). “Simultaneous Reductions of Smoke and NOx from a DI Diesel Engine with EGR and Dimethyl Carbonate", SAE Paper No. 952518.
25. Heywood, J.B. (1988). *Internal combustion engine fundamentals*. New York: McGraw-Hill.

26. Hoard, J., M. Abarham., D. Styles., J.M. Giuliano., S.C. Sluder., J. Storey., (2008). "Diesel EGR Cooler Fouling", SAE Paper No. 2008-01-2475.
27. Hoard, J., J.M. Giuliano., D. Styles., S.C. Sluder., J. Storey., S. Lewis., A. Strzelec., M. Lance., (2007). "EGR Catalyst for Cooler Fouling Reduction", DOE Diesel Engine Efficiency and Emission Reduction Conference, Detroit, MI, August 2007. http://www1.eere.energy.gov/vehiclesandfuels/resources/proceedings/2007_deer_presentations.html.
28. Merker, G.P., Schwarz, C., Stiesch, G., Otto, F. (2006). *Simulating combustion: simulation of combustion and pollutant formation for engine development*. Berlin: Springer-Verlag.
29. Girard, J.W., L.D. Gratz., J.H. Johnson., S.T. Bagley., D.G. Leddy., (1999). "A Study of the Character and Deposition Rates of Sulfur Species in the EGR Cooling System of a Heavy-Duty Diesel Engine", SAE Paper No. 1999-01-3566.
30. Epstein, N., (1997). "Elements of Particle Deposition onto Nonporous Solid Surfaces Parallel to Suspension Flows", *Experimental Thermal and Fluid Science*, 14(1), 323-334.
31. Teng, H., G. Regner., (2009). "Characteristics of Soot Deposits in EGR Coolers", SAE Paper No. 2009-01-2671.
32. Abarham, M., J. Hoard., D. Assanis., D. Styles., E.W. Curtis., N. Ramesh., C.S. Sluder., J. Storey., (2009). "Modeling of Thermophoretic Soot Deposition and Hydrocarbon Condensation in EGR Coolers", SAE Paper No. 2009-01-1939.
33. Chang, D.K., A. Sobh., J.S. Tjong., D. Styles., J.J. Szente., (2010). "Diesel EGR Cooler Fouling with Ni-Fe-Cr-Al DPF at Freeway Cruise", SAE Paper No. 2010-01-1955.
34. Mogi, H., K. Tajima., M. Hosoya., M. Shimoda., (1999). "The Reduction of Diesel Engine Emissions by Using the Oxidation Catalysts on Japan Diesel 13 Mode Cycle", SAE Paper No. 1999-01-3558.
35. Stone, R (1999). *Introduction to internal combustion engines* (3rd ed). Warrendale, Pa: Society of Automotive Engineers.
36. PMT Products, Inc., 2002, "Model SPT Amplified Output Pressure Transducers", www.ametekusg.com, Accessed November 2009.
37. Brock, J.R., (1962). "On the Theory of Thermal Forces Acting on Aerosol Particles", *Journal of Colloid Science*, 17(8), 768-780.
38. Dec, J.E., (1997). "A Conceptual Model of DI Diesel Combustion Based on Laser-Sheet Imaging", SAE Paper No. 970873.

39. Dec, J.E., R.E. Canaan., (1998). “PLIF Imaging of NO Formation in a DI Diesel Engine”, SAE Paper No. 980147.
40. Dieselnet, 2008, “Emission Standards”, http://www.dieselnet.com/standards, Accessed May 2008.
41. Hashemi, S., Goharrizi, A.S., (2009). "Prediction of Thermophoretic Deposition Efficiency of Particles in a Laminar Gas Flow along a Concentric Annulus: A Comparison of Developing and Fully Developed Flows", *Chinese Journal of Chemical Engineering*, 17(5), 727-733.
42. Hawley, J.G., F.J. Wallace., A. Cox., R.W. Horrocks., G.L. Bird., (1999). “Reduction of Steady State NOx Levels from an Automotive Diesel Engine Using Optimised VGT/EGR Schedules", SAE Paper No. 1999-01-0835.
43. Herzog, P.L., L. Bürgler., E. Winklhofer., P. Zelenka., W. Cartellieri., (1992). “NOx Reduction Strategies for DI Diesel Engines", SAE Paper No. 920470.
44. Ishikawa, N., Y. Ohkubo., K. Kudou., (2007). “Study on the Effects of EGR Cooler Performance on Combustion Properties of the Pre-mixed Compression Ignition Combustion by Multi Cylinder DI Diesel Engine", SAE Paper No. 2007-01-1881.
45. Kalsi, K.S., N. Collings., D.M. Heaton., S.A. Faulkner., (2008). “Study of Steady State of a Medium Duty Diesel Engine", SAE Paper No. 2008-01-2438.
46. Karagiorgis, S., U. Genc., J. Villegas., R. Tafner., M. Wellers., K. Tufail., (2009). “Relay Auto-tuning of PID Controllers for Calibration of EGR Controller Maps in Diesel Engines", SAE Paper No. 2009-01-2746.
47. Thome, J. R., Collier, J. G. (1996). *Convective boiling and condensation* (3rd ed.). Oxford: Clarendon Press.
48. Turns, S.R. (2000). *An introduction to combustion: concepts and applications* (2nd ed.). Boston: WCB/McGraw-Hill.
49. Yokomura, H., S. Kouketsu., S. Kotooka., Y. Akao., (2004). “Transient EGR Control for a Turbocharged Heavy Duty Diesel Engine", SAE Paper No. 2004-01-0120.
50. ETAS Inc., 2009,”ES611.1 A/D Module with Sensor Supply User Manual”, Ann Arbour, MI, USA.
51. ETAS Inc., 2009,”ES00 Network Module User Manual”, Ann Arbour, MI, USA.
52. ETAS Inc., 2009,”ES590 ETK, CAN and K-Line Module User Manual”, Ann Arbour, MI, USA.

53. ETAS Inc., 2009,"ES650 A/D and Thermo-Module User Manual", Ann Arbour, MI, USA.

APPENDIX A: Experimental Setup/Device Specifications

A.1 Fuel Specifications

The following table contains the specifications of the diesel fuel employed in the experiments:

Table A.1: Fuel specifications

Characteristic	**ASTM Test Method**	**Results**	
Distillation Temperature [°C] (Initial Boiling Point to End Point)	D86	IBP EP	188 337
Density [kg/m3] @15°C	D4052	851	
Kinematic Viscosity [cSt] @40°C	D445	2.4	
Total Sulphur [ppm wt]	D5453	14	
Reduced Chemical Formula (based on C/H/O)	D5291	CH1.8	
Composition, Aromatics [% vol]	D1319	30.4	
Composition, Olefins [% vol]	D1319	1.1	
Composition, Saturates [% vol]	D1319	68.5	
Total Aromatics [% wt]	D5186	30.7	
Polycyclic Aromatics [% wt]	D5186	4	
HHV (LHV)[MJ/kg] HHV (LHV) [MJ/l]	D240	44.93 (42.7) 38.34 (36.3)	
Cetane Number	D613	40.8	
Cetane Index	D4737-A	41.4	
Stoichiometric A/F (mass)*	D5291	14.4	

A.2 MAF/IAT Sensor Details

A 5 Volt power supply provides current flow through the resistive wire shown in Figure A.1. The supplied electric current causes the wire to heat up, ultimately increasing its electrical resistance while reducing the current flow. As air flows over the wire, there is a drop in temperature and the electrical resistance of the wire decreases while current flow increases. The air mass flowrate and the intake air temperature are proportional to the current flowing through the wire.

Figure A.1: MAF/IAT Sensor

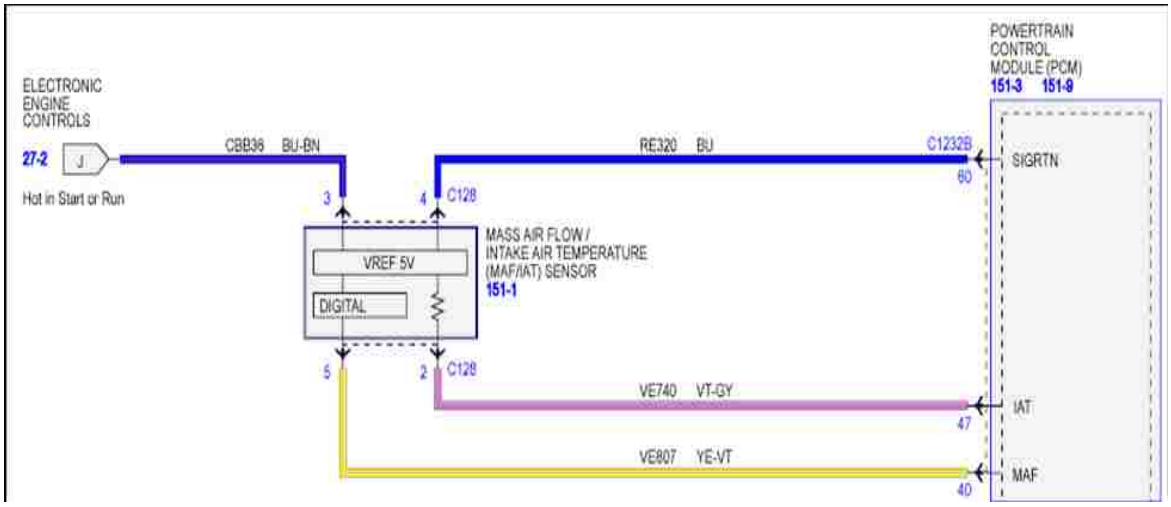

Figure A.2: MAF/IAT Sensor wiring diagram

A.3 ETAS ES600 Measurement Module Specifications

The following table summarizes the technical data of the ETAS data acquisition modules used for the experiments.

Table A.2: ES590 Technical specifications

ES590 Network Module	
Size and Weight	
Dimensions (HxWxD)	1.4 x 5 x 6.4 in
Weight	1.39 lbs
Environment	
Operating Temperature Range	-40 °C to +85 °C
Power Supply	
Operating Voltage	6 V to 32 V DC

Table A.3: ES600 Technical specifications

ES600 Network Module	
Size and Weight	
Dimensions (HxWxD)	1.4 x 5 x 6.3 in
Weight	1.35 lbs
Environment	
Operating Temperature Range	-40 °C to +70 °C
Power Supply	
Operating Voltage	6 V to 32 V DC

Table A.4: ES611 Technical specifications

ES611 A/D Module with Sensor Supply	
Analog Voltage Inputs	
Resolution	16 bits, higher at slower sampling rates
Sampling Rate	0.5 to 2000 samples/sec
Input Voltage range	-10V to +10V or -60V to +60V
Power Supply	
Operating Voltage	6 to 32 V DC
Sensor Supply	
Output Voltage (Vout)	0V to -15V, 0V to +15V

Table A.5: ES650 Technical specifications

ES650 A/D Thermo Module	
Analog Voltage Inputs	
Resolution	16 bits, higher at slower sampling rates
Sampling Rate	0.5 to 2000 samples/sec
Input Voltage range	-10V to +10V or -60V to +60V
Power Supply	
Operating Voltage	6 to 32 V DC
Thermocouple Inputs	
Resolution	21 bits, corresponding to 0.1 K for K-Type Thermocouples
Sampling Rate	0.1 to 10 Samples/sec
Measuring Range	-210 to +1372 C (Type K)
Maximum Inaccuracy of CJC	+/- 1 K

Table A.6: LA4 Lambda Meter

ES650 A/D Thermo Module	
Analog Voltage Inputs	
Resolution	16 bits, higher at slower sampling rates
Sampling Rate	0.5 to 2000 samples/sec
Input Voltage range	-10V to +10V or -60V to +60V
Power Supply	
Operating Voltage	6 to 32 V DC
Thermocouple Inputs	
Resolution	21 bits, corresponding to 0.1 K for K-Type Thermocouples
Sampling Rate	0.1 to 10 Samples/sec
Measuring Range	-210 to +1372 C (Type K)
Maximum Inaccuracy of CJC	+/- 1 K

A.4 EGR Cooler Design Details

DESIGN A

Cooler design A is classified as a shell and tube compact heat exchanger with 36 exhaust gas passages. The tubes are stacked in a 12 x 3 bundle, the gas inlet is curved and the exit is a centred diffuser as shown in Figure A.3. The coolant enters the cooler via a header which allows for even flow distribution of coolant amongst the tubes within the shell and exits via a collector.

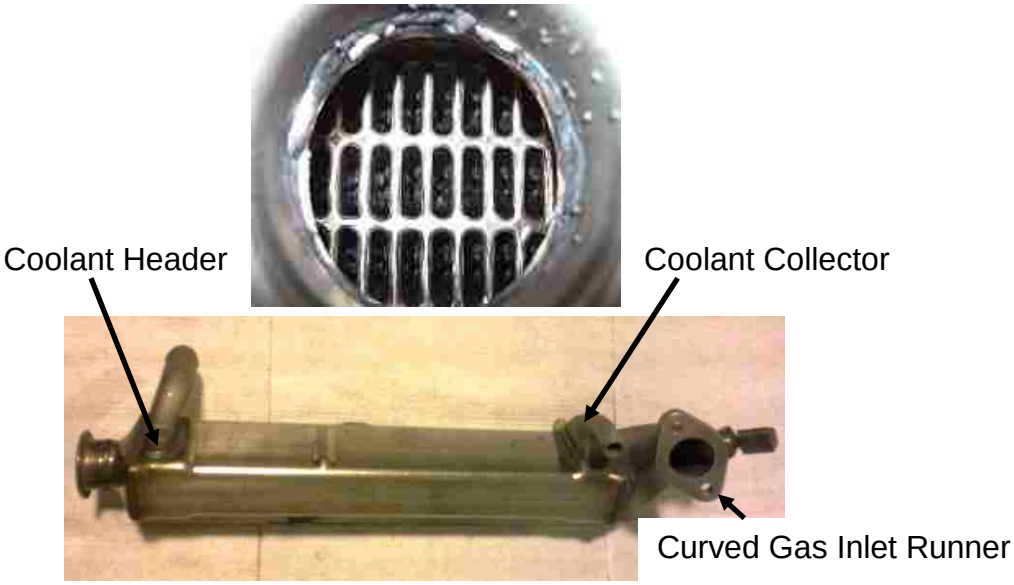

Figure A.3: Cooler design A

DESIGN B

Cooler design B is classified as a plate fin type compact heat exchanger with wavy fin construction. There are a total of 9 exhaust gas passages which contain wavy fins at a density of 9 fins per inch (FPI). The gas inlet is curved and the exit is an angled offset diffuser. The coolant enters the cooler via a header and exits via a collector.

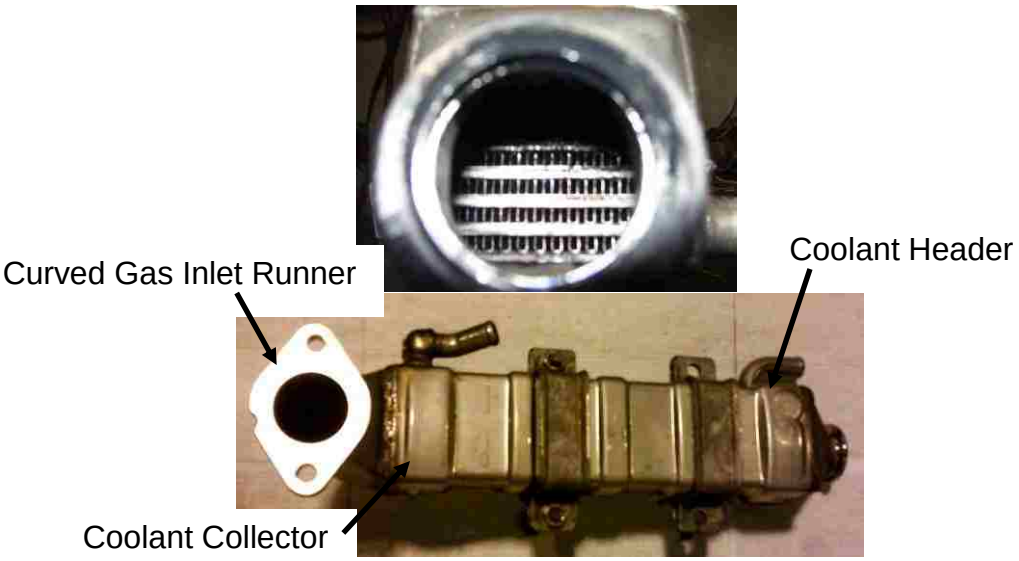

Figure A.4: Cooler design B

DESIGN C

Cooler design C is classified as a plate fin type compact heat exchanger with staggered offset fin construction. There are a total of 7 exhaust gas passages which contain staggered fins at a density of 11 fins per inch (FPI). The gas inlet and exit diffusers are straight and centred. The coolant enters the cooler via a header and exits via a collector.

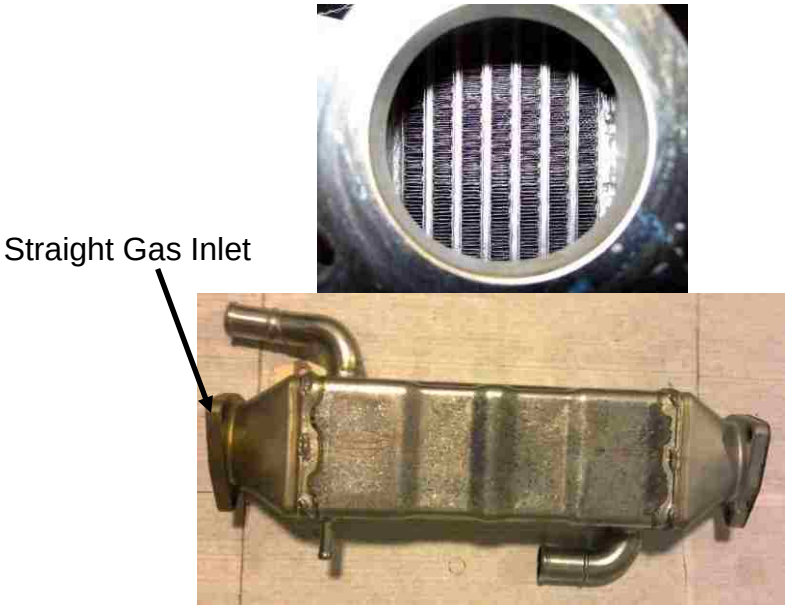

Figure A.5: Cooler design C

DESIGN D

Cooler design D is classified as a plate fin type compact heat exchanger with wavy fin construction. There are a total of 7 exhaust gas passages which contain wavy fins at a density of 9 fins per inch (FPI). The gas inlet and exit diffusers are straight and centred. The coolant enters the cooler via a header and exits via a collector.

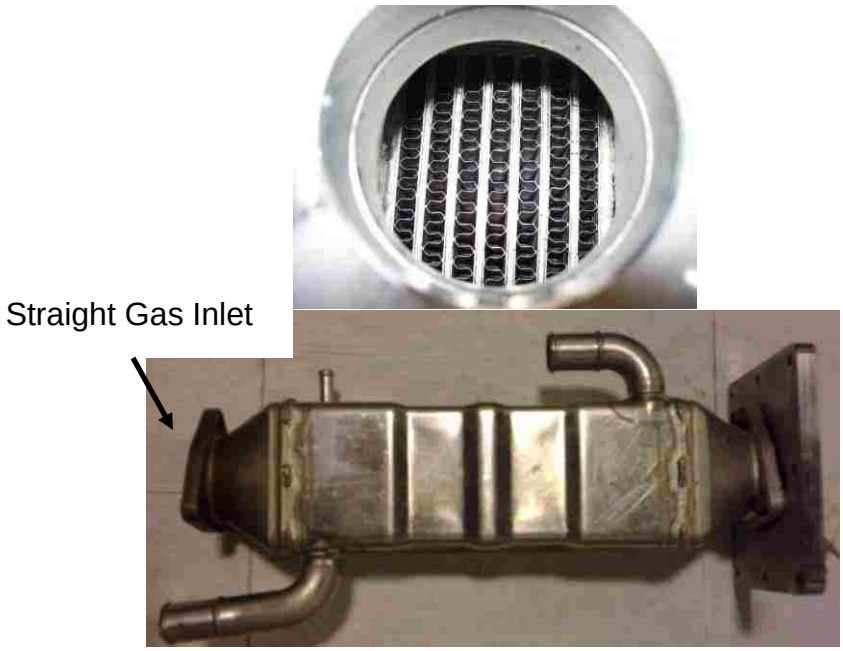

Figure A.6: Cooler design D

DESIGNS F, G, and H

Designs F, G, and H are classified as plate fin type compact heat exchangers with wavy fin construction. There are a total of 6 exhaust gas passages which contain wavy fins at a density of 7 fins per inch (FPI). The coolant enters the cooler via a header and exits via a collector. The lengths of F, G, and H are 270mm, 285mm, and 315mm respectively.

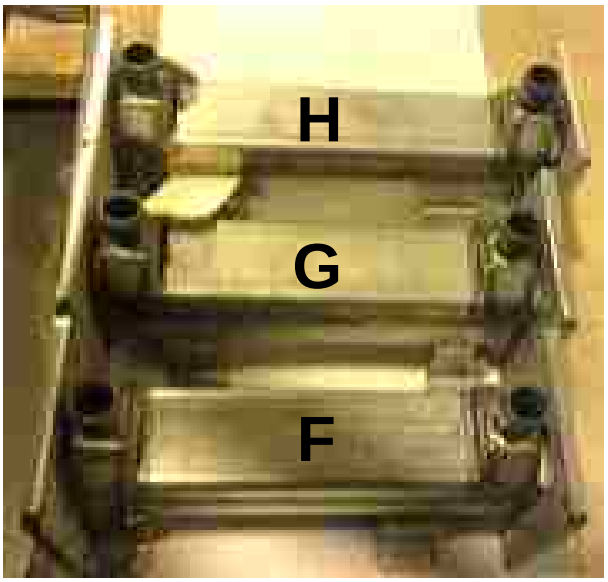

Figure A.7: Cooler designs F, G, and H

DESIGNS J, K, and L

Designs J, K, and L are classified as plate fin type compact heat exchangers with wavy fin construction. There are a total of 7 high temperature and 5 low temperature exhaust gas passages for each cooler which contain wavy fins at a density of 9, 11, and 14 fins per inch (FPI) for designs J, K, and L respectively. The high temperature and low temperature coolers are placed within an aluminum U-shaped housing assembly design.

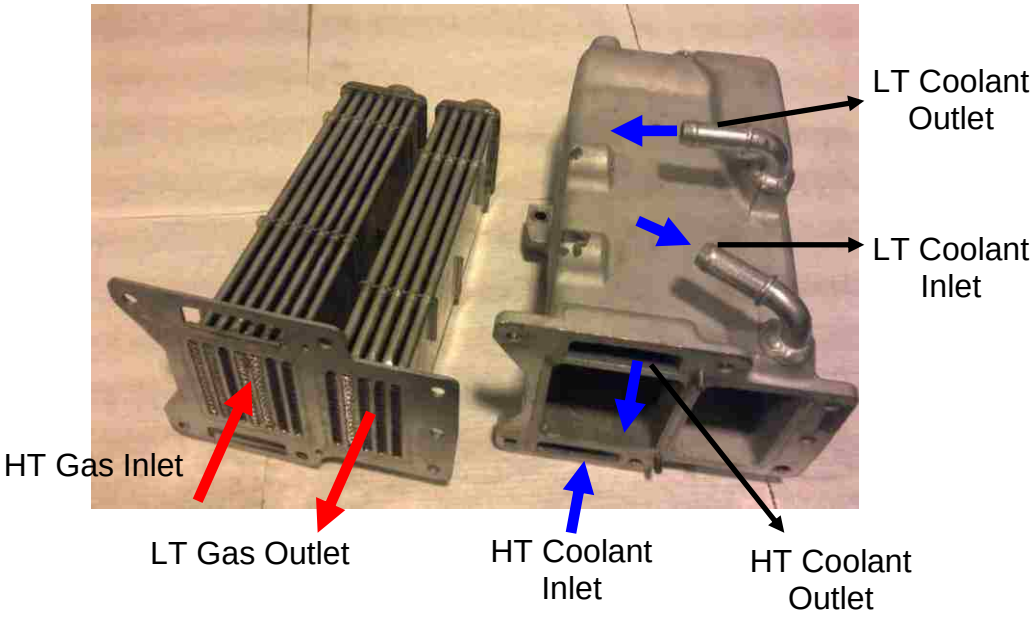

Figure A.8: Cooler designs J, K, and L with u-shaped housing assembly

APPENDIX B: Fluid Properties

B.1 Properties of Coolant

Table B.1: Properties of coolant

Property	Units	Average @ 95 °C	Average @ 35 °C
Density	kg/m^3	1038	1070
Specific Heat	J/kg-K	3607	3421

B.2 Properties of Exhaust Gas

Table B.2: Properties of exhaust gas

Property	Units	Average @ 400 °C
Density	kg/m^3	2.9083
Specific Heat	J/kg-K	1070
Thermal Conductivity	W/m-K	0.042295
Kinematic Viscosity	m^2/s	0.000019

VITA AUCTORIS

Ahmed Sobh was born in November 1985 and raised in Windsor, Ontario, Canada. He received his Bachelor of Applied Science degree from the University of Windsor in August of 2007 and began working as a Research Student at the Ford Powertrain Engineering and Research and Development Centre in September 2007. He is currently a candidate for the Master degree of Applied Sciences at the University of Windsor and hopes to graduate in Winter 2011.